On the Influence of Sea Surface Temperatures on Cyclone Characteristics in the Gulf Stream and Kuroshio Region

Leonidas Tsopouridis

Thesis for the degree of Philosophiae Doctor (PhD)
University of Bergen, Norway
2021

UNIVERSITY OF BERGEN

On the Influence of Sea Surface Temperatures on Cyclone Characteristics in the Gulf Stream and Kuroshio Region

Leonidas Tsopouridis

Thesis for the degree of Philosophiae Doctor (PhD)
at the University of Bergen

Date of defense: 29.01.2021

Year: 2021

Title: On the Influence of Sea Surface Temperatures on Cyclone Characteristics in the Gulf Stream and Kuroshio Region

Name: Leonidas Tsopouridis

Print: Skipnes Kommunikasjon / University of Bergen

Scientific environment

This thesis was carried out at the Geophysical Institute, University of Bergen. I have been enrolled in the Bjerknes Centre for Climate Research under the Global theme group and participated in a number of outreach activities. Most of the courses taken during this PhD have been completed at the Geophysical Institute, but also within the research school CHESS. Obligatory work (e.g., teaching, administrative tasks) accounted for 25% of the fixed term of my employment.

This PhD position has been funded by the University of Bergen (UiB) and was related to the NORPAN (Partnership between Norway and Japan for excellent Education and Research in Weather and Climate Dynamics) and UNPACC (Unifying Perspectives on Atmosphere-Ocean Interactions during Cyclone Development) projects.

CHESS
Research school on changing climates in the coupled earth system

UNIVERSITAS BERGENSIS

BJERKNES CENTRE
for Climate Research

Acknowledgements

First of all, I would like to thank my supervisor Thomas Spengler, for all the constructive discussions, for giving me the chance to attend several national and international meetings and conferences, and for all his guidance overall. I would also like to thank my co-supervisor Clemens Spensberger for sharing his deep knowledge in the field, raising my programming skills with understanding, patience and method, and for all the support when necessary. A special thank you also to my co-supervisor Hisashi Nakamura for all the inspiring discussions, enriching comments, and great hosting during my visits to the Research Center for Advanced Science and Technology, at the University of Tokyo (RCAST), and overall his belief in me.

Many people contributed to the completion of my PhD in different ways. Among them, I want to express my sincere gratitude to Clio Michel, Chris Weijenborg, Yuki Kanno, and Konstantinos Christakos, who either scientifically, or psychologically encouraged me to continue and to never give up. A big thank you to my roommate and friend Vasilis Tryfos for living with me (not easy to live with a PhD Candidate), cheering me up, and continuously reminding me to stay focused on my goal, no matter the difficulties.

Last, but definitely not least I want to thank my sister and my parents, who sidelining their own hard times, never stopped comforting me and reminding me that overall there is one thing in my life that is/should be non-negotiable: ethics. Σας ευχαριστώ και δε θα σταματήσω ποτέ να κυνηγάω τα όνειρά μου και να σας κάνω υπερήφανους.

Abstract

The Gulf Stream and the Kuroshio are the western boundary currents in the North Atlantic and North Pacific, respectively and are associated with maxima in midlatitude precipitation and air-sea heat exchange in the midlatitudes. Both regions are characterized by the strongest sea surface temperature (SST) gradients over the Northern Hemisphere's midlatitudes, able to anchor the storm track and influence the development of individual cyclones. Other mechanisms were also found to contribute significantly to the intensification of cyclones. These include the absolute SST values, the land-sea temperature contrast, latent heat release, surface fluxes from the ocean, and strong upper-level forcing.

The main goal of this thesis is to understand the characteristics of individual cyclones and the mechanisms leading to their intensification, as well as to document the changes on both individual cyclones and the storm track as a whole when a strong SST gradient is present/absent in the Gulf Stream and Kuroshio region. Individual cyclones were tracked using the University of Melbourne cyclone detection and tracking algorithm and categorised depending on their propagation relative to the Gulf Stream and Kuroshio SST fronts, which were detected automatically using an established algorithm that was originally used for detecting atmospheric fronts. Comparing results for the different categories we found that cyclones staying north of the Gulf Stream SST front and those crossing it northward were the ones with the maximum intensification, due to the increased low-level baroclinicity, arising primarily from the land-sea temperature contrast. Differently, in the Kuroshio region, we found cyclones crossing the SST front or remaining on its warm side, to intensify the most. We related this higher intensification to the propagation of cyclones near the left exit region of the jet stream, accounting also for higher precipitation. Even if the SST front contributes to the climatological low-level baroclinicity, no direct effect to the intensification of individual cyclones was found.

The latter was confirmed for both the Gulf Stream and the Kuroshio region, by comparing simulations with realistic and smoothed SSTs in the atmospheric general circulation model AFES. The experiments with smoothed SSTs revealed that the intensification of individual cyclones in the two regions was only marginally affected by reducing the SST gradient. In contrast, cyclone activity was reduced in the North Atlantic and North Pacific storm tracks, which found to shift equatorward in both basins. The mean values of precipitation, specific humidity and surface heat fluxes were found to considerably decrease after the SST smoothing, particularly in the Gulf Stream region, due to the stronger decrease in SST along the SST front. Moreover, to clarify whether the individual cyclones' behaviour is crucial for these changes, we subdivided the winter climatology into dates with/without cyclones in the Gulf Stream and Kuroshio regions

and we highlighted overall the secondary role of cyclones in building the mean state's differences between the SST experiments.

In summary, the results presented in this thesis indicate that despite the similarities between the Gulf Stream and Kuroshio western boundary currents, different mechanisms act to enhance the development and affect the characteristics of individual cyclones, which follow different pathways in the two regions. A weaker SST gradient was found to marginally affect the intensification of individual cyclones, but considerably affect the mean state, confirmed by a reduction in cyclone activity, a shift in the storm track position, a differently changed upper-level jet in the two basins, and a decrease in various meteorological parameters, such as humidity and surface heat fluxes. Considering the changes in the mean state between the experiments with realistic and smoothed SSTs, we found that SST fronts along the Gulf Stream and the Kuroshio region affect the winter climatology primarily in the absence of cyclones.

List of Papers

1. Tsopouridis L, Spensberger C, Spengler T., (2020) *Characteristics of cyclones following different pathways in the Gulf Stream region*, Quarterly Journal of the Royal Meteorological Society 1-16 (Accepted and published online, Oct 2020), https://doi.org/10.1002/qj.3924

2. Tsopouridis L, Spensberger C, Spengler T., (2020) *Cyclone Intensification in the Kuroshio Region and its relation to the Sea Surface Temperature Front and Upper-Level Forcing*, Quarterly Journal of the Royal Meteorological Society (Accepted and published online, Oct 2020), https://doi.org/10.1002/qj.3929

3. Tsopouridis L, Spengler T, Spensberger C., (2020) *SST fronts along the Gulf Stream and Kuroshio affect the winter climatology primarily in the absence of cyclones*, Weather and Climate Dynamics (under review), https://doi.org/10.5194/wcd-2020-50

Contents

Chapter 1

Introduction

1.1 Western Boundary Currents

Theories that explain the oceanic wind-driven circulation date back to the twentieth century. *Sverdrup* (1947) was the first to link the circulation in the upper kilometres of the ocean to the curl of the wind stress and to associate it with the latitudinal variations of the Coriolis force. Analogously, *Stommel* (1948) used the latitudinal variations of the Coriolis force to highlight the asymmetric circulation in the subtropical ocean gyres. *Munk* (1950) built upon Sverdrup's theory and by adding friction was among the first ones to explain the wind-driven ocean circulation, focusing on the Pacific Ocean.

Subtropical gyres are extensive and primarily wind-driven regions that cover approximately 40% of the Earths' surface and control the oceanic circulation at midlatitudes (*McClain et al.*, 2004). The poleward-moving parts of these subtropical gyres are known as western boundary currents (WBCs), since they are located at the western margin of the ocean basins. WBCs are narrow, fast moving, warm currents found in the major oceanic gyres at the midlatitudes (*Hu et al.*, 2015). Their typical width, speed and volume transport are of the order of 100 km, 100 cm s^{-1}, and 30-100 Sv, respectively (*Siedler et al.*, 2013). Wind stress, and particularly its horizontal gradient, is the main driving mechanism for the WBCs (*Hu et al.*, 2015). These oceanic features transport significant amounts of heat towards higher latitudes, contributing to the meridional heat transport and influencing the Earth's climate (e.g., *Kelly and Dong*, 2004; *Kwon et al.*, 2010; *Liu et al.*, 2010; *Nakamura et al.*, 2004; *Siedler et al.*, 2013). In the Northern Hemisphere, there are two WBCs, the Gulf Stream in the North Atlantic and the Kuroshio in the North Pacific Ocean.

The Gulf Stream is a warm ocean current owning its existence to the North Atlantic subtropical gyre. It originates from the Caribbean Sea and Gulf of Mexico, flows out of the Straits of Florida to North Carolina and extends to the east, in the higher latitudes of the North Atlantic Ocean (*Liu et al.*, 2010; *Meinen and Luther*, 2016). Due to its multiple segments, different names have been given in several studies, such as Florida current, Gulf Stream, and Gulf Stream Extension. *Stommel* (1965) underlined this confusion between the different studies and stated that "unfortunately, the naming of things is more a matter of common usage than of good sense". Focusing on the Gulf Stream, after separating from Cape Hatteras (35°N, 75°W), the Gulf Stream becomes one of the world's major currents with a maximum volume transport of approximately 140 Sv (*Talley*, 2011). As it flows over the western North Atlantic, the Gulf Stream grows by

a factor of two (*Hendry*, 1988; *Knauss*, 1969; *Leaman et al.*, 1989), and its transport increases by almost a factor of five (e.g., *Leaman et al.*, 1989). It is characterised by considerable meandering, has its narrowest width close to Cape Hatteras, and becomes wider downstream (*Talley*, 2011). The Gulf Stream water transport varies in time with a maximum (minimum) transport in fall (spring), in line with its documented northward (southward) shift (*Hogg and Johns*, 1995; *Kelly*, 1991). The Gulf Stream current is the upper branch of the meridional overturning circulation, leading to the transport of surface warm water to higher latitudes (e.g., *Liu et al.*, 2010) and driving the formation of tightened sea surface temperature (SST) gradients in the northwest Atlantic (*Brayshaw*, 2006).

The Kuroshio is the western boundary current of the subtropical North Pacific gyre. Kuroshio in Japanese means black stream (kuro-shio, respectively), due to its blackish colour, arising from the lack of organic material (*Qiu*, 2001). The Kuroshio Current originates east of the Philippines coast and as it flows northward, it meets the Luzon Strait, connecting the South China Sea with the North Pacific Ocean. The current becomes more detectable east of the Luzon Strait (*Centurioni et al.*, 2004). After crossing the Izu Ridge, its upper ocean structure resembles the Gulf Stream's, with a considerable core velocity and a westward recirculation, yet weaker compared to the Gulf Stream current (*Talley*, 2011). The Kuroshio flows then to the east of the Japan coast at 35°N, starting from 140°E, into the North Pacific Ocean where it is renamed Kuroshio Extension (KE) (*Kawai*, 1972; *Qiu*, 2001). The KE is highly unstable and characterised by large-amplitude meanders, with two distinct quasi-stationary meanders just east of the Japan coast, at 145°E and 150°E, respectively (*Qiu*, 2001, 2002; *Talley*, 2011). After 159°E, the main flow bisects into an eastward and a separate north-eastward flow, known as the Kuroshio Bifurcation Front, while after 170°E, the Kuroshio current has a broader structure and its separation from the Subarctic Current becomes unclear (*Qiu*, 2002).

The Northern Hemisphere's WBCs are regions of strong air-sea interactions and thus important components determining the climate of the Earth (e.g., *Kelly et al.*, 2010; *Kwon et al.*, 2010; *Nakamura et al.*, 2012; *Siedler et al.*, 2013). The WBCs bring warm waters poleward where they meet colder air with continental or subarctic origin (e.g., *Kelly et al.*, 2010; *Kwon et al.*, 2010; *Siedler et al.*, 2013; *Wallace and Hobbs*, 2006), leading to very large latent and sensible surface heat fluxes (with averaged values of about 200 W m^{-2} and 100 W m^{-2}, respectively) in both the Gulf Stream and Kuroshio regions (*Kwon et al.*, 2010; *Yu and Weller*, 2007). Apart from the ocean circulation, the existence of large surface heat fluxes is also affected by the proximity of the currents to a land nearby and the coastline geometry. Nonetheless, similar surface heat fluxes maxima are observed in both the North Atlantic and the North Pacific, despite the considerably longer distance between the Asian continent and the KE region. *Kelly et al.* (2010) reported this discrepancy and hypothesized that the Japan Sea has only a minor effect on warming the air above.

Along the strong SST gradients observed in the WBCs there are strong proofs of the ocean forcing the atmosphere. *Small et al.* (2008) showed a positive correlation between the SST, the wind speed, and the surface heat fluxes along the SST fronts. *Chelton et al.* (2004) using high-resolution data showed that the ocean currents affect the wind stress curl, which was found to intensify when the wind was blowing parallel to the SST fronts. The surface wind stress, heat fluxes, and boundary layer modifica-

tions across the WBCs arise from changes in surface stability as the air flows across the SST gradient (*Kelly et al.*, 2010). Moreover, instability over the warm SST increases the vertical exchange of momentum and results in enhanced winds and heat fluxes from the ocean to the atmosphere over warm SSTs (*Booth et al.*, 2010; *Chelton et al.*, 2004; *Kelly et al.*, 2010; *Xie*, 2004).

1.2 Storm Tracks

The Gulf Stream and the Kuroshio currents are the locations where the North Atlantic and North Pacific storm tracks are observed. *Hoskins and Valdes* (1990) showed that the warm WBCs to the east of the winter cold continents increase the low-level baroclinicity via diabatic heating and give rise to the genesis and maintenance of storm tracks. Storm tracks, through baroclinic waves, shape the Earth's climate by the poleward transport of heat, moisture, and energy (e.g., *Chang et al.*, 2002; *Hoskins and Valdes*, 1990; *Zhang et al.*, 2020). In addition, due to their momentum flux convergences, they determine the ocean's circulation via wind stress (*Yin*, 2005) and maintain the surface westerlies against friction (*Lau and Holopainen*, 1984; *Schneider*, 2006; *Shaw et al.*, 2016). Despite the different ways of defining a storm track, many studies agree that storm tracks are features of paramount importance for both the midlatitude weather and climate and that possible changes in their position could affect regional climates (*Bengtsson et al.*, 2006; *Chang et al.*, 2002; *Greeves et al.*, 2007).

There are two approaches to investigate the storm tracks: the "Eulerian" and the "Lagrangian" approach. The "Eulerian approach" is a statistical time-mean approach which quantifies the synoptic-scale wave activity by calculating the bandpass-filtered variance in the 500 hPa geopotential height field (e.g., *Blackmon*, 1976; *Blackmon et al.*, 1977). *Sawyer* (1970) was the first to identify a geographic relationship between regions with cyclone activity and transient eddy variance maxima at 500 hPa. *Blackmon* (1976) confirmed the collocation of those maxima and introduced the term "storm tracks" to refer to the geographically confined maxima of the bandpass eddy variance, while *Blackmon et al.* (1977, 1984) confirmed the latter and associated the band pass fluctuations of the 1000, 50 and 300 hPa geopotential height, and the 500 hPa meridional wind component and relative vorticity to propagating baroclinic waves. The eddy kinetic energy spatial distribution was used in this approach to detect the storm tracks. Despite the robustness of this method and the coverage of large amounts of data (*Pinto et al.*, 2007), the "Eulerian approach" does not give details about the cyclones themselves (e.g., *Guo et al.*, 2017; *Hoskins and Valdes*, 1990).

Therefore, cyclone detection and tracking algorithms, referred to as the Lagrangian approach, have been created (e.g., *Murray and Simmonds*, 1991a,b; *Sinclair and Shami*, 1997) to allow an in-depth study of individual cyclones by following them in time and space. Storm tracks in the "Lagrangian approach" are estimated as a group of cyclone tracks, based on individual storms (e.g., *Hoskins and Hodges*, 2002). This method has a more synoptic viewpoint as it "follows" the individual cyclones and enables the identification of their characteristics from their genesis to their lysis. The "Lagrangian approach" permits composites of cyclones during their evolution, providing knowledge on the structure and characteristics of cyclones (e.g., *Catto et al.*, 2010; *Tamarin and Kaspi*, 2017).

Different mechanisms have been suggested to justify the presence and localisation of the Northern Hemisphere storm tracks. *Sutcliffe* (1951) was the first to associate storm tracks and the thermal forcing, showing that the baroclinic development of cyclones was biased by the thermal forcing. *Hoskins and Valdes* (1990) highlighted diabatic heating as crucial to maintain the baroclinicity along the Northern Hemisphere storm tracks, associated the diabatic heating maxima with individual cyclones and proposed the "self-maintaining mechanism" for the storm tracks in the North Atlantic and the North Pacific.

The orography to the west of the North Atlantic storm track is another factor influencing the baroclinicity and controlling the storm track's orientation. Previous model studies confirmed the effect of orography on the propagation of Rossby waves in the midlatitudes (e.g., *Chen and Trenberth*, 1988; *Hoskins and Karoly*, 1981). *Broccoli and Manabe* (1992) using an atmospheric general circulation model (AGCM) showed that the absence of mountains weakens the stationary waves and is of paramount importance for the formation of zonally symmetric storm tracks. *Brayshaw et al.* (2009) highlighted the role of the Rocky Mountains as the strongest factor affecting the North Atlantic storm track. Specifically, they indicated that the orientation of the Rocky Mountains, as well as the southwest-northeast oriented shape of the North American continent lead to the respective tilt in both the storm track and the jet, downstream in the North Atlantic, and increase the low-level baroclinicity.

The role of the neighbouring continents relatively close to the storm track regions on the restoration of surface baroclinicity has been confirmed by previous studies (e.g., *Brayshaw et al.*, 2009; *Robinson*, 1996). The dry, rough, and winter cold continents, compared with the ocean nearby, were found to enhance the low-level baroclinicity, particularly off their eastern coasts. The temperature gradient between the cold continents and the warmer ocean during winter influences the atmosphere through enhancing the low-level baroclinicity and thus affects the storm track (e.g., *Inatsu et al.*, 2000). *Brayshaw et al.* (2009) through a semi-realistic framework explained the localization of the storm tracks, when the continents were present.

Even though baroclinicity has been considered as the most crucial factor for the storm growth and for determining the location of storm activity, their relationship should not be considered as granted (e.g., *Brayshaw*, 2006; *Chang et al.*, 2002; *McCabe et al.*, 2001). Consistent with the higher winter baroclinicity, the North Atlantic storm track is strongest in January, contrary to the North Pacific, where cyclonic activity peaks in autumn and early spring, despite the low-level baroclinicity and jet stream maxima in midwinter (*Chang*, 2003; *Christoph et al.*, 1997; *Nakamura*, 1992; *Park et al.*, 2010; *Zhang and Held*, 1999; *Zhao and San Liang*, 2019). *Nakamura* (1992) called this "midwinter suppression" and related it to the jet stream strength. In more detail, he found that the baroclinic wave activity was positively correlated with the upper-level jet when the upper-level wind speed was below 45 m s^{-1}, which is usually the case in the North Atlantic, whereas when it exceeded this value the correlation becomes negative. This "midwinter minimum" was found also in the sea level pressure variations, and transient eddy heat fluxes, but was more evident at the tropopause level. Since 1992, the midwinter suppression has been confirmed by more studies based on observations and AGCMs (e.g., *Chang*, 2003; *Christoph et al.*, 1997; *Park et al.*, 2010; *Zhang and Held*, 1999; *Zhao and San Liang*, 2019).

The SST fronts of the Gulf Stream and Kuroshio WBCs act to anchor the storm track

close to the front and, depending on their intensity, affect the storm track's intensity and position (e.g., *Kuwano-Yoshida and Minobe*, 2017; *Nakamura et al.*, 2004; *Sampe et al.*, 2010; *Small et al.*, 2014). Observational studies (e.g., *Nakamura et al.*, 2004; *Sinclair*, 1995) highlighted the collocation of the major storm tracks with regions of strong SST gradients along the WBCs, for both hemispheres. Through aquaplanet experiments, *Brayshaw et al.* (2008) associated the strong SST gradient with an enhancement of low-level baroclinicity, which was found to lead to the formation of a midlatitude storm track. They also revealed that strong SST gradients produce a stronger eddy-driven jet. The latter was confirmed by the aquaplanet experiments of *Sampe et al.* (2010) who also found that the elimination of the SST gradient decreases the eddy activity and leads to an equatorward shift of the westerlies and the jet stream. More studies based on model simulations (e.g., *Brayshaw et al.*, 2011; *Kuwano-Yoshida and Minobe*, 2017; *Kuwano-Yoshida et al.*, 2010; *Ma et al.*, 2015; *Piazza et al.*, 2016; *Small et al.*, 2014; *Zhang et al.*, 2020) showed that a smoothing of the SST leads to a weaker cyclone activity in the North Atlantic and the North Pacific region, as well as to an equatorward shift of the storm track.

1.3 Extratropical Cyclones

Extratropical cyclones form mainly along the midlatitude storm tracks (e.g., *Chang et al.*, 2002; *Hoskins and Valdes*, 1990) and are a crucial component of the midlatitude weather and climate (e.g., *Peixoto and Oort*, 1992). A large fraction of precipitation in the midlatitudes is related to extratropical cyclones (*Tierney et al.*, 2018), while when considering fronts, extratropical cyclones produce approximately 90% of the annual precipitation along the storm tracks (*Catto et al.*, 2012; *Hawcroft et al.*, 2012). As much as 80% of extreme precipitation is also related to the passage of extratropical cyclones in the midlatitudes (*Pfahl and Wernli*, 2012). Midlatitude storms -as extratropical cyclones are often called- are of paramount importance for the Earth's climate, as they transport heat, momentum, and energy from the subtropics towards the high-latitude regions (*Chang et al.*, 2002; *Hartmann*, 1994; *Hotta and Nakamura*, 2011; *Nakamura et al.*, 2004). Based on their influence on both the day-to-day weather and the climate as a whole, it becomes apparent why so many "extratropical cyclone-oriented" studies have been conducted over the last decades, trying to clarify their structure, characteristics and the mechanisms leading to their intensification, particularly along the WBC regions.

The study of the structure of extratropical cyclones as well as their dynamic processes and evolution dates back to the rise of the twentieth century. Following World War I, scientists in the Geophysical Institute in Bergen, Norway, led by Vilhelm Bjerknes, provided a conceptual model for the structure and evolution of extratropical cyclones and their accompanying fronts, the "Norwegian cyclone model", which was the cornerstone of observational synoptic meteorology (*Bjerknes*, 1919; *Bjerknes and Solberg*, 1922). Initially, the Norwegian model related an open-wave cyclone with two fronts with different characteristics: a cold and a warm front (*Bjerknes*, 1919). Later, *Bjerknes and Solberg* (1922) considered the life cycle of extratropical cyclones, which begins with a disturbance on the polar front, with winds blowing cyclonically around this disturbance, advecting warm air poleward to the east of the cyclone centre and cold

air equatorward to the west side of the cyclone while the low-pressure system propagates eastward, forced by the upper-level westerlies. Due to its faster rotation, the cold front "catches-up" with the warm front, and creates the so-called "occluded front", which gradually dissipates and leads to the maturity/death of the cyclone.

Due to weaknesses or inconsistencies between observations and the Norwegian model (*Dacre et al.*, 2012; *Schultz and Vaughan*, 2011) new conceptual models of extratropical cyclones have been proposed the following years leading to the Norwegian model's "sister" (*Schultz et al.*, 2018), the ShapiroKeyser cyclone model (*Shapiro and Keyser*, 1990). Analogous to the Norwegian cyclone model, this model includes 4 stages, with the first two being similar to the Norwegian model. However, during the third stage no "catch-up" occurs, but instead the warm front develops westward into the northern airstream of the low-pressure system, forming to what Shapiro and Keyser called "bent-back warm front" and lead to the so-called "T-bone structure", due to the shape of the perpendicularly oriented cold and warm fronts. During the final stage, the cold air and the bent-back warm front "surround" the centre of the low-pressure system and no occlusion process is observed, in contrast to the one described by the Norwegian cyclone model.

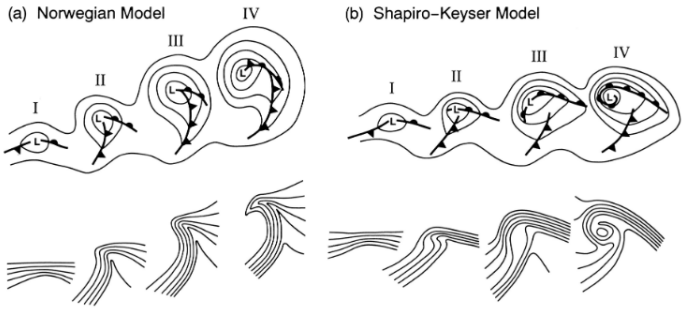

Figure 1.1: Conceptual models of cyclone evolution showing lower-tropospheric (e.g., 850-hPa) geopotential height and fronts(top), and lower-tropospheric potential temperature (bottom). (a) Norwegian cyclone model: (I) incipient frontal cyclone, (II) and (III) narrowing warm sector, (IV) occlusion; (b) ShapiroKeyser cyclone model: (I) incipient frontal cyclone, (II) frontal fracture, (III) frontal T-bone and bent-back front, (IV) frontal T-bone and warm seclusion. Panel (b) is adapted from Shapiro and Keyser (1990, their Fig. 10.27) to enhance the zonal elongation of the cyclone and fronts and to reflect the continued existence of the frontal T-bone in stage IV. The stages in the respective cyclone evolutions are separated by approximately 624 h and the frontal symbols are conventional. The characteristic scale of the cyclones based on the distance from the geopotential height minimum, denoted by L, to the outermost geopotential height contour in stage IV is 1000 km. Figure and caption text taken from Schultz et al. (1998). © American Meteorological Society. Used with permission.

Carl-Gustaf Rossby set the cornerstone regarding the vertical structure of extratropical cyclones by relating the presence of an extratropical cyclone at the surface to planetary waves in the upper-levels, the so-called Rossby waves (*Rossby*, 1939). These undulating wave disturbances, associated with the polar-front jet stream, are a result of the Earth's rotation and its spherical shape, the Coriolis effect, and the planetary vorticity gradient (*Rhines*, 2002). As these waves develop, cold air occupies troughs, which leads to the formation of a cyclone at the surface (cyclogenesis).

Based on Rossby's results, the pioneering works of *Charney* (1947) and *Eady* (1949) were the springboard to explain the origin of wave patterns of midlatitude cyclones, known as baroclinic instability. Baroclinic instability is denoted as the process by which perturbations draw energy from the mean flow available potential energy, which in turn depends on a horizontal temperature gradient. Baroclinic instability converts potential energy into kinetic energy of growing perturbations, that is the eddies. It is the primary ingredient for cyclones' growth and it is affected by both horizontal and vertical temperature gradients, making it easy to understand why extratropical cyclones tend to intensify where baroclinicity is stronger and why the jet stream influences their speed and propagation (*Shaw et al.*, 2016).

Apart to the baroclinic instability arising from small perturbations, as described before, waves of larger amplitudes at either the upper or lower levels can cause cyclone growth. In this manner, *Hoskins et al.* (1985) introduced the so-called "potential vorticity thinking/PV-thinking" to show that baroclinic instability required for the development of midlatitude cyclones could also arise from the interaction of anomalous features, between different levels of the atmosphere. Potential vorticity conservation and PV-invertibility were used in Hoskins' framework to interpret the dynamics of a balanced flow. The conservation principle means that potential vorticity is conserved for adiabatic, frictionless flow, while the potential vorticity invertibility implies that the potential vorticity can be inverted in such a way to allow one to obtain meteorological fields, by assuming an appropriate balanced state. The PV-thinking framework has been applied -among others- to explain the genesis of extratropical cyclones (e.g., *Davis and Emanuel*, 1991; *Whitaker and Davis*, 1994).

During the last decades, several attempts were made to clarify whether the upper-level forcing was necessary for the genesis and subsequent development of cyclones or if cyclones could be the result of the lower level forcing. The first and perhaps the most complete classification scheme came from *Petterssen and Smebye* (1971), who classified cyclones into two types, type A and type B, based on the relative roles of upper and low-level forcing. Cyclones in type A form in the zone of maximum baroclinicity, in the absence of a pre-existing upper-level trough, even if a trough occurs during the cyclone's development and the distance of separation between the upper-level trough and the cyclone doesn't change until the time of maximum cyclone intensity (*Petterssen and Smebye*, 1971). They found that thermal advection is the main mechanism for the intensification of type A cyclones. *Gray and Dacre* (2006) focusing on the North Atlantic vicinity found that 30% of the North Atlantic cyclones belong to this category, of which 60% of these type A cyclones are found to develop. They also indicated that type A-cyclones mainly occur in the region east of the Rocky Mountains. Type B cyclones found to develop when an upper-level trough exists and moves over a warm advection region, in which fronts can be absent or present (*Petterssen and Smebye*, 1971). Contrary to cyclones of type A, the distance of separation between the upper-level trough and the low-level cyclone decreases as the cyclone intensifies, whereas low-level baroclinicity increases. Based on the analysis of *Gray and Dacre* (2006), type B accounts for 38% of cyclones in the North Atlantic, while 56% of these cyclones found to deepen, primarily near the United States East Coast.

In advance to the two types proposed by *Petterssen and Smebye* (1971), *Deveson et al.* (2002) suggested a third type, the so-called type C, which is an extension of type B and consists of cyclones with a very strong upper-level forcing and a weak

cyclogenesis-tilt correlation. They found that these cyclones form at an early stage over high latitude regions. *Gray and Dacre* (2006) found these cyclones to account for 32% of the total number of the North Atlantic cyclones and found to dominate over the ocean, in regions with weak low-level baroclinicity, such as the Eastern Atlantic (*Dacre and Gray*, 2009).

1.3.1 Mechanisms of Extratropical Cyclone Intensification

Focusing on the intensification of individual cyclones, there are many mechanisms which act in a way to intensify extratropical cyclones. Cyclone intensification is considered to be the sum of a number of processes, rather than the result of a single mechanism (e.g., *Roebber*, 1989). Among them, baroclinicity is considered as a primary mechanism. Several studies highlighting the role of a strong SST gradient along the Gulf Stream and Kuroshio region to increase low-level baroclinicity and thus influencing cyclone intensification. Several studies underline the importance of diabatic effects, such as latent heating to enhance cyclone growth (e.g., *Chagnon and Gray*, 2015; *Davis et al.*, 1993; *Fink et al.*, 2012; *Kuo et al.*, 1991). The intensification of cyclones along the regions with strong SST gradients has been also related to the pronounced low-level baroclinicity arising either from sensible heat fluxes (e.g., *Hotta and Nakamura*, 2011) or from latent heating (e.g., *Papritz and Spengler*, 2015). Consistently, *Booth et al.* (2012) through model simulations highlighted latent heat release as an important factor for storm growth, However, they highlighted the absolute SST value as the main driver leading to the storm growth, even when a weaker SST gradient was present in the Gulf Stream region.

Apart from the SST front, the pronounced land-sea temperature contrast, between the cold continent and the warmer ocean has been also proved to affect the intensification of midlatitude cyclones (e.g., *Brayshaw et al.*, 2009; *Inatsu et al.*, 2000; *Tsopouridis et al.*, 2020a), while some studies focusing in the North Atlantic region (e.g., *Brayshaw et al.*, 2009; *Wang and Rogers*, 2001) showed cyclones to be associated with higher baroclinicity in the western part of the basin, due to their proximity to the land. The land-sea temperature gradient is more evident in the North Atlantic region, where both the cold North American continent and the Rockies enhance the pool of cold, dry continental air over the warmer ocean, contributing to the strong temperature contrast and higher low-level baroclinicity along the East Coast (*Brayshaw et al.*, 2009).

In addition to low-level baroclinicity the strong upper-level forcing can contribute significantly to the deepening of extratropical cyclones (e.g., *Evans et al.*, 1994; *Riviere and Joly*, 2006; *Schultz et al.*, 1998), because the baroclinicity associated with the jet stream is beneficial for cyclone intensification. Individual cyclones were found to intensify rapidly when they are located in the left-exit region of the jet, due to the upper-level divergence and vertical lifting (e.g., *Oruba et al.*, 2013; *Ritchie and Elsberry*, 2003; *Uccellini*, 1990). Analogously, pronounced cyclone intensification was observed when a storm crossed the jet axis from the anticyclonic to its cyclonic side (e.g., *Baehr et al.*, 1999; *Riviere and Joly*, 2006).

Chapter 2

Motivation

The western North Atlantic and western North Pacific regions are characterized by strong SST gradients associated with the Gulf Stream and the Kuroshio western boundary currents, respectively. Both regions are preferential locations for cyclogenesis and cyclone intensification. Different reasons have been proposed to explain the regions of pronounced cyclone intensification, including the SST, SST gradient, land-sea temperature contrast, diabatic heating, maxima in air-sea heat exchange, as well as forcing from the upper levels. However, a detailed analysis of the characteristics of individual cyclones in these regions which propagate differently relative to the SST front position is missing. Moreover, while the Gulf Stream and Kuroshio Extension regions share some common characteristics, there are also certain differences between them, such as the orientation of the currents, the proximity of propagating cyclones to the neighbouring continent and the difference in terms of the strength and position of the upper-level jet. All these differences could exert a significant response to the cyclone characteristics, such as their associated surface heat fluxes, moisture, precipitation, and wind speed. Similarly, different mechanisms could evolve and affect differently the development of individual cyclones in the two regions.

The strong SST gradient along the Gulf Stream and the Kuroshio regions has been also considered to anchor the respective storm tracks. Several studies, through numerical experiments and sensitivity tests revealed a shift to both the storm track and the upper-level jet, when the SSTs were smoothed. Nonetheless, there is only a limited number of studies focusing on the influence of such a smoothing on individual cyclones and this was made primarily through case studies. Previous studies confirmed that such an SST smoothing had a certain impact to the mean state's characteristics, that is a decrease on the surface heat fluxes and precipitation. However, the role of cyclones explaining independently or in conjunction with the SST changes the mean state's differences between the SST experiments is unclear and needs to be further investigated.

Chapter 3

Summary of Results and Outlook

3.1 Summary of Scientific Publications

Paper I: Characteristics of cyclones following different pathways in the Gulf Stream region

Tsopouridis L, Spensberger C, Spengler T. (2020), Q J R Meteorol. Soc., 1-16
https://doi.org/10.1002/qj.3924

To understand the characteristics of individual cyclones propagating differently in the Gulf Stream region and to highlight the respective influences of the sea surface temperature (SST) front and land-sea contrast, as well as the role of the jet stream on cyclone intensification, we track individual cyclones and categorize them depending on their propagation relative to the SST front. For the cyclone propagation, we considered five categories, yet concentrated on cyclones staying either on the cold (C1) or warm (C2) side of the SST front, and those crossing the SST front from the warm to the cold side (C3). We tracked cyclones using the University of Melbourne cyclone detection and tracking algorithm and identified SST fronts using an objective frontal detection scheme, originally developed to identify atmospheric front lines. To compare the characteristics of the different propagating cyclones and to investigate the mechanisms leading to cyclone development, we performed a composite analysis around the time of maximum intensification.

We found cyclones in C1 and C3, which form and propagate closer to the continent to intensify more rapidly compared to cyclones in C2, which are characterised by a more maritime propagation and remain more distant from both the land and the SST front. Both cyclones of C1 and C3 are characterised by stronger upper-level forcing and higher low-level baroclinicity, with the higher baroclinicity in C1 highlighting the superiority of the land-sea contrast versus the SST front for cyclone intensification in the region. Nevertheless, cyclones of C3 feature the highest fraction of explosive cyclones, related to the increased latent heat release within the cyclones' warm conveyor belt.

Maxima in surface heat fluxes were observed during maximum cyclone intensity, approximately 12 hours after their maximum intensification. We recognised a pronounced dipole structure in the sensible heat fluxes in cyclones of C1 and C3, with positive values (from the ocean to the atmosphere) to the west and negative values

(from the atmosphere to the ocean) to the east of the cyclone core. Despite the dipole's detrimental role in reducing baroclinicity, the highest low-level baroclinicity in C1 and C3 indicates a rather minor role on cyclone intensification.

Regarding precipitation, different conclusions were drawn for the two types. We found convective precipitation to be strongly modulated by the absolute SST values, no matter if cyclones do or do not cross the SST front. On the other hand, cyclones that crossed the SST front were accompanied by higher large-scale precipitation, confirming the importance of cyclone intensity and moisture availability for increased large-scale precipitation. Interestingly, we found cyclones in C1 and C2 to be associated with similar average large-scale precipitation, despite the limited moisture availability for C1-cyclones. We associated this discrepancy to cyclones in C1 propagating in the left-exit region of an upper-level jet and to an increased isentropic upglide, arising from the strong land-sea temperature contrast.

Paper II: Cyclone Intensification in the Kuroshio Region and its relation to the Sea Surface Temperature Front and Upper-Level Forcing

Tsopouridis L, Spensberger C, Spengler T. (2020), Q J R Meteorol. Soc.
https://doi.org/10.1002/qj.3929

The different characteristics of the Kuroshio region compared to the Gulf Stream region, such as the different orientation and meandering of the Kuroshio current, the stronger Pacific jet and a weaker SST front, as well as the location of a cold continental air mass further away from the Kuroshio SST front, indicated the need of a separate analysis for the North Pacific. To this end, we tracked individual cyclones and categorised them depending on their propagation relative to the SST front in the north western Pacific, following the methods of *Tsopouridis et al.* (2020a) (Paper I).

We considered as mechanisms low-level baroclinicity, upper level forcing by the jet, as well as moisture transport and precipitation. Low-level baroclinicity is generally weaker around the Kuroshio compared to the Gulf Stream region. In addition, cyclones have on average less moisture available. Consequently, both low-level baroclinicity and moisture availability play a less important role for cyclone intensification in the Kuroshio region and account for less of the differences between the cyclone categories.

We found cyclones staying always on the warm side of the SST front (C2) and those crossing the SST front from the warm to the cold side (C3) to deepen more rapidly compared to cyclones remaining on the cold side (C1). The higher intensification of both C2 and C3 cyclones in the Kuroshio region was consistent with their location close to the left exit of a strong jet stream. The forced ascent at the left exit region of the jet likely contributed also to the higher observed large-scale precipitation for cyclones in C2, despite the more limited moisture than in the Gulf Stream region. Even though our results do not suggest a direct impact of the Kuroshio SST front on cyclone intensification, we suggest that the higher baroclinicity observed for cyclones in C3 is partially attributable to the SST front, providing a conducive environment for cyclone growth.

Even if the role of the absolute SSTs is rather secondary in the Kuroshio region for the intensification of cyclones on synoptic timescales, we found the SSTs to con-

siderably modulate the local surface heat fluxes, convective precipitation, and moisture availability. Nonetheless, cyclones are associated with less convective precipitation compared to the ones propagating in the Gulf Stream region, consistent with the overall lower SSTs in the Kuroshio region.

Overall, we underlined the importance of both the upper level jet and low-level baroclinicity on cyclone intensification for the Kuroshio region, with low-level baroclinicity not arising from the land-sea contrast as in the Gulf Stream region. Our results indicated the pronounced role of the intense upper tropospheric jet for the increased precipitation for cyclones propagating near its left exit region.

Paper III: **SST fronts along the Gulf Stream and Kuroshio affect the winter climatology primarily in the absence of cyclones**

Leonidas Tsopouridis, Thomas Spengler, and Clemens Spensberger (2020), Weather Clim. Dynam. Discuss.
https://doi.org/10.5194/wcd-2020-50

Using the atmospheric general circulation model AFES and comparing simulations with realistic (CNTL) and smoothed SSTs for the North Atlantic (SMTHG) and North Pacific (SMTHK), respectively, we quantified and attributed differences in the atmospheric response for the winter period (December-February) 1982-2000. To evaluate the model's results, we compared the CNTL simulation to the ERA-Interim reanalysis dataset and found a good agreement among them, except for considerably larger latent heat fluxes in CNTL, which are most likely associated with the lower SST resolution in ERA-Interim prior to 2002.

We first examined the impact of the SST smoothing on the intensification of individual cyclones. Considering only cyclones with a maximum intensification in the Gulf Stream or the Kuroshio region, analogously classified into 3 categories as in *Tsopouridis et al.* (2020a,b)(Paper I,II), we found similar deepening rates for all the cyclone-categories between the CNTL and SMTHG/SMTHK experiments. The latter confirms the rather minor role of the SST gradient on the intensification of individual cyclones (as in *Tsopouridis et al.* (2020a,b)) and is particularly relevant for the Gulf Stream region where the SST smoothing dramatically weakened a previously strong SST gradient.

Nevertheless, considering all cyclones propagating in the North Atlantic and the North Pacific we found that the SST gradient weakening led to a decreased cyclone density in the storm track, more pronounced in the Gulf Stream region. An equatorward shift in cyclone density was observed in both basins, particularly over their central and eastern parts, in line with previous studies. An analogous southward shift was observed in the upper-level jet for the North Atlantic, whereas for the North Pacific the experiments revealed instead a more meridionally focused and zonally extended jet when the SSTs were smoothed.

Despite the minor impact of the SST smoothing on the characteristics and intensification of individual cyclones, the smoothing of the SST substantially affected the mean state's characteristics. A considerable decrease was observed in the surface heat fluxes, large-scale and particularly convective precipitation, as well as specific humid-

ity, mainly over the warm side of the Gulf Stream SST front. In contrast, a less pronounced decrease was observed in the Kuroshio region, related to the smaller differences in SST between the CNTL and SMTHK experiments.

The different influence of the SST smoothing, that is the largely unaffected characteristics of individual cyclones and the evident changes in the climatological mean state of the storm track, led us to decompose the winter climatology into dates with and without cyclones propagating through either the Gulf Stream or the Kuroshio region. We found the contribution from time-steps without cyclones propagating in the Gulf Stream or Kuroshio region to more closely resemble the climatological differences in surface heat fluxes, whereas differences in precipitation were more closely associated with cyclones propagating in the Gulf Stream or Kuroshio region.

Regarding differences in specific humidity and the upper-level wind speed, different results arise for the two regions. Differences in specific humidity at 850 hPa in the Gulf Stream region are mainly attributable to days with no cyclones in the region, while for the Kuroshio the differences are almost equally attributed between time-steps with and without cyclones present in the region. In like manner, the presence of cyclones in the Gulf Stream region does not seem to affect the difference between CNTL and SMTHG, whereas cyclones in the Pacific act to enhance the observed differences in upper-level wind.

Differences in specific humidity in the Gulf Stream region between CNTL and SMTHG are mainly attributable to days when cyclones are absent in the region. For the Kuroshio, however, the differences are almost equally attributed between time-steps with and without cyclones present in the region. Likewise, while cyclones in the Gulf Stream region do not seem to have a considerable imprint on the differences in the upper-level wind, differences in the Kuroshio region are mainly attributable to time-steps when cyclones are present. We associate this discrepancy between the two basins to cyclones in the Pacific propagating more closely to the climatological jet position in SMTHK, thereby intensifying its eddy-driven component. We related the latter to cyclones propagating closer to the climatological position of the North Pacific jet in SMTHK, thereby intensifying its eddy-driven component.

Overall, our analysis highlights that SST fronts only have a minor impact on the characteristics and intensification of individual cyclones propagating in the Gulf Stream or Kuroshio region, but significantly affect the large-scale response. This effect was stronger in the Gulf Stream, consistent with a more pronounced weakening of the SST gradient. Subdividing the winter climatology into dates with/without cyclones present in the Gulf Stream and Kuroshio regions, we find that cyclones play overall only an inferior role in explaining the mean state's differences between the SST experiments.

3.2 Main Conclusions

Mutually in the three papers we used both Reanalysis and model data, as well as objective detection schemes to capture cyclones, SST fronts, and the jet stream to understand the mechanisms leading to cyclone intensification in the Gulf Stream and Kuroshio region. Categorizing cyclones in the two regions with respect to their propagation

relative to the SST front we provide new insights into the differently propagating cyclones' characteristics and evolution and into the different mechanisms leading to the development of cyclones along the major western boundary currents of the Northern Hemisphere. Finally, through sensitivity tests we revealed the different influence of smoothing the SST to individual cyclones and to the climatological mean state's characteristics and clarified the role of cyclones in explaining the mean state's differences. The main conclusions are:

- There is no direct impact of the SST front on the intensification of individual cyclones, even though the SST front contributes to the climatological low-level baroclinicity.

- Low-level baroclinicity and the upper-level forcing are the main mechanisms leading to the intensification of cyclones in the Gulf Stream and Kuroshio region. For the Gulf Stream region, we highlighted the importance of the land-sea temperature contrast for supplying baroclinicity to cyclones propagating close to the continent. In the Kuroshio region, the land-sea contrast plays a less prominent role and the North Pacific jet stream was found to considerably promote cyclone development.

- We confirmed cyclone intensity and moisture availability as important factors enhancing large-scale precipitation around the cyclone, as well as the corresponding effect when cyclones propagate near the left exit region of the jet. Moreover, we hypothesized that low-level baroclinicity might be an additional factor determining precipitation intensity in the Gulf Stream region.

- Comparing simulations with realistic and smoothed SSTs in an AGCM we found that the intensification of individual cyclones is only marginally affected by reducing the SST gradient in the Gulf Stream and Kuroshio region.

- In contrast, we observed considerable changes in the climatological mean state, with reduced cyclone activity and a southward shift in the North Atlantic and North Pacific storm tracks. Moreover, we recognised a different influence of the SST smoothing in the upper levels, with an equatorward shift of the upper-level jet in the North Atlantic and a stronger and more eastward extended North Pacific jet.

- We marked decreased surface heat fluxes, specific humidity, and precipitation, particularly along the warm side of the Gulf Stream SST front after the SST smoothing and found overall cyclones to play only a secondary role in explaining the mean state's differences between the SST experiments.

3.3 Outlook

I aim to extend the scientific knowledge provided by the above described papers through 2 different analyses:

1) Following the categorization of cyclones into different categories with respect to their propagation relative to the SST front, I aim to produce case studies of specific cyclones, belonging to each of the previously mentioned categories by using a high-resolution atmospheric model. Improving grid spacing and resolution could be beneficial for resolving the cyclone strength, precipitation, and surface heat fluxes distribution around the cyclones. It has been also been proven that a finer model resolution and grid spacing accounts for a more accurate capture of the diabatic features and small scale SST-anomalies, important for the evolution of cyclones (e.g., *Feliks et al.*, 2004; *Minobe et al.*, 2008; *Willison et al.*, 2013).

2) Despite their quantitative differences, climate models, supported by recent observations, qualitatively agree on an increase in the SST and specific humidity the years to come (e.g., *Allen and Ingram*, 2002; *Hartmann et al.*, 2013; *Held and Soden*, 2006; *Knutson et al.*, 2013). This could lead to stronger cyclones through enhanced latent heat release due to the increased moisture availability (e.g., *Stocker et al.*, 2001). Analogously to the methods and analysis of Paper III, I would be interested in designing an experiment in which the SSTs will be equally increased all over the Gulf Stream and Kuroshio domain, differently from the SST smoothing (Paper III), which found to increase the SSTs north of the SST front and decrease them towards its warm side. This will keep the SST gradient unchanged and the changes in the characteristics and intensification of cyclones would be causally linked to the change of the absolute SST values. It would be interesting to investigate the differences arising from an increase of the SST on the frequency, intensity, and characteristics of individual, differently propagating cyclones, as well as to document the mean state's characteristics along the western boundary currents in the projection of a warmer world.

Chapter 4

Scientific results

Paper I

Characteristics of cyclones following different pathways in the Gulf Stream region

Tsopouridis L, Spensberger C, Spengler T.
Quarterly Journal of the Royal Meteorological Society, 1-16, (2020)
https://doi.org/10.1002/qj.3924

Received: 9 March 2020 | Revised: 5 September 2020 | Accepted: 24 September 2020

DOI: 10.1002/qj.3924

Quarterly Journal of the Royal Meteorological Society RMetS

RESEARCH ARTICLE

Characteristics of cyclones following different pathways in the Gulf Stream region

Leonidas Tsopouridis | Clemens Spensberger | Thomas Spengler

Geophysical Institute, University of Bergen, and Bjerknes Centre for Climate Research, Bergen, Norway

Correspondence
L. Tsopouridis, Geophysical Institute, University of Bergen, Postboks 7803, 5020 Bergen, Norway.
Email: leonidas.tsopouridis@uib.no

Funding information
Research Council of Norway (RCN), Grant/Award Number: 262220

Abstract

The Northwest Atlantic is a region of strong temperature gradients and hence is a favourable location for wintertime cyclone intensification co-located with the storm track. The temperature gradient is associated with both the sea surface temperature front along the Gulf Stream and the land–sea contrast. To understand the respective influences of the sea surface temperature (SST) front and land–sea contrast in the Gulf Stream region, as well as the role of upper-level forcing on cyclone development, we track individual cyclones and categorise them depending on their propagation relative to the SST front. We concentrate on cyclones staying either on the cold (C1) or warm (C2) side of the SST front, and on cyclones that cross the SST front from the warm to the cold side (C3). Comparing these categories, we find that the land–sea contrast is more important for supplying baroclinicity to cyclones in C1, while the strong low-level baroclinicity in C3 is also partially attributable to the SST front. The propagation of cyclones in C1 and C3 near the left exit region of the North Atlantic jet explains the higher intensification and precipitation.

KEYWORDS

cyclone intensification, Gulf Stream, extratropical cyclones, land–sea contrast, SST front

1 | INTRODUCTION

The western North Atlantic region is characterized by both strong sea surface temperature (SST) gradients associated with the Gulf Stream (Tomczak and Godfrey, 2003) and strong land–sea temperature contrasts during winter (Thompson *et al.*, 1988). The region is a preferential location for cyclogenesis (Hoskins and Hodges, 2002), cyclone intensification (e.g., Wang and Rogers, 2001; Lim and Simmonds, 2002; Jacobs *et al.*, 2008), and cyclonic bomb formation (Sanders and Gyakum, 1980). Roebber (1989) indicated that the deepening rates of extratropical cyclones (hereafter cyclones) "arise as a sum of processes", such as latent heat release (e.g., Rogers and Bosart, 1991; Kuo *et al.*, 1991; Whitaker and Davis, 1994) and baroclinic instability (e.g., Sanders, 1986; Manobianco, 1988; 1989; Catto, 2016). The origin of the baroclinicity has been argued to be due to the Gulf Stream SST gradient (Sanders, 1986) and the land-sea contrast (Wang and Rogers, 2001). We aim to clarify the relative roles of the SST front and the

land–sea contrast by categorising the intensification of cyclones in the Gulf Stream region with respect to their position relative to the SST front.

Several studies have highlighted the importance of diabatic heating and surface heat fluxes on maintaining low-level baroclinicity in the area of strong SST gradients (Kuo *et al.*, 1991; Reed *et al.*, 1993; Nakamura *et al.*, 2004; Hotta and Nakamura, 2011; Papritz and Spengler, 2015). Hotta and Nakamura (2011) underlined the significance of sensible heat fluxes for restoring low-level baroclinicity along oceanic frontal zones, while Papritz and Spengler (2015) emphasised latent heat release as a major contributor maintaining baroclinicity in the Gulf Stream region. The SST front has also been argued to increase convection and large-scale precipitation along the SST front (Minobe *et al.*, 2008; Parfitt *et al.*, 2016; Vannière *et al.*, 2017b). However, studies based on composite analysis found cyclone intensity and moisture availability to be the dominant factors altering precipitation (Field and Wood, 2007; Rudeva and Gulev, 2011; Pfahl and Sprenger, 2016). Consistently, de Vries *et al.* (2019) found that cyclones respond to both the low-level baroclinicity associated with the SST front as well as the additional moisture provided by altered surface latent heat fluxes associated with changes in the SSTs.

In addition to the SST front, the wintertime temperature contrast between the cold continent to the west and the warmer ocean to the east can also influence the baroclinicity and the storm track (Cione *et al.*, 1993); Inatsu *et al.*, 2000; 2003; Brayshaw *et al.*, 2009; Booth *et al.*, 2012). In particular, Wang and Rogers (2001) and Brayshaw *et al.* (2009) showed that cyclones in the Northwest Atlantic are associated with a greater amount of baroclinicity due to their proximity to the land–sea boundary than cyclones in the Northeast Atlantic. Furthermore, the triangular shape of the North American continent together with the Rocky Mountains support the growth of the pool of cold air in the northeast of the continent, contributing to the surface temperature contrast along the Eastern North American continental margin which increases low-level baroclinicity and thereby cyclone intensification (Brayshaw *et al.*, 2009).

In addition to the low-level baroclinicity, the upper-level forcing, determined by the relative position of the jet stream, can contribute to cyclogenesis (e.g., Sanders and Gyakum, 1980; Uccellini *et al.*, 1984; Sinclair and Revell, 2000), as well as influence the subsequent evolution and intensification of cyclones (e.g., Evans *et al.*, 1994; Schultz *et al.*, 1998). Sanders and Gyakum (1980) noted that explosive cyclogenesis mainly occurs on the poleward side of the jet stream and is associated with an upper-level trough. This rapid cyclone intensification is due to the location close to the poleward exit region of the jet, because the upper-level divergence and vertical lifting stimulate both cyclone deepening and precipitation (e.g., Johnson and Daniels, 1954; Uccellini, 1990; Ritchie and Elsberry, 2003; Oruba *et al.*, 2013; Milrad, 2017).

To better understand the relative roles of the SST front, the land–sea contrast and upper-level forcing to cyclone intensification in the Gulf Stream region, we need to consider the evolution on synoptic time-scales (e.g., Parfitt *et al.*, 2016; Vannière *et al.*, 2017b; Ogawa and Spengler, 2019). This can be accomplished either through composite analysis or by investigating individual case-studies. While case-studies can provide great detail of the different physical processes during the development of an individual cyclone, it is often difficult to draw more general conclusions on the dominant mechanisms. Analyses of composites of developing cyclones, on the other hand, have proven to be advantageous, as the basic features and general characteristics of the evolution are maintained, while not relying on arguments built around individual events with large case-to-case variability (Sinclair and Revell, 2000; Rudeva and Gulev, 2011).

For instance, using cyclone-centric composites, Wang and Rogers (2001) compared the dynamical structure and evolution of cyclones in different sectors of the North Atlantic. However, their analysis is based on explosive cyclones only. More recent studies evaluated surface heat fluxes and atmospheric moisture content for cyclones at different stages of their development over the Gulf Stream region (Rudeva and Gulev, 2011; Dacre *et al.*, 2020). However, none of these studies examined the specific contribution of the SST front to the intensification of cyclones. We thus complement these studies by including both explosive and non-explosive cyclones in the composite analysis and by evaluating the significance of the SST front on cyclone growth, where we divide cyclone propagation into different categories based on the path of cyclone trajectories relative to the SST front. Thereby, we shed light on the aspects of cyclone intensification in the Gulf Stream region and highlight the structural differences of cyclones following different paths relative to the Gulf Stream SST front.

2 | DATA AND METHODS

2.1 | Data

We use 6-hourly data from the ERA-Interim reanalysis (Dee *et al.*, 2011) with a horizontal resolution of $0.5° \times 0.5°$ for all winter months (December–February) in the period 1979–2016. Both cyclone intensity and distribution (Hodges *et al.*, 2011) as well as precipitation (Hawcroft *et al.*, 2012; Booth *et al.*, 2018) in ERA-Interim compare well to other reanalyses. For our analysis, we use mean sea level pressure (MSLP), SST, temperature at 850 hPa,

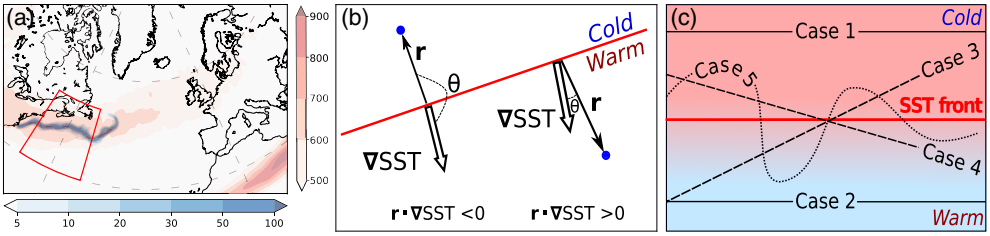

FIGURE 1 (a) Density of SST fronts (km of line (100 km)$^{-2}$, blue shading) and of the climatological jet stream (km of jet axis line (1000 km)$^{-2}$, light red shading) for the North Atlantic. The Gulf Stream region is marked with a red box. (b) Illustration describing the scalar product method to derive the relative position between the cyclone and the SST front. (c) Schematic of the cyclone classification based on the cyclone position relative to the SST front

total column water vapour (TCWV), vertically integrated water vapour flux (IWVF), wind at 925 hPa, large-scale and convective precipitation, as well as latent and sensible surface heat fluxes. Surface heat fluxes and precipitation are derived from the twice-daily forecasts (initialised at 0000 and 1200 UTC) and are accumulated ±3 hr around the respective timesteps, following the same procedure as Ogawa and Spengler (2019) and Weijenborg and Spengler (2020). Specifically, we use the cumulative values from the 0000 UTC forecasts between 3 and 9 hr lead time, as well as between 9 and 15 hr lead time to derive fluxes and precipitation for the analyses of 0600 and 1200 UTC, respectively. Analogously, we use the 1200 UTC forecasts to derive precipitation and fluxes at 1800 and 0000 UTC.

2.2 | SST front detection

We identify SST fronts using an objective frontal detection scheme that is based on the "thermal" method (Hewson, 1998). This scheme has been applied to detect atmospheric fronts in several previous studies (Jenkner *et al.*, 2010; Berry *et al.*, 2011; Schemm *et al.*, 2015). The method by Hewson (1998) identifies frontal lines in a two-dimensional thermal field τ using the thermal frontal parameter (Renard and Clarke, 1965)

$$\mathrm{TFP} = -\nabla|\nabla\tau| \cdot \frac{\nabla\tau}{|\nabla\tau|}\,, \tag{1}$$

where we chose τ to be the SST. The TFP indicates "the gradient of the magnitude of the gradient of a thermodynamic scalar quantity, resolved into the direction of the gradient of that quantity" (Renard and Clarke, 1965). Hewson (1998)'s framework is based on identifying the maxima of TFP, which correspond to the warm side of a frontal zone. In our study, however, we choose TFP=0 to identify the centre of the frontal zone (following e.g., Jenkner *et al.*, 2010), and apply a masking criterion

$$\nabla|\nabla\tau| < 0 \tag{2}$$

to exclude the detection of minima in SST gradients.

We perform the detection using SST data filtered with a triangular truncation T84 and require a minimum frontal length of 500 km to retain only fronts with a length-scale comparable to atmospheric fronts. To capture the most prominent parts of the SST fronts along the Gulf Stream, we found a temperature gradient threshold $|\nabla\tau| > 2\mathrm{K}/100\,\mathrm{km}$ to yield the most accurate results. Consistent with oceanographic studies (e.g., Lee and Cornillon, 1996; Meinen and Luther, 2016), the SST front climatology for the North Atlantic basin features the highest frequency of SST fronts along the Gulf Stream (Figure 1a). To account for the convergence of the grid towards the poles, we normalise the front line detections to an average line length per unit area γ, with

$$\gamma = \frac{1}{AN}\sum_{i=1}^{N} l_i\,. \tag{3}$$

Here, A is the area covered by a grid cell, N the number of time steps in the climatology, and l_i the length of a SST front line over the respective grid cell during time step i (zero if no front is detected).

2.3 | Jet stream detection

To diagnose the role of upper-level forcing on cyclone intensification, we employ a jet detection, based on automatically detected jet axes, following the method and criteria of Spensberger *et al.* (2017). The jet axes are identified by lines separating the cyclonic from the anticyclonic wind shear. The climatological position of the North Atlantic jet

coincides with the location of the SST front (compare blue and light red shadings in Figure 1a).

2.4 | Cyclone detection and tracking

We employ the University of Melbourne cyclone detection and tracking algorithm (Murray and Simmonds, 1991a; 1991b). The algorithm defines cyclones as maxima in the Laplacian of the MSLP field and tracks them over time using a nearest-neighbourhood method together with the most probable direction of propagation (Murray and Simmonds, 1991a; 1991b; Michel *et al.*, 2018) The Appendix gives the chosen parameters.

For the selection of tracks, we require cyclones to spend at least 12 hr (three consecutive time steps) in the area of interest (30–50°N and 290–310°E), henceforth referred to as the Gulf Stream region. We also require that the minimum of pressure along the track occurs during December–February (DJF) and only consider tracks with maximum intensification, defined as the most rapid decrease in surface pressure, in the Gulf Stream region. In addition, we require the Great Circle distance between cyclogenesis and cyclolysis to be greater than 300 km to remove quasi-stationary systems. Furthermore, all cyclones positioned over terrain higher than 1000 m are discarded. By applying the criteria described above, we obtain 222 tracks over the 38 winters.

2.5 | Classification of cyclone tracks based on position to SST front

We find the shortest distance between each cyclone position and the SST front for every timestep along the cyclone track and define the vector $\mathbf{r}$ directed from the SST front to the cyclone. We then use the scalar product

$$\mathbf{r} \cdot \nabla SST = |\mathbf{r}||\nabla SST| \cos\theta \tag{4}$$

to calculate the angle θ between $\mathbf{r}$ and ∇SST to detect which side of the SST front the cyclone is located (Figure 1b). If a cyclone is located on the warm (cold) side of the SST front, the scalar product is positive (negative). Note that the SST front lines do not have to follow the SST contours and that the front lines therefore do not have to be perpendicular to the SST gradient.

Using the relative position of the cyclone to the SST front within the Gulf Stream region, we categorise cyclone propagation into five categories (Figure 1c). For category 1 (C1) the cyclone always stays on the cold side of the SST front, while the cyclone always stays on the warm side of the SST front for category 2 (C2). Cyclones crossing the SST front from the warm to the cold side belong to category 3 (C3), whereas they belong to category 4 (C4) if they cross the SST front from the cold to the warm side. Finally, cyclones that cross the SST front multiple times belong to category 5 (C5).

3 | RESULTS

3.1 | Cyclone occurrence and intensification

The cyclone density for the winter season (DJF) over the North Atlantic exhibits three major regions of cyclone activity: East of Greenland, the Gulf Stream, and along the Scandinavian coastline (Figure 2a). The cyclone density pattern is in good spatial agreement with previous studies (e.g., Hanley and Caballero, 2012; Neu *et al.*, 2013). We observe small quantitative differences compared to the density climatology presented by either Neu *et al.* (2013) or Murray and Simmonds (1991a), who also used the Melbourne University algorithm. These small deviations are most likely due to the neglect of shallow and weak systems in our database.

A large number of cyclones (84) stay on the cold side of the SST front (C1) (Figure 2b), whereas fewer cyclones (26) stay on the warm side of the SST front (C2) (Figure 2c). When crossing the SST front in the Gulf Stream region, the great majority of cyclones (64) cross the SST front towards its cold side (C3) (Figure 2d). A common feature for the three categories of cyclones is their propagation from the southwest to the northeast, whether or not they cross the SST front. Brayshaw *et al.* (2009) associated this tilt of the storm track with both the orientation of the North American east coast, as well as stationary waves from the Rocky Mountains. Only 13 cyclones cross the SST front from the cold to the warm side (C4) (Figure 2e) while 35 cyclones cross the SST front multiple times (C5) (Figure 2f). In order to assess the influence of the SST front on cyclones, we discard C4 and C5, because of the small number of tracks and multiple crossings, respectively. We will thus focus exclusively on C1, C2, and C3.

Cyclones in C1 and C2 never cross the SST front in the Gulf Stream region and mostly stay at a distance greater than 300 km on the cold or warm side, respectively (Figure 3a). In contrast, cyclones in C3 cross the SST front on average 6 hr after their maximum intensification (Figure 3a,b). Overall, cyclones in C1 and C3 feature the highest deepening rates (Figure 3b), with a maximum deepening rate of approximately 1.2 hPa·h^{-1} (28 hPa·day^{-1}), while cyclones of C2 experience a lower, yet notable intensification of 0.8 hPa·hr^{-1} (19 hPa·day^{-1}). C2 has a qualitatively similar,

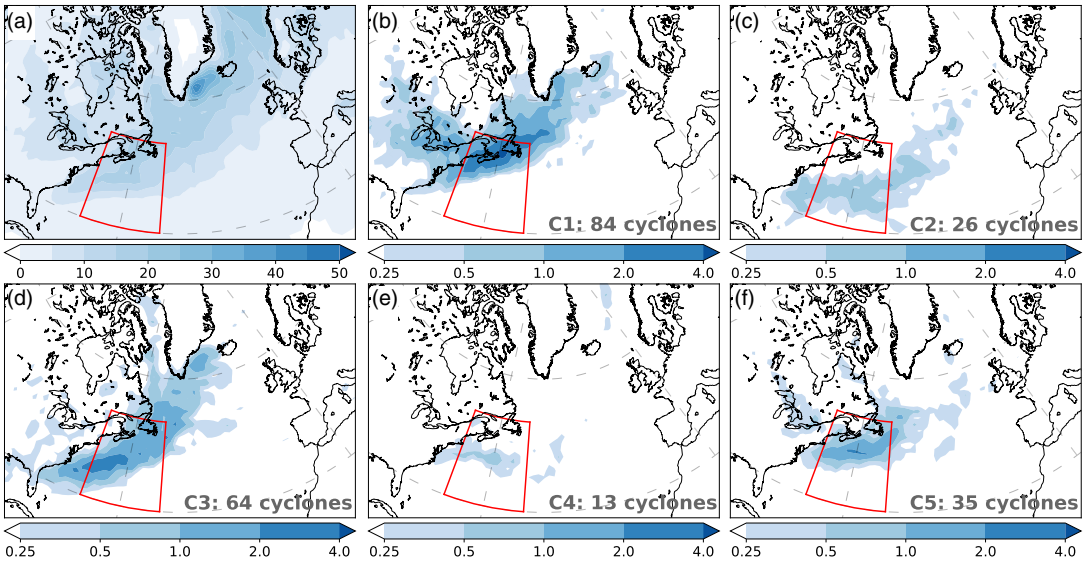

FIGURE 2 (a) Cyclone density (10^{-6} km^{-2}) based on the ERA-Interim reanalysis for the winter seasons in 1979–2016. (b)–(f) are as (a) but for cyclones with maximum intensification in the Gulf Stream region in categories C1 to C5, respectively. See main text for more details on the cyclone detection and categorisation

but more variable distribution, due to the lower number of cyclones than in C1 and C3. Following the definition of Sanders and Gyakum (1980), 40% of the cyclones in C3 (26 cyclones), 23% of the cyclones in C1 (19 cyclones), and only 11% of the cyclones in C2 (3 cyclones) are explosively developing cyclones. The total number of explosive cyclones is smaller than in the climatologies of Lim and Simmonds (2002) and Allen *et al.* (2010), as we restrict our analysis to the Gulf Stream region.

The location of maximum intensification is equally spread on the cold and warm sides of the SST front for categories C1 and C2, while the locations are spread along the main SST gradient for C3 (Figure 4a–c). For C1, and in particular C3, the location of maximum intensity is close to the location of maximum intensification. In contrast, cyclones of C2 reach their maximum intensity further downstream.

3.2 | Cyclone-relative SST and wind composites

We present cyclone-relative composites for C1, C2, and C3 to clarify the potential role of the SST front, the land–sea contrast, and upper-level forcing on the cyclone structure and intensity. Cyclone centres in the composites represent the minimum sea level pressure. In the following, we will contrast the non-crossing categories C1 and C2 with the crossing category C3. We present composites for the time of maximum intensification (centre column in Figures 5–9) as well as 12 hr before and after this time (left and right columns in Figures 5–9, respectively).

Due to the cyclones in C1 moving towards higher SSTs (Figures 2b and 3a), we observe an increase in SST with time in the southeastern quadrant before the time of maximum intensification (Figure 5a,b). Due to the southern position of cyclones in C2 (Figure 2c), they are propagating over higher SSTs than in C1. In contrast to C2 (Figure 5d–f), cyclones in C1 are associated with the strongest temperature gradient at 850 hPa, most likely due to the proximity of the cyclones to the United States east coast throughout their evolution (Figure 5a–c). However, in both categories there is a gradual increase of the maximum wind speed at 925 hPa from 18 m·s^{-1} at 12 hr prior to maximum intensification to 24 m·s^{-1} 24 hr later (Figure 5a-c,d-f), with the maximum wind speed observed in the southeastern quadrant, due to the superposition of the cyclonic circulation and the eastward propagation.

Twelve hours prior to their maximum intensification, cyclones of C3 are located on the warm side of the SST front, similar to cyclones of C2. However, cyclones of C3 propagate closer to both the SST front and the landmass (Figures 3a and 5g), which likely explains the stronger temperature gradient at 850 hPa observed in C3 than in C2. Drawing air both from the warm side of the SST front and the cold continent, cyclones of C3 can make use of the

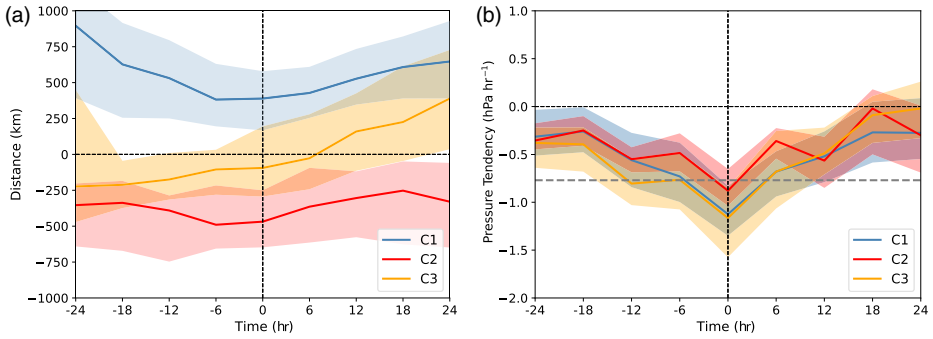

FIGURE 3 (a) Distance (km) between cyclone centres and the SST front relative to the time of maximum intensification. Lines indicate the 50th percentile and the shading the interquartile range. (b) is as (a), but for the pressure tendency (hPa·hr^{-1})

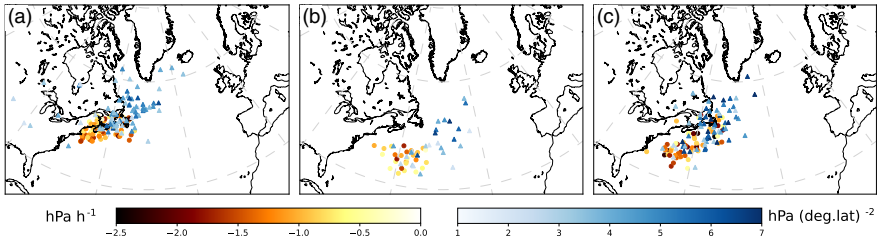

FIGURE 4 Locations of cyclone maximum intensification (hPa·h^{-1}, yellow-red circles) and cyclone maximum intensity (hPa· (deg lat)$^{-2}$, blue triangles) for category (a) C1, (b) C2, and (c) C3

combined thermal gradient across both the SST front and the coastline. This interpretation is in line with Brayshaw *et al.* (2009), who documented increased near-surface low-level baroclinicity along the United States east coast, where the cold dry continental air meets the warmer and moist air over the ocean.

Contrary to C1, the SST decreases with time for C3, consistent with the propagation towards the cold side of the SST front (Figures 2d and 5g–i). As for C1 and C2, the wind speed increases with time for C3 (Figure 5g–i), and the highest wind speed, exceeding 30 m·s^{-1}, is observed 12 hr after maximum intensification (Figure 5i). The wind decays 18 hr after the maximum intensification (not shown).

3.3 | Cyclone-relative surface heat flux composites

For both C1 and C2, the latent heat fluxes are always upward (Figure 6a–c,d–f) and largest in the southwestern quadrant south of the SST front due to the increase in surface saturation mixing ratio with increasing SST. Likewise, sensible heat fluxes are directed towards the atmosphere in the southwestern quadrant, within the cyclone's cold sector (Figure 6a–c,d–f). Both fluxes are highest south of the SST front due to an increase in SST (consistent with, e.g., Zolina and Gulev, 2003; Vannière *et al.*, 2017a). Twelve hours before maximum intensification, there are on average significantly lower fluxes for C1 than for C2. This is most likely associated with the propagation of the C2 cyclones over higher SSTs than for C1 (Figure 2b,c). However, for both categories, there is a marked increase in both latent and sensible heat fluxes in the southwestern quadrant within 24 hr (Figure 6a–c,d–f) associated with the proximity of the SST front. Consistent with Businger *et al.* (2005) and Rudeva and Gulev (2011), the maximum sensible and latent heat fluxes are almost collocated, with a slight northward shift of the sensible heat fluxes compared to the latent heat fluxes. Similar to C1, surface heat fluxes increase within the 24 hr period (Figure 6d–f).

C3 can be considered a combination of C1 and C2, as cyclones are initially located on the warm side of the SST front (C2) before crossing to the cold side (C1). At 12 hr before maximum intensification, latent and sensible

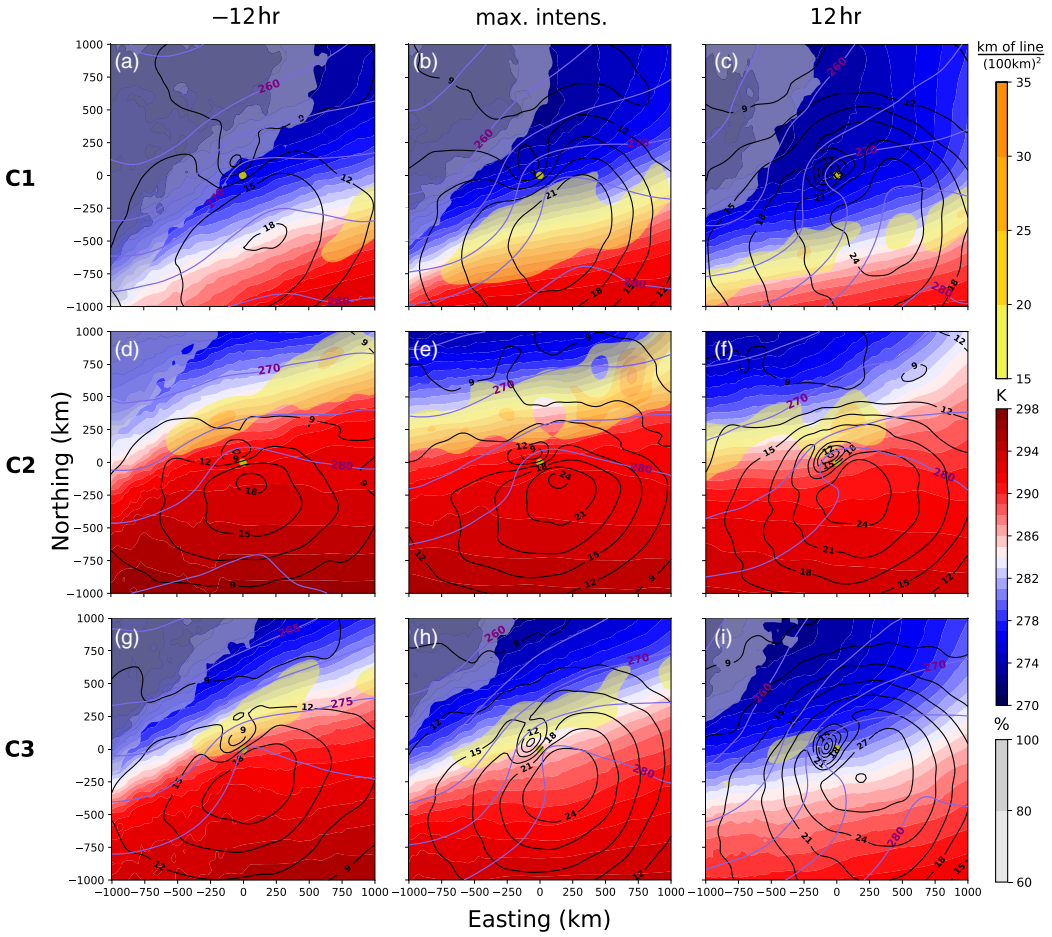

FIGURE 5 Composite evolution of cyclone-centred SST (blue-red shading, K), temperature at 850 hPa (purple contours with interval 5 K), wind speed at 925 hPa (black contours with interval 3 $m \cdot s^{-1}$), SST front density (yellow shading, in $10^{-5} km^{-1}$) and probability of being over land (grey shading, 60–100%). (a, d, g) are at 12 hr prior to maximum intensification, (b, e, h) at maximum intensification, and (c, f, i) at 12 hr after maximum intensification, for categories (a–c) C1, (d–f) C2, and (g–i) C3

heat fluxes are relatively high, exceeding 240 $W \cdot m^{-2}$ and 100 $W \cdot m^{-2}$, respectively (Figure 6g). These values are higher than for C2 (Figure 6d), because the cyclones are located closer to the SST front (Figure 3a) and the wind is stronger (Figure 5d,g). Similar to C1, C3 consists of cyclone tracks located closer to the continent at the early stage of development (Figure 2b,d) and are thus more strongly influenced by cold continental air masses (Figure 5d,g) than C2.

During maximum intensification, sensible (latent) heat fluxes increased to more than 100 (160) $W \cdot m^{-2}$ for C1 (Figure 6b). Twelve hours past maximum intensification, upward sensible heat fluxes increased to approximately 160 $W \cdot m^{-2}$ in the southwestern quadrant (Figure 6c). Besides that, downward sensible heat fluxes appear in the eastern quadrant due to warm air advection over relatively lower SST (Figure 6b,c), yielding a dipole structure in the sensible heat flux, with positive values to the west and negative sensible heat fluxes to the east (consistent with Rudeva and Gulev, 2011; Dacre *et al.*, 2020). This tongue of warm air is wrapped cyclonically around the cyclone centre. For C3, the heat fluxes (Figure 6h,i) are equivalent to C1 (Figure 6b,c) with a similar dipole emerging in the sensible heat fluxes 12 hr after maximum intensification (Figure 6i).

In C2, this dipole in sensible heat fluxes is much less pronounced, because these cyclones generally form further away from the North American continent than

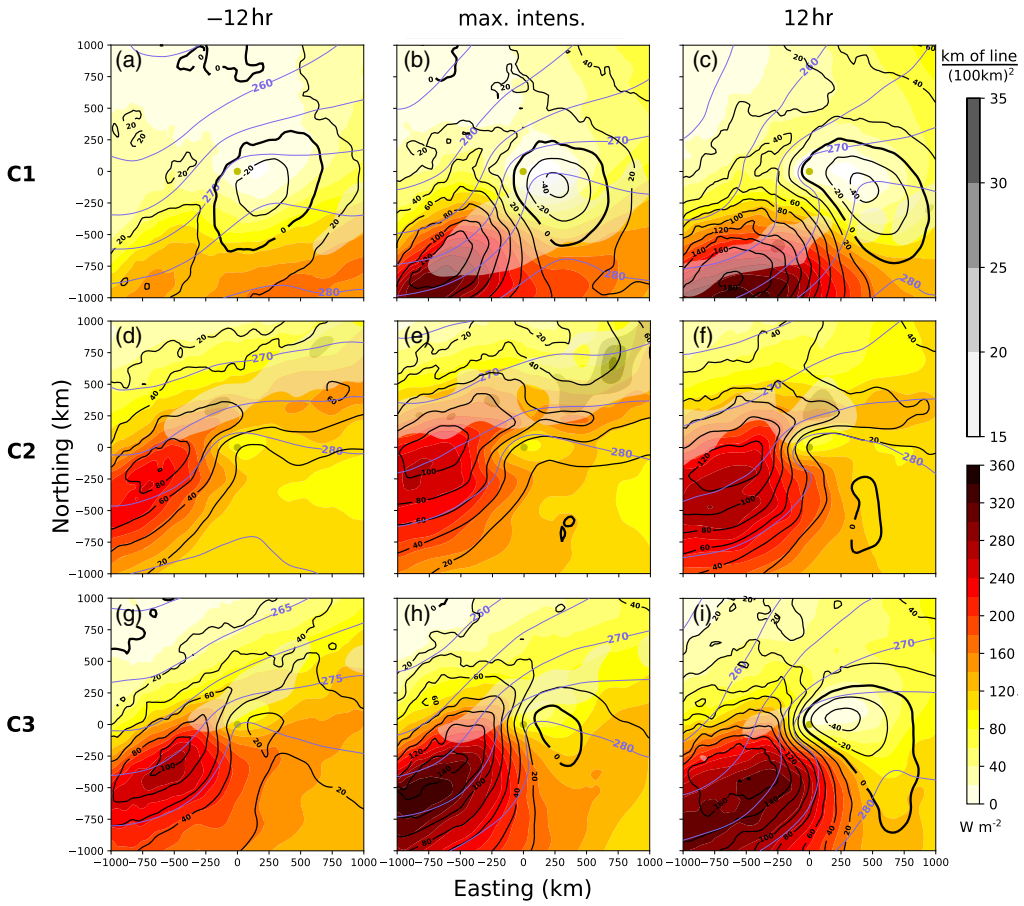

FIGURE 6 As Figure 5, but showing evolution of cyclone-centred latent heat fluxes (yellow-red shading, $W \cdot m^{-2}$), sensible heat fluxes (black contours with interval 20 $W \cdot m^{-2}$, with thick line for zero), and temperature at 850 hPa (purple contours with interval 5 K). Here, SST front density is shown as grey shading

those in C1 and C3 (Figure 5). The surface upward heat fluxes slightly increase with time (Figure 6e,f), but only weak downward sensible heat fluxes appear 12 hr after maximum intensification (Figure 6f). This is due to both the warm airstream not crossing the SST front (Figure 6f) and the tongue of warm air wrapped around the cyclone centre being less pronounced for C2 than for C1 and C3.

3.4 | Cyclone-relative moisture and precipitation composites

C2 is characterised by higher values of TCWV, exceeding 30 $kg \cdot m^{-2}$, and stronger moisture transport (Figure 7d–f) than C1 (Figure 7a–c). The increase of TCWV with SST is expected from the Clausius–Clapeyron relation, as cyclones in C2 propagate towards the warm and moist side of the SST front. The maximum values of TCWV for C2 occur 12 hr before maximum intensification (Figure 7d). Thereafter, the values slightly decrease with time as the cyclones propagate to the northeast towards lower SSTs. Nonetheless, TCWV remains relatively high (>27 $kg \cdot m^{-2}$) throughout the evolution as the cyclones remain on the warm side of the SST front (Figure 7e,f).

In contrast, cyclones of C1 remain on the cold side of the SST front, propagate over lower SSTs (Figure 7a–c) and are thus associated with lower TCWV. However, higher values of TCWV in excess of 27 $kg \cdot m^{-2}$ appear during maximum intensification (Figure 7b) compared to 12 hr before (Figure 7a), located approximately 750 km to the south of the cyclone centre. We associate the maximum values

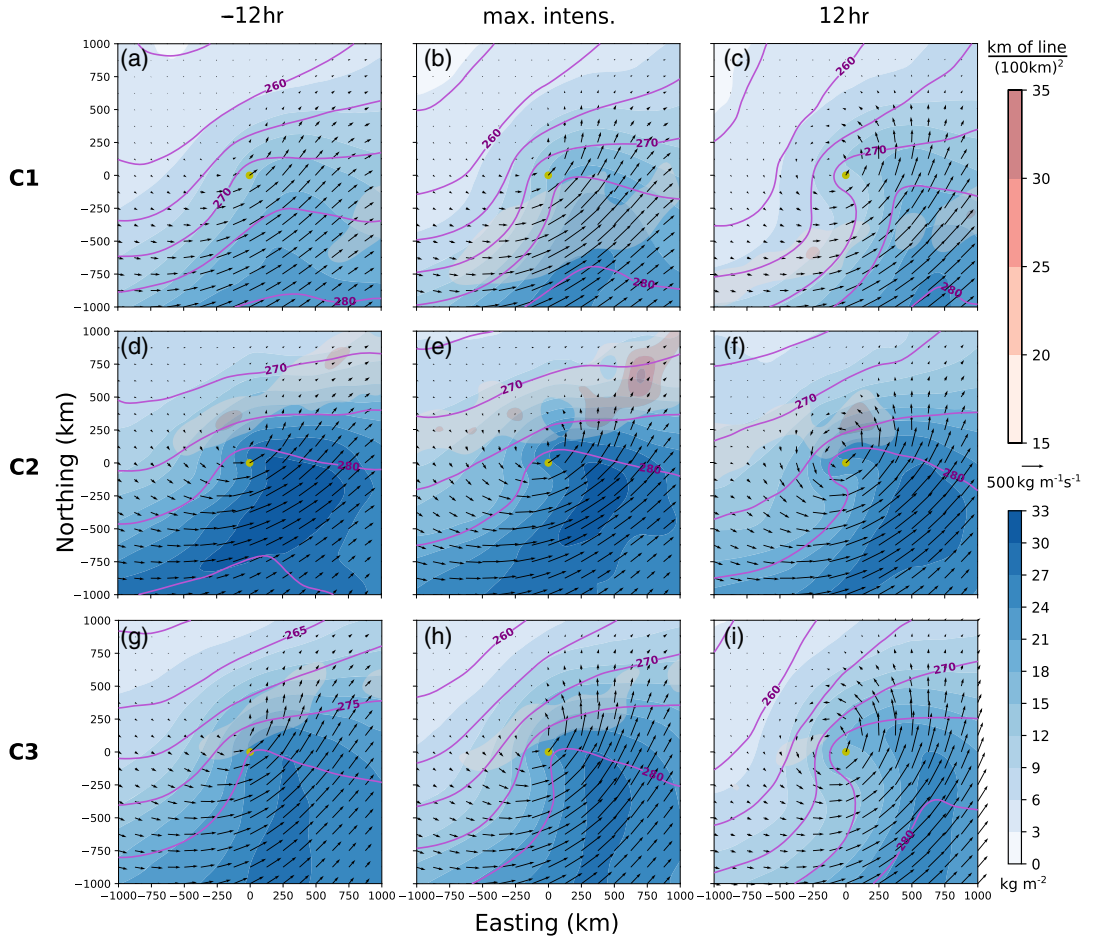

FIGURE 7 As Figure 5, but showing evolution of cyclone-centred total column water vapour (blue shading, kg·m^{-2}), integrated water vapour flux (black vectors), and temperature at 850 hPa (purple contours with interval 5 K). Here, SST front density is shown as pink shading

of TCWV, during the maximum intensification with the smaller distance between the cyclones and the SST front (Figure 3a), which enables moisture uptake from the warm side of the SST front.

For both C1 and C2, the moisture transport increases in the 12 hrs before the time of maximum intensification (Figure 7a,b,d,e). At the time of maximum intensification, the transport peaks around 400–500 km to the south-southeast of the cyclone core (Figure 7b,e). At 12 hr after maximum intensification, the strong moisture transport persists, but occurs at a greater distance, approximately 600 km southeast of the cyclone centre (Figure 7c,f). The cyclonic wrap-up of the warm sector is also evident in TCWV as well as the moisture transport for both C1 and C2, though more distinctly for C2 (Figure 7f).

Both C1 and C2 are characterised by similar average large-scale precipitation. For C1, large-scale precipitation increases gradually throughout the cyclone evolution (Figure 8a–c). For C2, large-scale precipitation rate is generally higher (Figure 8d–f) than for C1 (Figure 8a–c), however the average large-scale precipitation rate is similar to C1, despite the higher availability of moisture (compare Figure 7d–f with Figure 7a–c). Based on the 925 hPa wind speeds for the two categories, we conclude that the cyclones of the two categories are rather similar, in terms of intensity. Surprisingly though, they result in the same amount of precipitation, which could be due to the isentropic ascent of the baroclinic moisture flux that leads to higher precipitation (McTaggart-Cowan *et al.*, 2017). Based on the larger temperature gradient in C1

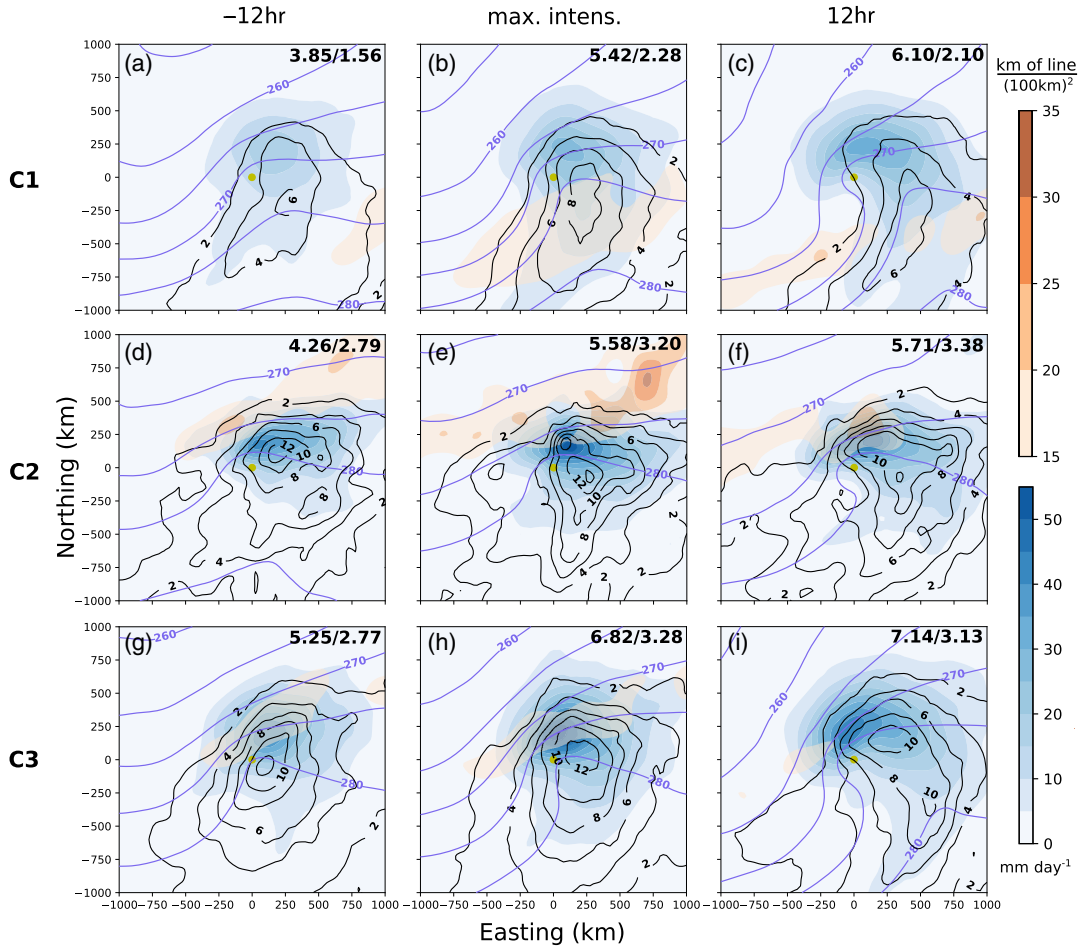

FIGURE 8 As Figure 5, but showing evolution of cyclone-centred large-scale precipitation rate (blue shading, mm·day^{-1}), convective precipitation rate (black contours, mm·day^{-1}), and temperature at 850 hPa (purple contours with interval 5 K). Here, SST front density is shown as orange shading. Numbers in the top right of each panel represent the average large-scale/convective precipitation rate in the composite domain in mm·day^{-1}

(Figure 5a–c) than in C2 (Figure 5d–f), we hypothesise that the increased isentropic upglide in C1 indeed results in more precipitation compared to the sole contributions of cyclone intensity and moisture availability, as described in Pfahl *et al.* (2015).

Conversely, the convective precipitation for C2 is higher (Figure 8d–f) than for C1 (Figure 8a–c), due to higher TCWV (Figure 7d–f) and higher SSTs (compare Figure 5d-f with Figure 5a–c). For both C1 and C2, the highest convective precipitation rate coincides with the time of maximum intensification (Figure 8b,e), exceeding 14 mm·day^{-1} for C2. A maximum of convective precipitation is observed during maximum intensification for C1, when cyclones are typically closer to the SST front (Figure 3a) and thus reside in a region with higher SSTs (Figure 5b) and moisture (Figure 7b) than 12 hr previously and subsequently (Figure 5a,c). For C2, the cyclones always stay on the warm and moist side of the SST front and thus it is the increase in intensity that increases convective precipitation.

Structurally, precipitation occurs in a relatively broad region tracing the cyclone's cold front in C1, whereas it is more confined within the cyclone core in C2 (Figure 8a–f). These structural differences of the cyclone are in line with the findings of Pfahl *et al.* (2015), who compared the structure of cyclones in warmer and colder climates. Therefore,

the difference in the spatial distribution of precipitation most likely arises due to the higher SST in C2 (Figure 5f) than in C1 (Figure 5c).

The decrease of TCWV with time in C3 is consistent with the gradual propagation of cyclones over lower SSTs. Maximum values of TCWV exceed 27 $kg \cdot m^{-2}$ up to the time of maximum intensification and are located to the southeast of the cyclone core within the cyclone's warm sector (Figure 7g,h). They decrease slightly until 12 hr after maximum intensification when cyclones propagate towards the cold side of the SST front (Figure 7i). This evolution and location of the maximum values of TCWV is similar to C1 and C2 (Figure 7b,e). However, the maximum values of TCWV are observed in a south–north direction and not from the southwest to the northeast as in C1 and C2. Consistent with the TCWV, the largest moisture transport also occurs to the southeast of the cyclone core and has again a more meridional component, contrary to C1 and C2, where the transport is oriented from the southwest to the northeast.

Similar to C2, the strongest convective precipitation in C3 occurs during maximum intensification (Figure 8h). At this point in time, cyclones in C3 are propagating over regions of higher SSTs and, based on the higher wind speed (Figure 5g,h), are stronger than at 12 hr prior to maximum intensification. At 12 hr after maximum intensification, convective precipitation is reduced, in line with the cyclones propagating over lower SSTs (Figure 5i) compared to 12 hr before (Figure 5h). Thus, more rapidly intensifying cyclones propagating over regions with higher SSTs are associated with higher convective precipitation.

Cyclones in C3 are associated with the highest average large-scale precipitation (Figure 8g–i) rate among the three categories, with the maximum average large-scale precipitation rate of 7.14 $mm \cdot day^{-1}$ occurring 12 hr after maximum intensification. The distribution of large-scale precipitation in C3 (Figure 8g–i) is similar to C1 (Figure 8a–c), affecting a broader area around the cyclone core, which is different from the locally confined distribution in C2 (Figure 8d–f). The fact that cyclones in C1 and C3 propagate over regions with lower SSTs (Figure 6c,i) than in C2 (Figure 6f) during this later stage of development further supports the connection between the SST and the spatial distribution of precipitation. The observation that C3 features the highest precipitation is also consistent with the higher intensification (Figures 3b and 8i), high wind speed (Figure 5i), and stronger surface heat fluxes (Figure 6i) than in the other categories.

Contrary to C1 and C2, the maximum of large-scale precipitation for C3 at 12 hr after maximum intensification is located to the north-northwest of the cyclone core (Figure 8i), which is consistent with the more wrapped-up structure of the cyclones in C3 than in C1 and C2 (compare Figures 6c,f,i). This structure indicates a faster development of cyclones in C3, consistent with cyclones reaching their maximum intensity sooner after their maximum intensification than in the other categories (Figure 4a–c). Given that all cyclones passed their time of maximum intensification, it is likely that they feature an occlusion, which is commonly associated with a maximum in precipitation (Sanders, 1986; Martin, 1998). The more rapid wrap-up and occlusion process in C3 than in C1 and C2 explains the increased precipitation.

Overall, the features in large-scale precipitation for C3 can be seen as a combination of C1 and C2. For C1, we concluded that the larger temperature gradient than in C2 mainly explains the increased precipitation, whereas for C2 it is mainly the higher values of TCWV that contribute to the increased precipitation. With both cyclone strength and moisture availability resulting in increased large-scale precipitation (Pfahl and Sprenger, 2016), it is straightforward that C3 has higher values than C1 and C2 due to the cyclones in C3 being both stronger (Figure 5g–i) and featuring higher TCWV (Figure 7g–i) than C1 and C2.

3.5 | Cyclone-relative geopotential and wind at 300 hPa

Cyclones in C2 evolve at a greater distance from the climatological position of the North Atlantic jet compared to the other categories (Figures 1a and 2b–d). Consistently, cyclones of C2 are associated with the lowest wind speed maximum at 300 hPa during maximum intensification (Figure 9e). The structure in the geopotential field indicates a gradual development of an upper-level trough in the northwest quadrant and a corresponding shift in the position of the wind maximum to the south (Figure 9d–f).

Compared to C2, cyclones of C1 and C3 propagate at a smaller distance from the North Atlantic jet (Figures 1a and 2b,d). Consequently, the isohypses are distributed tighter than in C2 (Figure 9a–c,g–i) and feature a jet streak of 50–60 $m \cdot s^{-1}$ to the southwest of the cyclone centre. While all categories are associated with a trough at 300 hPa, this trough is much more pronounced in C1 and C3 than in C2 (Figure 9).

Cyclones in C1 are associated with the strongest jet and most pronounced upper-level trough among the three categories, with cyclones being located near the left exit of the jet (Figure 9a–c), a position favourable for the increase of large-scale precipitation via forced ascent (e.g., Johnson and Daniels, 1954; Brown *et al.*, 1994; Milrad, 2017). The upper-level forcing is thus a plausible explanation for why cyclones in C1 and C2 produce a similar area-averaged precipitation rate (Figure 8a–f), although considerably more moisture is available for C2

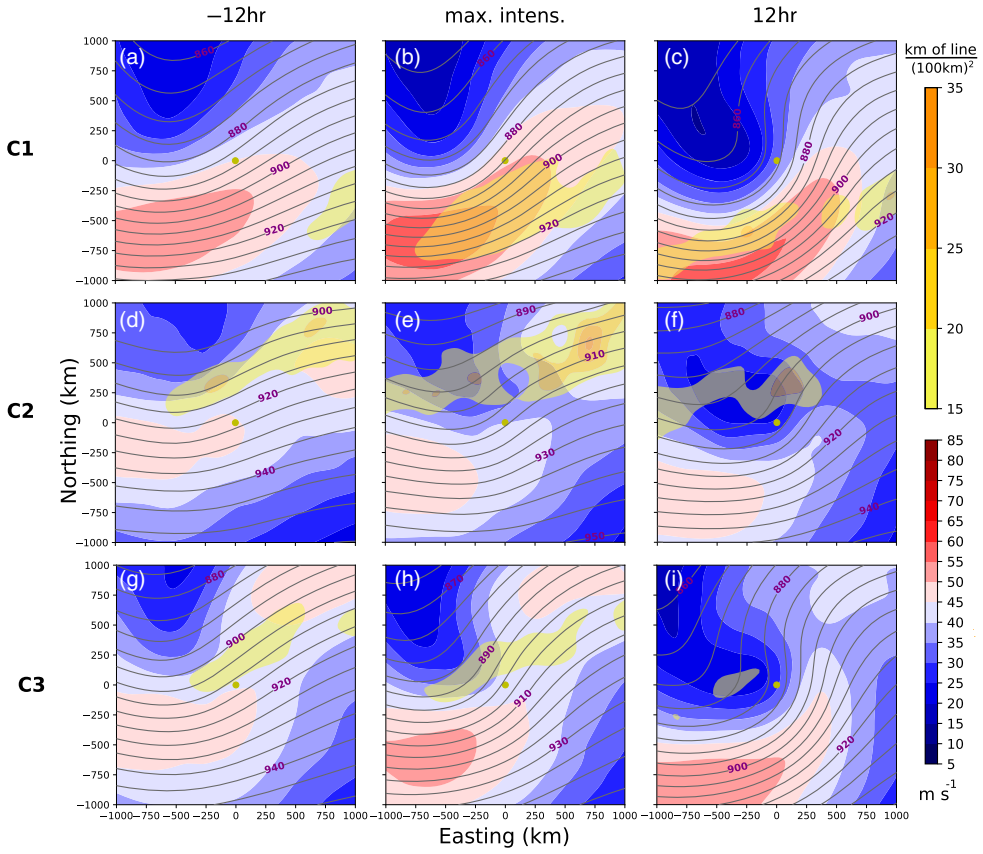

FIGURE 9 As Figure 5, but showing evolution of cyclone-centred SST front density (yellow shading, in 10^{-5}km^{-1}), wind speed at 300 hPa (blue-red shading, m·s^{-1}) and geopotential height at 300 hPa (grey contours with interval 5 gpdm). Here, SST front density is shown as yellow shading

(Figure 7a–f). We thus confirm the previously highlighted (e.g., Uccellini, 1990; Riviere and Joly, 2006; Milrad, 2017) contribution of the upper-level forcing to cyclone intensification and increased average large-scale precipitation rate for cyclones in C1. The average large-scale precipitation rate in C2 can be related to the higher moisture availability, in line with previous studies (e.g., Field and Wood, 2007; Pfahl and Sprenger, 2016).

4 | DISCUSSION AND CONCLUDING REMARKS

We classified cyclones in the Gulf Stream region with respect to their propagation relative to the SST front, which we detected automatically using an established algorithm that was originally developed to identify atmospheric front lines. We considered cyclones which stay either on the cold (C1) or warm (C2) side of the SST front, and those crossing the SST front from the warm to the cold side (C3). A high density of cyclone tracks associated with the North Atlantic storm track (Figure 2a) coincides with the region of the highest SST front density (Figure 1a). To compare the characteristics of cyclones following different tracks relative to the SST front, we performed a composite analysis around the time of maximum intensification. We use composites to analyse the respective roles of the SST front, the land–sea contrast, and the upper-level forcing on cyclone development.

Cyclones in C1 and C3 intensify more rapidly than cyclones in C2 (Figure 3b). Cyclones in C1 and C3 frequently form over land (Figure 2b–d) and propagate closer to the continent during their evolution than cyclones in C2 (Figure 5). Thus, they commonly include continental

air masses in their cold sector (Figure 5a,g). The continental air mass provides additional baroclinicity which is conducive for cyclone intensification. Cyclones in C1 propagate closer to the land, yet at a greater distance from the SST front than cyclones in C3. However, for most of the evolution, low-level baroclinicity is lower around C3 cyclones than around C1 cyclones. This comparison between C1 and C3 suggests that the role of the SST front is secondary compared to that of the land–sea contrast for the low-level baroclinicity. Nevertheless, cyclones of C3 deepen most rapidly on average and feature the highest fraction of explosive cyclones. Based on the rather similar orientation of the upper-level wave in C1 and C3, we relate the more rapid intensification for cyclones in C3 to the increased latent heat release within the cyclones' warm conveyor belt, as cyclones in C3 are associated with the highest average large-scale precipitation rate among the three categories (Figure 8).

Contrary to cyclones of C1 and C3, cyclones of C2 remain distant from both the SST front and the continent (Figures 2c and 5d–f) resulting in a less pronounced temperature gradient across the cyclone. In addition, C2 cyclones are typically furthest away from the upper-level jet and associated with the least pronounced trough. They thus receive considerably less upper-level forcing than C1 and C3 cyclones, which both develop in the left exit region of a pronounced jet.

Cyclones for all categories reach their maximum surface heat fluxes 12 hr after their maximum intensification (Figure 6c,f,i), the time when they tend to reach their maximum intensity. Cyclones of C1 and C3 are associated with a pronounced dipole structure in the sensible heat flux, with positive (negative) values to the west (east) of the cyclone core, which is absent for cyclones of C2 (Figure 6a–c,h,i). This dipole structure is detrimental to cyclone intensification as it reduces baroclinicity and thus available potential energy in the cyclone. However, cyclones of C1 and C3 are still associated with a higher intensification than cyclones in C2 (Figure 3b). Thus, the intensification of cyclones is not directly associated with the surface heat fluxes. Instead, the strength of the surfaces fluxes is closely tied to the different pathways of the cyclones and in particular the proximity to the SST front and the cold continent.

We find convective precipitation to be closely related to the SSTs under the cyclone. For example, convective precipitation is strongest for C2, in which the cyclones propagate over the highest SSTs (Figure 5d–f). Further, for C3, convective precipitation evolves parallel to the SSTs. Before maximum intensification (Figure 8d,e,g,h), SSTs and convective precipitation are both most intense, and both decrease in tandem with the cyclone crossing the SST fronts. As this relation between SSTs and convective precipitation holds for all our categories, we conclude that convective precipitation is strongly modulated by the absolute SST, independent of whether or not the cyclones cross the SST front.

Strongest average large-scale precipitation is associated with cyclones in C3. Cyclones in this category are the most intense as measured by 925 hPa wind speeds, and have available nearly as much moisture as cyclones in C2. However, the average large-scale precipitation for C1 and C2 are rather similar, despite the larger moisture availability in C2 (Figure 8a–f). Thus, C2 seems to be less efficient than C1 in making use of the available moisture. We identified two likely reasons for this reduced efficiency. First, cyclones in C1 intensify more due to considerably stronger upper-level forcing than in C2. Second, temperature gradients across C2 cyclones are smaller than across C1 cyclones, which implies a reduced isentropic upglide. We consequently hypothesize that low-level baroclinicity might be an additional factor determining precipitation intensity, in addition to moisture availability and cyclone intensity as documented by Pfahl and Sprenger (2016). Our hypothesis is supported by McTaggart-Cowan *et al.* (2017) who document that the strongest precipitation in a cyclone is co-located with the strongest moist isentropic upglide.

Overall, we identified that the land–sea contrast has a clear influence on cyclone intensification in the Gulf Stream region for cyclones staying to the north of the SST front (C1) through increased low-level baroclinicity. For cyclones crossing the SST front from the warm to the cold side (C3), low-level baroclinicity is slightly weaker than in C1, but is nevertheless attributable to both the land–sea contrast and the SST front. Furthermore, both C1 and C3 are associated with stronger upper-level forcing, which contributes to cyclone intensification in addition to the low-level baroclinicity. However, given the specific geographic features of the western North Atlantic, a generalisation of our results to SST fronts associated with other western boundary currents is not straightforward. Therefore, a similar study should be conducted for the Kuroshio Extension region. The cold continental air masses in the West Pacific are located further away from the SST front than in the Gulf Stream region. This would allow us to further assess the relative role of the land–sea contrast and the SST front for cyclone intensification in these two regions with the strongest western boundary currents in the Northern Hemisphere.

ORCID

Leonidas Tsopouridis https://orcid.org/0000-0002-2043-0871
Clemens Spensberger https://orcid.org/0000-0002-9649-6957
Thomas Spengler https://orcid.org/0000-0002-1747-6385

REFERENCES

Allen, J.T., Pezza, A.B. and Black, M.T. (2010) Explosive cyclogenesis: A global climatology comparing multiple reanalyses. *Journal of Climate*, 23, 6468–6484.

Berry, G., Reeder, M.J. and Jakob, C. (2011) A global climatology of atmospheric fronts. *Geophysical Research Letters*, 38, L04809.

Booth, J.F., Naud, C.M. and Willison, J. (2018) Evaluation of extratropical cyclone precipitation in the North Atlantic basin: An analysis of ERA-Interim, WRF, and two CMIP5 models. *Journal of Climate*, 31, 2345–2360.

Booth, J.F., Thompson, L., Patoux, J. and Kelly, K.A. (2012) Sensitivity of midlatitude storm intensification to perturbations in the sea surface temperature near the Gulf Stream. *Monthly Weather Review*, 140, 1241–1256.

Brayshaw, D.J., Hoskins, B.J. and Blackburn, M. (2009) The basic ingredients of the North Atlantic storm track. Part I: Land–sea contrast and orography. *Journal of the Atmospheric Sciences*, 66, 2539–2558.

Brown, R.H., Baker, D.J. and Friday, E.W. (1994) *The Great Flood of 1993*. Natural disaster survey report, NOAA National Weather Service, Silver Spring, MD.

Businger, S., Graziano, T.M., Kaplan, M.L. and Rozumalski, R.A. (2005) Cold-air cyclogenesis along the Gulf Stream front: Investigation of diabatic impacts on cyclone development, frontal structure, and track. *Meteorology and Atmospheric Physics*, 88, 65–90.

Catto, J. (2016) Extratropical cyclone classification and its use in climate studies. *Reviews of Geophysics*, 54, 486–520.

Cione, J.J., Raman, S. and Pietrafesa, L.J. (1993) The effect of Gulf Stream-induced baroclinicity on U.S. East Coast winter cyclones. *Monthly Weather Review*, 121, 421–430.

Dacre, H.F., Josey, S.A. and Grant, A.L. (2020) Extratropical cyclone induced sea surface temperature anomalies in the 2013/14 winter. *Weather and Climate Dynamics*, 1, 27–44.

de Vries, H., Scher, S., Haarsma, R., Drijfhout, S. and Van Delden, A. (2019) How Gulf Stream SST-fronts influence Atlantic winter storms. *Climate Dynamics*, 52, 5899–5909.

Dee, D.P., Uppala, S.M., Simmons, A.J., Berrisford, P., Poli, P., Kobayashi, S., Andrae, U., Balmaseda, M.A., Balsamo, G., Bauer, P., Bechtold, P., Beljaars, A.C.M., van de Bergd, L., Bidlot, J., Bormann, N., Delsol, C., Dragani, R., Fuentes, M., Geer, A.J., Haimberger, L., Healy, S.B., Hersbach, H., Holm, E.V., Isaksen, L., Kållberg, P., Köhler, M., Matricardi, M., McNally, A.P., Monge-Sanz, B.M., Morcrette, J.-J., Park, B.-K., Peubey, C., de Rosnay, P., Tavolato, C., Thépaut, J.-N. and Vitart, F. (2011) The ERA-Interim reanalysis: configuration and performance of the data assimilation system. *Quarterly Journal of the Royal Meteorological Society*, 137, 553–587.

Evans, M.S., Keyser, D., Bosart, L.F. and Lackmann, G.M. (1994) A satellite-derived classification scheme for rapid maritime cyclogenesis. *Monthly Weather Review*, 122, 1381–1416.

Field, P.R. and Wood, R. (2007) Precipitation and cloud structure in midlatitude cyclones. *Journal of Climate*, 20, 233–254.

Hanley, J. and Caballero, R. (2012) The role of large-scale atmospheric flow and Rossby wave breaking in the evolution of extreme windstorms over Europe. *Geophysical Research Letters*, 39(21). https://doi.org/10.1029/2012GL053408.

Hawcroft, M.K., Shaffrey, L.C., Hodges, K.I. and Dacre, H.F. (2012) How much Northern Hemisphere precipitation is associated with extratropical cyclones?. *Geophysical Research Letters*, 39(24). https://doi.org/10.1029/2012GL053866.

Hewson, T.D. (1998) Objective fronts. *Meteorological Applications*, 5, 37–65.

Hodges, K.I., Lee, R.W. and Bengtsson, L. (2011) A comparison of extratropical cyclones in recent reanalyses ERA-Interim, NASA MERRA, NCEP CFSR, and JRA-25. *Journal of Climate*, 24, 4888–4906.

Hoskins, B.J. and Hodges, K.I. (2002) New perspectives on the Northern Hemisphere winter storm tracks. *Journal of the Atmospheric Sciences*, 59, 1041–1061.

Hotta, D. and Nakamura, H. (2011) On the significance of sensible heat supply from the ocean in the maintenance of mean baroclinicity along storm tracks. *Journal of Climate*, 24, 3377–3401.

Inatsu, M., Mukougawa, H. and Xie, S.-P. (2000) Formation of subtropical westerly jet core in an idealized GCM without mountains. *Geophysical Research Letters*, 27, 529–532.

Inatsu, M., Mukougawa, H. and Xie, S.-P. (2003) Atmospheric response to zonal variations in midlatitude SST: Transient and stationary eddies and their feedback. *Journal of Climate*, 16, 3314–3329.

Jacobs, N., Raman, S., Lackmann, G. and Childs, P.Jr. (2008) The influence of the Gulf Stream induced SST gradients on the US East Coast winter storm of 24–25 January 2000. *International Journal of Remote Sensing*, 29, 6145–6174.

Jenkner, J., Sprenger, M., Schwenk, I., Schwierz, C., Dierer, S. and Leuenberger, D. (2010) Detection and climatology of fronts in a high-resolution model reanalysis over the Alps. *Meteorological Applications*, 17, 1–18.

Johnson, D. and Daniels, S. (1954) Rainfall in relation to the jet stream. *Quarterly Journal of the Royal Meteorological Society*, 80, 212–217.

Kuo, Y.-H., Shapiro, M.A. and Donall, E.G. (1991) The interaction between baroclinic and diabatic processes in a numerical simulation of a rapidly intensifying extratropical marine cyclone. *Monthly Weather Review*, 119, 368–384.

Lee, T. and Cornillon, P. (1996) Propagation and growth of Gulf Stream meanders between 75° and 45°W. *Journal of Physical Oceanography*, 26, 225–241.

Lim, E.-P. and Simmonds, I. (2002) Explosive cyclone development in the Southern Hemisphere and a comparison with Northern Hemisphere events. *Monthly Weather Review*, 130, 2188–2209.

Manobianco, J. (1988) *On the observational and numerical aspects of explosive east coast cyclogenesis*. Report No. 88-7, Department of Meteorology, Florida State University, Tallahassee, FL.

Manobianco, J. (1989) Explosive East Coast cyclogenesis over the west-central North Atlantic Ocean: A composite study derived from ECMWF operational analyses. *Monthly Weather Review*, 117, 2365–2383.

Martin, J.E. (1998) The structure and evolution of a continental winter cyclone. Part II: Frontal forcing of an extreme snow event. *Monthly Weather Review*, 126, 329–348.

McTaggart-Cowan, R., Gyakum, J.R. and Moore, R.W. (2017) The baroclinic moisture flux. *Monthly Weather Review*, 145, 25–47.

Meinen, C.S. and Luther, D.S. (2016) Structure, transport, and vertical coherence of the Gulf Stream from the Straits of Florida to the southeast Newfoundland Ridge. *Deep-Sea Research Part I: Oceanographic Research Papers*, 112, 137–154.

Michel, C., Terpstra, A. and Spengler, T. (2018) Polar mesoscale cyclone climatology for the Nordic Seas based on ERA-Interim. *Journal of Climate*, 31, 2511–2532.

Milrad, S. (2017) *Synoptic Analysis and Forecasting: An Introductory Toolkit*. Elsevier, Amsterdam, Netherlands.

Minobe, S., Kuwano-Yoshida, A., Komori, N., Xie, S.-P. and Small, R.J. (2008) Influence of the Gulf Stream on the troposphere. *Nature*, 452, 206–210.

Murray, R.J. and Simmonds, I. (1991a) A numerical scheme for tracking cyclone centres from digital data. Part I: Development and operation of the scheme. *Australian Meteorological Magazine*, 39, 155–166.

Murray, R.J. and Simmonds, I. (1991b) A numerical scheme for tracking cyclone centres from digital data. Part II: Application to January and July general circulation model simulations. *Australian Meteorological Magazine*, 39, 167–180.

Nakamura, H., Sampe, T., Tanimoto, Y. and Shimpo, A. (2004) Observed associations among storm tracks, jet streams and midlatitude oceanic fronts. *Geophysical Monograph Series*, 147, 329–345.

Neu, U., Akperov, M.G., Bellenbaum, N., Benestad, R., Blender, R., Caballero, R., Cocozza, A., Dacre, H.F., Feng, Y., Fraedrich, K., Grieger, J., Gulev, S., Hanley, J., Hewson, T., Inatsu, M., Keay, K., Kew, S.F., Kindem, I., Leckebusch, G.C., Liberato, M.L.R., Lionello, P., Mokhov, I.I., Pinto, J.G., Raible, C.C., Reale, M., Rudeva, I., Schuster, M., Simmonds, I., Sinclair, M., Sprenger, M., Tilinina, N.D., Trigo, I.F., Ulbrich, S., Ulbrich, U., Wang, X.L. and Wernli, H. (2013) IMILAST: A community effort to intercompare extratropical cyclone detection and tracking algorithms. *Bulletin of the American Meteorological Society*, 94, 529–547.

Ogawa, F. and Spengler, T. (2019) Prevailing surface wind direction during air–sea heat exchange. *Journal of Climate*, 32, 5601–5617.

Oruba, L., Lapeyre, G. and Rivière, G. (2013) On the poleward motion of midlatitude cyclones in a baroclinic meandering jet. *Journal of the Atmospheric Sciences*, 70, 2629–2649.

Papritz, L. and Spengler, T. (2015) Analysis of the slope of isentropic surfaces and its tendencies over the North Atlantic. *Quarterly Journal of the Royal Meteorological Society*, 141, 3226–3238.

Parfitt, R., Czaja, A., Minobe, S. and Kuwano-Yoshida, A. (2016) The atmospheric frontal response to SST perturbations in the Gulf Stream region. *Geophysical Research Letters*, 43, 2299–2306.

Pfahl, S., O'Gorman, P.A. and Singh, M.S. (2015) Extratropical cyclones in idealized simulations of changed climates. *Journal of Climate*, 28, 9373–9392.

Pfahl, S. and Sprenger, M. (2016) On the relationship between extratropical cyclone precipitation and intensity. *Geophysical Research Letters*, 43, 1752–1758.

Reed, R.J., Grell, G.A. and Kuo, Y.-H. (1993) The ERICA IOP 5 storm. Part I: analysis and simulation. *Monthly Weather Review*, 121, 1577–1594.

Renard, R.J. and Clarke, L.C. (1965) Experiments in numerical objective frontal analysis. *Monthly Weather Review*, 93, 547–556.

Ritchie, E.A. and Elsberry, R.L. (2003) Simulations of the extratropical transition of tropical cyclones: Contributions by the midlatitude upper-level trough to reintensification. *Monthly Weather Review*, 131, 2112–2128.

Riviere, G. and Joly, A. (2006) Role of the low-frequency deformation field on the explosive growth of extratropical cyclones at the jet exit. Part II: Baroclinic critical region. *Journal of the Atmospheric Sciences*, 63, 1982–1995.

Roebber, P.J. (1989) The role of surface heat and moisture fluxes associated with large-scale ocean current meanders in maritime cyclogenesis. *Monthly Weather Review*, 117, 1676–1694.

Rogers, E. and Bosart, L.F. (1991) A diagnostic study of two intense oceanic cyclones. *Monthly Weather Review*, 119, 965–996.

Rudeva, I. and Gulev, S.K. (2011) Composite analysis of North Atlantic extratropical cyclones in NCEP–NCAR reanalysis data. *Monthly Weather Review*, 139, 1419–1446.

Sanders, F. (1986) Explosive cyclogenesis in the west-central North Atlantic Ocean, 1981–84. Part I: Composite structure and mean behavior. *Monthly Weather Review*, 114, 1781–1794.

Sanders, F. and Gyakum, J.R. (1980) Synoptic-dynamic climatology of the "bomb". *Monthly Weather Review*, 108, 1589–1606.

Schemm, S., Rudeva, I. and Simmonds, I. (2015) Extratropical fronts in the lower troposphere – global perspectives obtained from two automated methods. *Quarterly Journal of the Royal Meteorological Society*, 141, 1686–1698.

Schultz, D.M., Keyser, D. and Bosart, L.F. (1998) The effect of large-scale flow on low-level frontal structure and evolution in midlatitude cyclones. *Monthly Weather Review*, 126, 1767–1791.

Sinclair, M.R. and Revell, M.J. (2000) Classification and composite diagnosis of extratropical cyclogenesis events in the southwest Pacific. *Monthly Weather Review*, 128, 1089–1105.

Spensberger, C., Spengler, T. and Li, C. (2017) Upper-tropospheric jet axis detection and application to the boreal winter 2013/14. *Monthly Weather Review*, 145, 2363–2374.

Thompson, K., Loucks, R. and Trites, R. (1988) Sea surface temperature variability in the shelf-slope region of the Northwest Atlantic. *Atmosphere Ocean*, 26, 282–299.

Tomczak, M. and Godfrey, J. (2003) *Regional Oceanography: An Introduction*. Elsevier Science, Oxford, UK.

Uccellini, L.W. (1990) Processes contributing to the rapid development of extratropical cyclones, pp. 81–105 in Extratropical Cyclones. Springer, Berlin.

Uccellini, L.W., Kocin, P.J., Petersen, R.A., Wash, C.H. and Brill, K.F. (1984) The Presidents' Day cyclone of 18–19 February 1979: Synoptic overview and analysis of the subtropical jet streak influencing the pre-cyclogenetic period. *Monthly Weather Review*, 112, 31–55.

Vannière, B., Czaja, A. and Dacre, H.F. (2017a) Contribution of the cold sector of extratropical cyclones to mean state features over the Gulf Stream in winter. *Quarterly Journal of the Royal Meteorological Society*, 143, 1990–2000.

Vannière, B., Czaja, A., Dacre, H.F. and Woollings, T. (2017b) A "Cold Path" for the Gulf Stream–troposphere connection. *Journal of Climate*, 30, 1363–1379.

Wang, C.-C. and Rogers, J.C. (2001) A composite study of explosive cyclogenesis in different sectors of the North Atlantic. Part I: Cyclone structure and evolution. *Monthly Weather Review*, 129, 1481–1499.

Weijenborg, C. and Spengler, T. (2020) Diabatic heating as a pathway for cyclone clustering encompassing the extreme storm *Dagmar*. *Geophysical Research Letters*, 47(8). https://doi.org/10.1029/2019GL085777.

Whitaker, J.S. and Davis, C.A. (1994) Cyclogenesis in a saturated environment. *Journal of the Atmospheric Sciences*, 51, 889–908.

Zolina, O. and Gulev, S.K. (2003) Synoptic variability of ocean–atmosphere turbulent fluxes associated with atmospheric cyclones. *Journal of Climate*, 16, 2717–2734.

How to cite this article: Tsopouridis L, Spensberger C, Spengler T. Characteristics of cyclones following different pathways in the Gulf Stream region. *Q.J.R. Meteorol. Soc*. 2020;1–16. https://doi.org/10.1002/qj.3924

APPENDIX

Namelists used when running the cyclone detection and tracking algorithm

TABLE A1 Values of the parameters for the detection and tracking namelists used by the algorithm (Murray and Simmonds, 1991a; 1991b; Michel *et al.*, 2018)

Cyclone detection					
ni, nj	301	drmx1	0.7	fccmn	0.0
rproj	150	drmx2	0.3	cvarad	1.25
rdiff	2.0	itmx1, itmx2	10	nrrdir	18
rdifz	2.0	diflt1, diflt2	2.0	rdincr	0.25
iopmxc	1	cmnh, cmnc	0.0	sphtrg	.false.
istmxc	11	cmnc1	0.5	rdpgrd	5.0
nshell	12	cmnc2	1.3	npgdir	12
mscrn	2	dpmn	0.1	ftopeq	0.005
sdrmx	10	zsmax	1000	cmncw	2.0
Tracking					
irevmx	400	refdt	0.25	qmxnew	0.75
wsteer	0.6	wpten	0.3	qmxopn	0.75
fsteer	2.0	wmotn	1.0	qmxwek	0.5
asteer	0.5	rcprob	12.0	rpbell	0.5

Paper II

Cyclone Intensification in the Kuroshio Region and its relation to the Sea Surface Temperature Front and Upper-Level Forcing

Tsopouridis L, Spensberger C, Spengler T.
Quarterly Journal of the Royal Meteorological Society, 1-16, (2020)
https://doi.org/10.1002/qj.3929

Received: 15 May 2020 | Revised: 5 August 2020 | Accepted: 30 September 2020

DOI: 10.1002/qj.3929

Quarterly Journal of the Royal Meteorological Society RMetS

RESEARCH ARTICLE

Cyclone intensification in the Kuroshio region and its relation to the sea surface temperature front and upper-level forcing

Leonidas Tsopouridis | Clemens Spensberger | Thomas Spengler

Geophysical Institute, University of Bergen, and Bjerknes Centre for Climate Research, Bergen, Norway

Correspondence
L. Tsopouridis, Geophysical Institute, University of Bergen, Bergen, Norway.
Email: leonidas.tsopouridis@uib.no

Funding information
Research Council of Norway (RCN) 262220

Abstract

The Northwest Pacific features strong sea surface temperature (SST) gradients providing favourable conditions for wintertime cyclone intensification in the midlatitudes. To estimate the relative contribution of the SST front to the evolution of cyclones and identify the mechanisms for cyclone intensification, we track individual cyclones and categorise them depending on their propagation relative to the SST front. We focus on cyclones remaining on either the cold or warm side of the SST front, as well as those crossing the SST front from the warm to the cold side. Cyclones crossing the SST front or remaining on its warm side propagate near the left exit region of the jet and are associated with higher precipitation, consistent with higher moisture availability and cyclone intensity. Comparing the different cyclone categories, there is no direct effect of the SST front on cyclone intensification. However, the SST front contributes to the climatological low-level baroclinicity, providing a conducive environment for cyclone intensification for the cyclones crossing the SST front. Compared with the Gulf Stream region, the land–sea contrast plays a less prominent role for the low-level baroclinicity in the Kuroshio region.

KEYWORDS

cyclone intensification, extratropical cyclones, jet stream, Kuroshio Extension, low-level baroclinicity

1 | INTRODUCTION

The Kuroshio and the Gulf Stream are the western boundary currents in the North Pacific and North Atlantic, respectively, and are associated with maxima in midlatitude air–sea heat exchange along the sea surface temperature (SST) front (Ogawa and Spengler, 2019). Both boundary-current regions are areas of frequent cyclogenesis (Hoskins and Hodges, 2002; Nakamura *et al.*, 2004), where a sum of processes favours storm development (Roebber, 1989). Upper-level forcing (e.g., Sanders and Gyakum, 1980; Uccellini *et al.*, 1984; Sinclair and Revell,

2000), low-level baroclinicity (e.g., Sanders, 1986; Wang and Rogers, 2001), and diabatic processes (e.g., Kuo *et al.*, 1991; Fink *et al.*, 2012; Chagnon and Gray, 2015) have been identified as the main mechanisms influencing the development of extratropical cyclones (hereafter cyclones: e.g., Petterssen and Smebye, 1971; Uccellini *et al.*, 1984; Nuss and Anthes, 1987). In this study, we will clarify the role of these mechanisms for cyclone intensification in the Kuroshio region, with a particular focus on the role of the SST front.

While the Kuroshio Extension and the Gulf Stream region have several characteristics in common, there are some important differences. For example, the Kuroshio is located further away from the Asian continent than the Gulf Stream from the North American continent. In addition, the characteristics of the wintertime upper-level jet differ considerably, with the Pacific jet being stronger and more confined meridionally at comparatively lower latitudes than the Atlantic jet (Spensberger and Spengler, 2020). We will clarify the extent to which these differences affect the cyclogenetic forcing in the Kuroshio Extension region.

Low-level temperature gradients, arising from either horizontal differences in the SST or due to the land–sea contrast, increase the low-level baroclinicity and thus facilitate cyclone intensification. Recent studies highlighted the role of the SST front in determining the wintertime low-level baroclinicity along the western boundary currents (e.g., Hotta and Nakamura, 2011; Papritz and Spengler, 2015). Here, the SST gradient both anchors the storm track (Nakamura *et al.*, 2008) and triggers convection and precipitation (Minobe *et al.*, 2008; Parfitt *et al.*, 2016; Vannière *et al.*, 2017). In addition to SST anomalies around the Gulf Stream and Kuroshio SST front, the comparatively cold North American land mass can also affect low-level baroclinicity strongly in winter (Nakamura and Yamane, 2009). Previous studies confirmed that the land–sea contrast contributes considerably to low-level baroclinicity in the Gulf Stream region (e.g., Cione *et al.*, 1993; Inatsu *et al.*, 2000; Wang and Rogers, 2001; Brayshaw *et al.*, 2009; Tsopouridis *et al.*, 2020) and also rapidly developing cyclones over the Northwestern Pacific have been associated with cold continental airmasses (Yoshida and Asuma, 2004).

Yoshida and Asuma (2004), however, also identified the strong and zonal upper tropospheric jet stream as a contributor to cyclogenesis in the Kuroshio region. Indeed, Jacobs *et al.* (2008) attribute up to 74% of the variance in deepening to differences in upper-level forcing. Cyclogenesis is fundamentally linked to the occurrence of jets (e.g., Sanders and Gyakum, 1980; Uccellini *et al.*, 1984; Schultz *et al.*, 1998; Sinclair and Revell, 2000), because the baroclinicity associated with the jet stream provides a source of energy for cyclone intensification (Riviere and Joly, 2006). Rapid intensification of cyclones typically occurs in the left-exit region of jet streams (Uccellini, 1990), which is associated with enhanced upper-level divergence yielding vortex stretching (e.g., Ritchie and Elsberry, 2003; Oruba *et al.*, 2013).

In addition to low-level baroclinicity and upper-level forcing, diabatic heating associated with surface fluxes and latent heat release can contribute to cyclone intensification (e.g., Kuo *et al.*, 1991; Reed *et al.*, 1993; Nakamura *et al.*, 2004). With the Kuroshio Extension region featuring the highest surface heat fluxes in the wider North Pacific region (e.g., Josey *et al.*, 1998; Ogawa and Spengler, 2019), it is not surprising that strong surface heat and moisture fluxes significantly influenced the deepening of a Pacific cyclone that experienced weak upper-level forcing (Reed and Albright, 1986). Using numerical simulations, Kuwano-Yoshida and Asuma (2008) indeed found that latent heat release is important for the rapid intensification of cyclones over the Northwestern Pacific Ocean. Further, Hirata *et al.* (2018) demonstrated that surface fluxes can affect the intensity of an explosive cyclone and its bent-back front. However, the effect of surface fluxes remains small compared with other influences such as latent heat release (Reed *et al.*, 1993).

We perform a synoptic analysis to elucidate the different contributions of the aforementioned mechanisms to cyclone intensification in the Kuroshio region, where we focus on wintertime cyclones with maximum intensification in the Kuroshio Extension region. To evaluate the significance of the SST front on cyclone growth, we categorise these cyclones depending on their trajectories with respect to the SST front. Using these categories, we discuss the respective roles of upper- and lower-level forcing for cyclone intensification. We contrast our results for the Kuroshio Extension region with the Gulf Stream (documented by Tsopouridis *et al.*, 2020, hereafter TSS20), with special emphasis on similarities and differences between these regions.

2 | DATA AND METHODS

2.1 | Data

We use the ERA-Interim reanalysis data with a four-dimensional variational data assimilation scheme and a spectral truncation of T255 and 60 levels in the vertical (Dee *et al.*, 2011). We use fields pre-interpolated onto a $0.5° \times 0.5°$ horizontal grid and 6-hr temporal resolution for the winter period (December–February) from 1979–2016.

For our analysis, we acquired the following data, in line with TSS20: mean sea-level pressure (MSLP),

geopotential height at 300 hPa, sea surface temperature (SST), temperature at 850 hPa, total column water vapour (TCWV), vertically integrated water-vapour flux (IWVF), wind at 925 and 300 hPa, large-scale and convective precipitation, as well as latent and sensible surface heat fluxes. Surface heat fluxes and precipitation data are derived from the twice daily forecasts (initialized at 0000 and 1200 UTC) and are accumulated ±3 hr around the respective timesteps (such as in Ogawa and Spengler, 2019).

2.2 | SST front

We identify the position of SST fronts using an objective frontal detection scheme. The scheme is based on the "thermal" method and has been used to detect atmospheric fronts (Jenkner *et al.*, 2010; Berry *et al.*, 2011; Schemm *et al.*, 2015). Further details are described in TSS20. To capture the most prominent SST fronts in the Kuroshio Extension region, we have chosen an SST gradient threshold of 1.25 K·100 km^{-1}. Our choice is based on a sensitivity analysis where we varied the threshold between 1.0 and 2.0 K·100 km^{-1} in steps of 0.25 K·100 km^{-1}. The chosen threshold is a trade-off between consistently detecting the main SST front, and avoiding too many detections of secondary SST gradient maxima as fronts. TSS20 used a larger threshold (2K·100 km^{-1}) for the Gulf Stream region, consistent with the stronger SST gradient in the Atlantic (e.g., Nakamura *et al.*, 2004). Our climatological SST front position coincides with the region of the maximum SST gradient, as presented in the SST climatologies of Yao *et al.* (2016), Tozuka *et al.* (2018), and Wang *et al.* (2019).

Following Masunaga *et al.* (2015), we divided the full period encompassing 38 winters into two time segments, prior to and after 2002, to assess the potential impact of the change in resolution of the SST in the ERA-Interim data on our results. Although the detected SST fronts are more variable after 2002, the mean position of the SST fronts, the SST distribution, and the propagation of cyclones relative to the SST front remain consistent across the time segments (see Appendix Figure A1). Further, the evolution of cyclone characteristics, assessed by separate composite analyses for the two time segments (not shown), is qualitatively unchanged. Thus, in line with Ogawa and Spengler (2019), we only present the results for the entire period from 1979–2016 (SST front climatology in Figure 1a). The unit of the SST front distributions in Figure 1a is a result of a normalisation to account for variations in the size of a grid cell. We thus sum the total length of all front lines within a given grid cell and divide this quantity by the number of time steps and the size of the grid cell.

2.3 | Jet stream detection

In order to assess the potential impact of upper-level forcing, we diagnose the upper-level flow for the cyclones in our database. This is also motivated by the North Pacific jet occurring most frequently slightly to the south of the Kuroshio Extension region (orange shading in Figure 1a), consistent with previous climatologies (e.g., Riehl *et al.*, 1954; Nakamura, 1992; Jaffe *et al.*, 2011; Spensberger and Spengler, 2020). The presented jet position is based on automatically detected jet axes, following the method and criteria of Spensberger *et al.* (2017) identifying lines separating cyclonic from anticyclonic wind shear on the 2-potential vorticity unit (PVU) surface (where 1 PVU $= 10^{-6}$ m^2·s^{-1}·K·kg^{-1}). The unit of the jet axis distributions is the result of the same normalisation process applied for the SST front distributions, as described in Section 2.2.

2.4 | Cyclone detection and tracking

We utilize the University of Melbourne cyclone detection and tracking algorithm (Murray and Simmonds, 1991a; 1991b). The algorithm detects maxima in the Laplacian of the MSLP field and tracks them over time, employing a nearest-neighbour method together with the most likely direction of propagation (Murray and Simmonds, 1991a; 1991b; Michel *et al.*, 2018, TSS20).

Analogous to the analysis for the Gulf Stream region in TSS20, we apply a number of track selection criteria. We require cyclones to propagate for at least 12 hr (three consecutive time steps) in the Kuroshio Extension region (30–50°N and 145–170°E), henceforth referred to as the "Kuroshio region". The minimum in the evolution of the surface pressure along the track must occur during December–February (DJF) and we only include tracks with maximum intensification, defined as the most rapid decrease in MSLP, in the Kuroshio region. Moreover, we require the great circle distance between cyclogenesis and cyclolysis to be greater than 300 km to remove quasistationary systems.

2.5 | Classification of cyclone tracks based on their position relative to the SST front

We identify the shortest distance between each cyclone position and the SST front for every timestep along the cyclone track and define a vector $\mathbf{r}$ pointing from the SST front to the cyclone. The orientation of $\mathbf{r}$ relative to the SST gradient ∇SST at the SST front allows us to classify the cyclone position relative to the SST front, with $\mathbf{r} \cdot \nabla\text{SST} < 0$

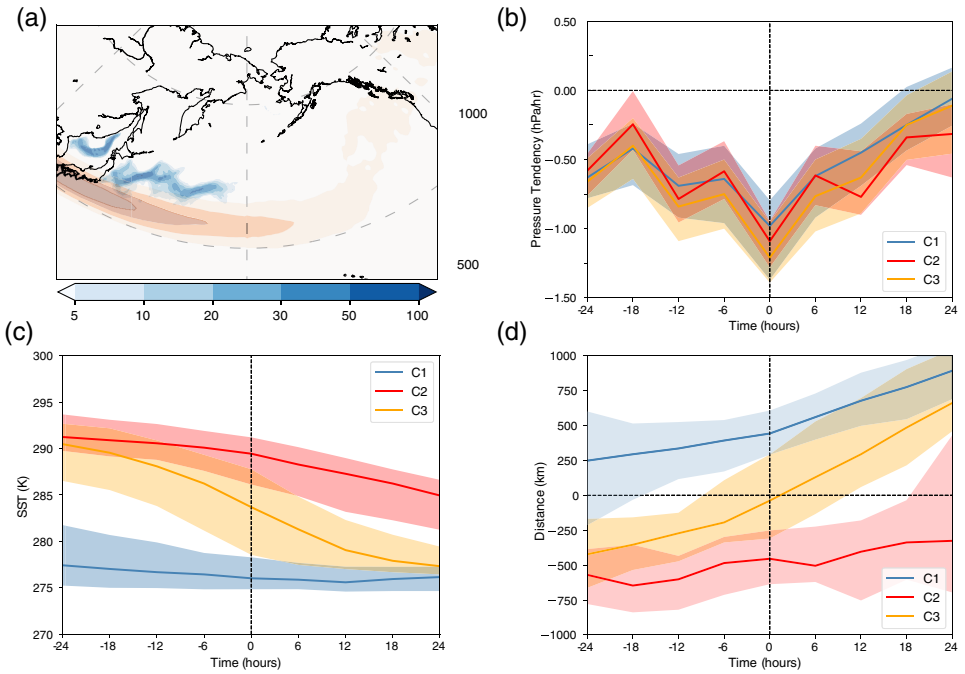

FIGURE 1 (a) SST front distributions (blue shading, km of line (100 km)$^{-2}$) and jet axis distributions (orange shading, km of jet axis line (1,000 km)$^{-2}$) for the North Pacific. The Kuroshio region is marked with a red box. (b) Pressure tendency (hPa·hr^{-1}) for the three categories relative to the time of maximum intensification. Lines indicate the median and the shading the interquartile range. (c) As (b), but for the SST. (d) Distance (km) between cyclone centres and the SST front relative to the time of maximum intensification

on the cold side of the SST front and vice versa on the warm side. Further details are described in TSS20. With the positions of both the SST fronts and the cyclone tracks, we follow TSS20 and categorize the propagation of cyclones relative to the SST fronts only within the Kuroshio region (red rectangle in Figure 1a) into five categories. In category C1, cyclones always remain on the cold side of the SST front, whereas for category C2 cyclones always stay on the warm side of the SST front. In category C3, cyclones are crossing the SST front from the warm to the cold side, contrarily to category C4, in which cyclones cross the SST front from the cold to the warm side. Finally, cyclones that belong to category C5 cross the SST front multiple times.

3 | RESULTS

3.1 | Cyclone occurrence and intensification

Analogously to TSS20 for the Gulf Stream region, we restrict our focus to categories C1, C2, and C3 during the winter season (DJF) over the North Pacific Ocean. Category C4 comprises only 28 cyclones that cross the SST front from the cold to the warm side, making it challenging to deduce statistically robust results. As cyclones in C5 cross the SST front multiple times, it is impossible to diagnose the role of the SST front in the cyclone evolution. However, 142 cyclones consistently stay on the cold side (C1, Figure 2a), 97 cyclones stay on the warm side (C2, Figure 2b), and 188 cyclones cross from the warm to the cold side (C3, Figure 2c). For these three categories, the cyclones all propagate from the southwest to the northeast. Cyclones in C1 and C3 remain closer to the Asian continent than the ones in C2, which propagate northwards the least (Figure 2b).

Amongst these three categories, cyclones in C3 deepen the most from 12 hr prior to maximum intensification to 6 hr after, undergoing a maximum six-hourly deepening corresponding to 30 hPa·day^{-1} (median in Figure 1b). Cyclones in C2 intensify slightly more slowly compared with C3, with a maximum deepening rate corresponding to approximately 26 hPa·day^{-1}. From 12 hr after maximum intensification onward, however, C2 becomes the category

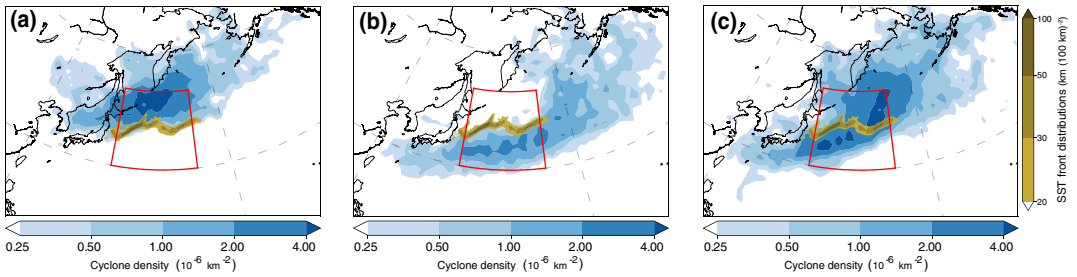

FIGURE 2 (a) Cyclone density for category C1 (blue shading, 10^{-6} km^{-2}) based on the ERA-Interim reanalysis for the winter seasons in 1979–2016 for cyclones with maximum intensification in the Kuroshio region. Density of the SST fronts (brown shading, km of line(100km)$^{-2}$) as in Figure 1, but for the most prominent SST fronts in the Kuroshio region. (b,c) As (a), but for categories C2–3, respectively. See main text for more details on the cyclone detection and categorisation

that deepens the most (median in Figure 1b). Cyclones in C1 intensify least, with a maximum deepening rate corresponding to 22 hPa·day^{-1}. Based on the definition of Sanders and Gyakum (1980), 13.5% of the cyclones in C1 (19 cyclones), 17.5% of the cyclones in C2 (17 cyclones), and 21% of the C3 cyclones (40 cyclones) are explosive. The higher percentages for C2 and C3 are consistent with the study of Iwao *et al.* (2012), who found that the majority of explosive cyclones in the Kuroshio region originate southwest of Japan (Figure 2b,c).

The intensification for the different categories is different compared with the Gulf Stream region, where cyclones in C2 were shown to intensify considerably less than those in C1 and C3 (TSS20). Further, in the Gulf Stream region, 23% of cyclones in C1 and 40% of cyclones in C3 are explosive, compared with 13.5 and 21%, respectively, in the Kuroshio region. Despite the overall lower fraction of explosive cyclones in the Pacific, 17.5% in C2 cyclones in the Kuroshio region are explosive, compared with 11% in the Gulf Stream region.

The higher percentage of explosive cyclones in the Gulf Stream region for C1 and C3 compared with the Kuroshio region could be associated with the additional low-level baroclinicity in the Atlantic due to the land–sea contrast (TSS20). During the early stages, cyclones in C1 and C3 in the Gulf Stream region propagate closer to the cold continental landmass, which enhances the low-level baroclinicity (TSS20). Conversely, cyclones in C1 and C3 in the Kuroshio region are further away from the continent and thus have a more maritime character and weaker low-level baroclinicity. With diabatic processes playing a key role for explosive cyclogenesis, precipitation and latent heat fluxes could also play a crucial role.

However, a higher fraction of C2 cyclones in the Pacific are associated with explosive cyclogenesis compared with those propagating in the Gulf Stream region, despite the similar distribution of surface heat fluxes and the propagation over lower SSTs in the Pacific. We suggest that the reason for the higher explosive fraction for C2 cyclones in the Pacific is the proximity of cyclones to a stronger upper-level jet (Figure 1a) compared with the Gulf Stream region (cf. TSS20).

To estimate the possible effect of the SST front on cyclone intensity, we present its distribution in Figure 3. The location of the maximum intensity is rather equally spread on the cold side of the SST front for C1 and C3, with the latter being closer to the main SST gradient (Figures 1a and 3a,c) and associated with the highest peak intensity among the three categories (not shown). For cyclones of C1 and C3, the location of maximum intensity is close to the location of maximum intensification (not shown). Similarly to C3, cyclones of C2 are also characterized by higher intensity than those in C1 (Figure 3b), but they reach their maximum intensity further downstream, similar to the Atlantic C2 cyclones (TSS20).

3.2 | Cyclone-relative SST and wind composites

We present cyclone-relative composites for the first three categories around the time of maximum intensification to better understand the role of the different forcing mechanisms in the Kuroshio region.

For C1, cyclones propagate over comparatively low SSTs (approximately 277 K) throughout their evolution (Figure 1c), as cyclones remain on the cold side of the SST front (Figure 1d). Over time, cyclones gradually propagate away from the SST front over even lower SSTs (Figure 4a–c). Compared with C1, cyclones in C2 propagate over approximately 15 K higher SSTs (Figure 1c), although SSTs are still about 4 K lower compared with

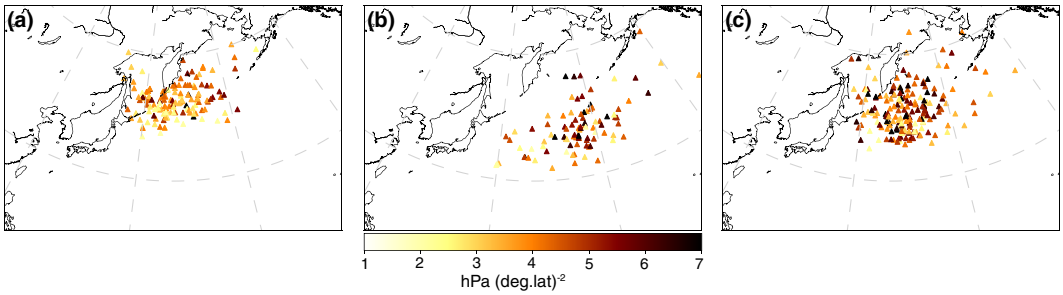

FIGURE 3 (a) Maximum Laplacian of the MSLP (hPa·(deg lat)$^{-2}$) for cyclones in C1. (b,c) As in (a), but for cyclones in C2 and C3, respectively

cyclones in C2 in the Atlantic (TSS20). However, 12 hr after maximum intensification, cyclones in C2 propagate over slightly lower SSTs (Figure 4f), consistent with the cyclones getting closer to the SST front (Figure 1d).

C3 can be seen as a combination of C1 and C2. Prior to the time of maximum intensification, cyclones propagate on the warm side of the SST front (Figure 1d) and thus over higher SSTs (Figures 1c and 4g). After crossing the SST front around the time of maximum intensification (Figures 1d and 4h), cyclones propagate gradually over lower SSTs (Figures 1c and 4i). The cross-frontal SST difference in C3 is, however, less sharp than the one observed in the Gulf Stream region (TSS20), due to a more spatially confined SST front in the Gulf Stream compared to the Kuroshio region (e.g., Nakamura *et al.*, 2004).

For all categories, the maximum wind at 925 hPa increases gradually throughout the cyclone development. This increase is more apparent in C2 and C3, with the wind speed increasing from 18 to 27 m·s^{-1} within 24 hr (Figure 4d–i), compared with C1, where there is an increase of 6 m·s^{-1} (Figure 4a–c). Thus, in contrast to the Gulf Stream region, C2 cyclones are stronger on average than C1 cyclones (cf. TSS20). Nonetheless, in both the Pacific and the Atlantic, the maximum wind speed occurs in the south–southeast quadrant, due to the superposition of circulation and these cyclones their east–northeastward propagation.

Cyclones in C1 and C3 in the Kuroshio region develop in environments with about equally strong low-level baroclinicity (850-hPa temperatures in Figure 4a–c,g–i), while less low-level baroclinicity is observed for C2 (Figure 4d–f). The temperature gradient at 850 hPa is overall smaller compared with the Gulf Stream region for cyclones of categories C1 and C3, while being rather similar for C2 (cf. figure 4 in TSS20). Following the argument of TSS20, the higher low-level baroclinicity in the Gulf Stream region is most likely associated with the proximity of the cyclones to the cold continental landmass. Their argument is consistent with our results for the Kuroshio region, where cyclones are located further away from the cold-air reservoir over the Asian continent and exhibit weaker low-level baroclinicity.

3.3 | Cyclone-relative surface heat flux composites

For all three categories, upward surface heat fluxes dominate around the cyclones (Figure 5). The sensible heat fluxes are largest in the southwest quadrant on the warm side of the SST front, yielding a larger atmosphere–ocean temperature contrast. Averaged over the composite domain, cyclones in C2 are associated with higher sensible heat fluxes (Figure 5d–f) than those in C1 (Figure 5a–c), due to the propagation over higher SSTs (Figure 1c). Similarly to the sensible heat fluxes, the latent heat fluxes are also higher in the southwest quadrant, with the maximum values appearing slightly to the south of the sensible heat fluxes (consistent with, for example, figure 6a,b in Rudeva and Gulev, 2011). This offset in the location of the flux maxima is most likely associated with the saturation mixing ratio increasing exponentially with increasing SSTs following the Clausius–Clapeyron relation.

Sensible and latent heat fluxes follow a distribution for all three categories very similar to that in the Gulf Stream region, except that the amplitude of the fluxes is larger in the Atlantic (cf. TSS20). This is most likely attributable both to the SST gradient being larger in the Gulf Stream compared with the Kuroshio Extension and to cyclones being located closer to the SST front during the time of maximum intensification.

At 12 hr prior to maximum intensification, cyclones in C3 are still located on the warm side of the SST front and consequently feature intense latent and sensible heat fluxes exceeding 280 and 120 W·m^{-2}, respectively

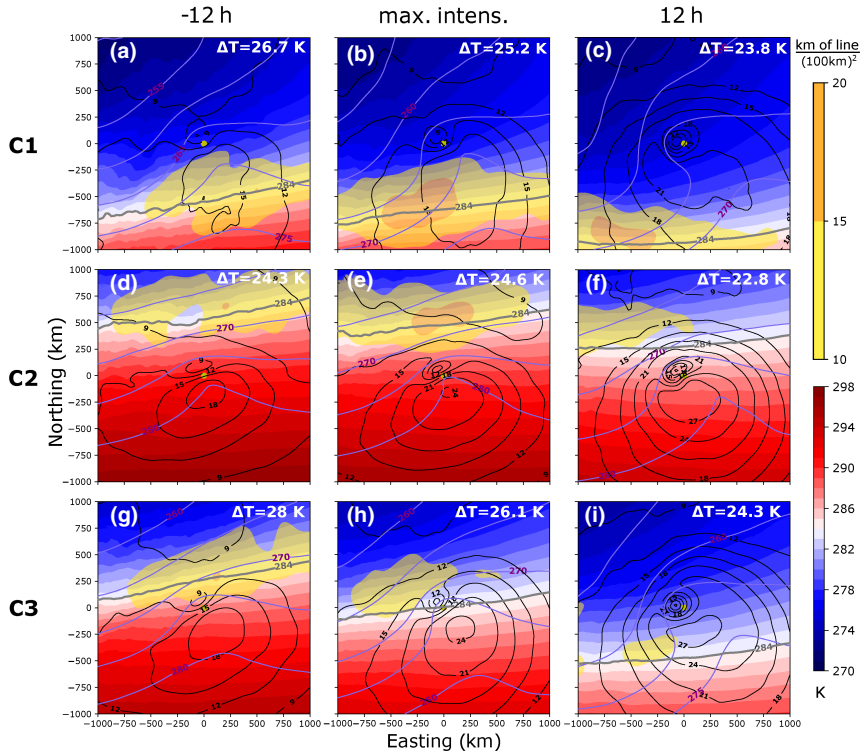

FIGURE 4 Composite evolution of cyclone-centred SST (blue–red shading, K), temperature at 850 hPa (purple contours, interval: 5 K), wind speed at 925 hPa (black contours, interval: 3 m·s^{-1}), and SST front density (yellow shading, in 10^{-5} km $^{-1}$). The isotherm of 284 K (grey contour) estimates the position of the SST front. Numbers in the top right of each panel represent the temperature difference at 850 hPa in the composite domain. Left, middle, and right panels are for 12 hr prior to maximum intensification, maximum intensification, and 12 hr after maximum intensification, respectively. Top, middle, and bottom panels show the categories C1, C2, and C3, respectively

(Figure 5g). At this point in time, both latent and sensible heat fluxes are even slightly higher than for cyclones in C2. Considering the relatively similar wind speeds between the two categories, the higher surface heat fluxes in C3 compared with C2 can be related to the closer proximity of cyclones to the SST front (Figure 1d). During the development, the amplitude of the surface heat fluxes remains more or less unchanged, but the location shifts southwards as cyclones in C3 move away from the SST front. At the same time, downward sensible heat fluxes appear to the east of the cyclone core (Figure 5i).

For all three categories, the highest upward sensible heat fluxes occur in the west–southwest quadrant and are associated with cold-air advection across the SST front (consistent with Vannière *et al.*, 2017). While latent heat fluxes are directed upwards throughout the evolution, sensible heat fluxes can also be directed towards the ocean within the cyclones' warm sector (Figure 5). For C1, a small area of downward sensible heat fluxes appears during the maximum intensification in the southeast quadrant, due to warm-air advection over relatively lower SSTs (Figure 5b). Downward fluxes for C2 only occur in a small region 12 hr after maximum intensification. As the cyclone and its warm sector remain on the warm side of the SST front, the warm air only marginally exceeds the SST in some locations. Once the cyclone crosses the SST front, downward fluxes appear more widespread for C3 (Figure 5i), but remain weak. Overall, the dipole structure becomes more apparent for C2 and C3 at 12 hr, due to the higher intensity of cyclones compared with C1 (Figure 4). Thus, stronger cyclones feature more pronounced dipole structures in surface heat fluxes.

Downward sensible heat fluxes to the east of the cyclone core are more pronounced in the Gulf Stream region throughout the evolution in C1, and after maximum intensification for C3 (TSS20). We relate these more pronounced downward fluxes in the Atlantic to the sharper SST front in the Gulf Stream region, increasing

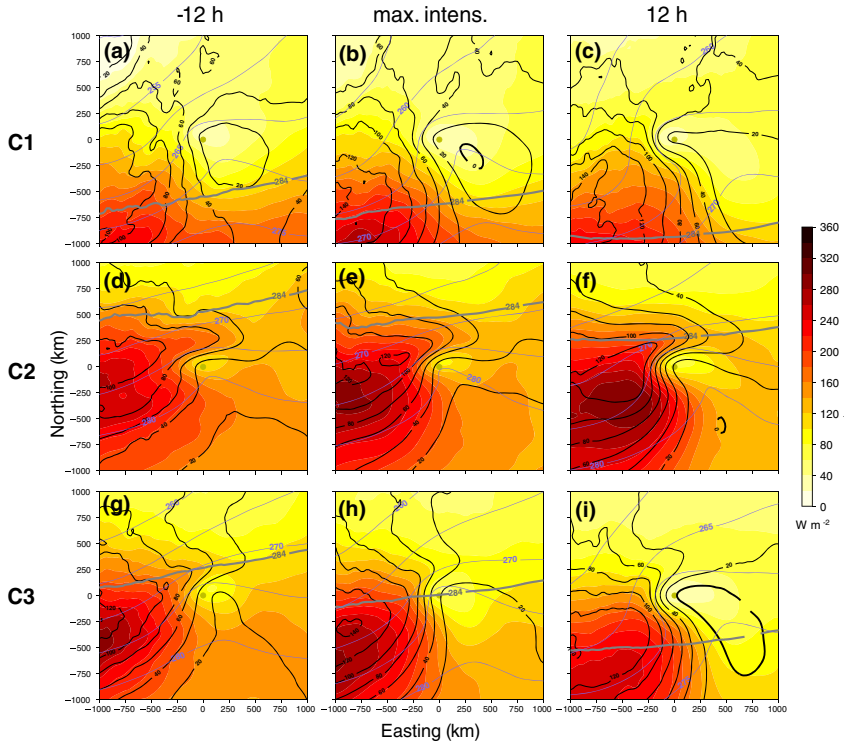

FIGURE 5 Composite evolution of cyclone-centred latent heat fluxes (yellow–red shading, $W \cdot m^{-2}$), sensible heat fluxes (black contours, thick line for the zero contour, interval: $20\ W \cdot m^{-2}$), and temperature at 850 hPa (purple contours, interval: 5 K). Panel setup and SST front position ($T = 284$ K) as in Figure 4

the likelihood that warm air originating from the south reverses the air–sea temperature contrast. Brayshaw *et al.* (2009) showed that the orientation of the North American continent increases the low-level baroclinicity by amplifying the pool of cold continental air to the east. Analogous to their argument for the Atlantic, we suggest that the more tilted SST front in the Gulf Stream region, compared with the Kuroshio region, could further contribute the amplification of temperature differences across the SST front and thus lead to more pronounced downward sensible heat fluxes to the east of the cyclone core, as documented for the Gulf Stream region (TSS20). For C2, the dipole is roughly similar in both regions. Nonetheless, in the Gulf Stream region it becomes more apparent at 12 hr, due to cyclones propagating closer to the SST front than in the Kuroshio region (TSS20).

Overall, the highest sensible heat fluxes are located close to the SST front on its warm side and the highest fluxes occur during maximum intensity of the cyclones. This is consistent with the study of Rudeva and Gulev (2011), which highlights that the SST front determines the location of the maximum surface heat fluxes, whereas the cyclones' intensity regulates when the maximum fluxes will occur.

3.4 | Cyclone-relative moisture composites

C2 is the category with the highest values of TCWV (hereafter moisture content), exceeding $27\ kg \cdot m^{-2}$ at all time steps shown and peaking at maximum intensification (Figure 6e), also featuring the strongest IWVF (hereafter moisture transport) (Figure 6d–f). This is not unexpected, as cyclones in C2 stay on the warm side of the SST front, where the large amount of moisture can be explained by the Clausius–Clapeyron relation.

For C1, the highest moisture content occurs prior to maximum intensification (between −12 and 0 hrs), reaching $21\ kg \cdot m^{-2}$ (Figure 6a,b) nearly 1,000 km to the south of the cyclone centre. At 12 hr after maximum intensification, the maximum moisture content decreases by about

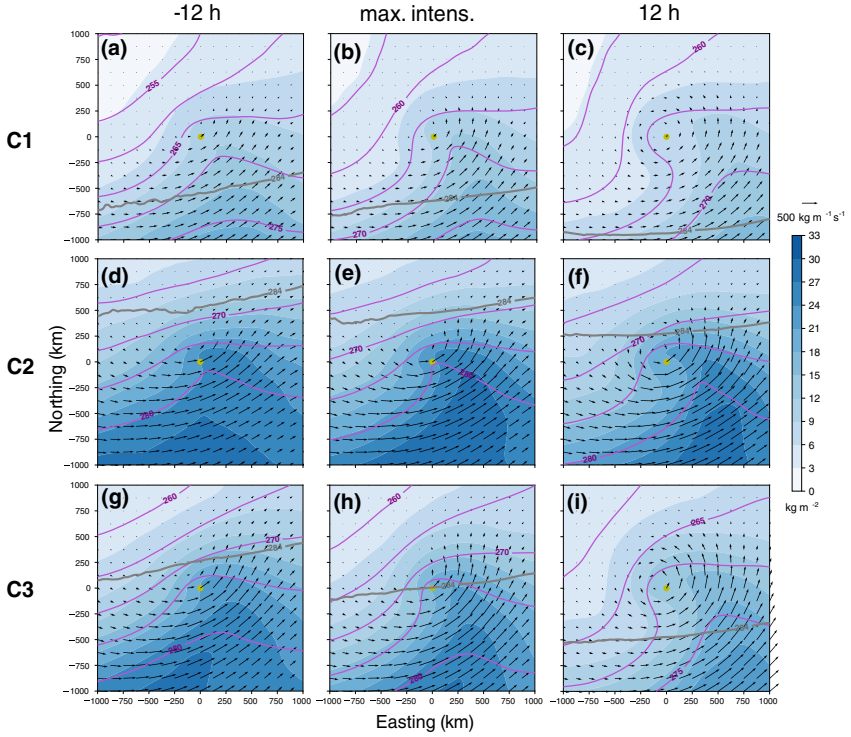

FIGURE 6 Composite evolution of cyclone centred total column water vapour (blue shading, kg·m^{-2}), integrated water vapour flux (black vectors), and temperature at 850 hPa (purple contours, interval: 5 K). Panel setup and SST front position as in Figures 4 and 5

3 kg·m^{-2} and is now located near the southeastern corner of the composite domain (Figure 6c). We relate this gradual reduction in moisture to the propagation of cyclones to the northeast (Figure 2a), moving at a greater distance from the SST front during the evolution of C1 cyclones (Figure 1d).

For C3, the moisture content peaks initially between 27 and 30 kg·m^{-2} at a distance of 750 km to the south of the cyclone centre (Figure 6g). This maximum gradually decays as the cyclones propagate towards the cold side of the SST front (Figure 6g–i), with a corresponding shift of the maximum towards the southeastern sector of the cyclone. The largest moisture transport occurs during maximum intensification in C3 (Figure 6h).

For all three categories, we note the development of a cyclonic wrap-up of both moisture content and transport around the cyclone core, which is progressively more evident throughout the cyclone development (Figure 6). The wrap-up of the warm sector is more distinct for C2 and C3 at 12 hr (Figure 6f,i), consistent with a higher cyclone intensity compared with C1 (cf. low-level wind speeds in Figures 3 and 4c,f,i).

The spatiotemporal evolution of moisture content and transport is similar for the Gulf Stream region. However, both moisture content and transport are consistently lower in the Kuroshio region compared with the Gulf Stream region (cf. TSS20). We relate these differences to the generally higher SSTs on the warm side of the Gulf Stream compared with the Kuroshio region. Due to this difference, Atlantic cyclones of all categories have on average a larger reservoir of moisture to tap into than Pacific cyclones.

3.5 | Cyclone-relative precipitation composites

C1 is the category with the lowest large-scale precipitation among the three categories and is characterized by a gradual yet minor increase of average large-scale precipitation during cyclone development (Figure 7a–c). Twelve hours past maximum intensification, cyclones in C2 are accompanied with on average about 2.5 mm·day^{-1} more intense large-scale precipitation compared with C1 (Figure 7c,f). Precipitation is thus consistent with the higher moisture

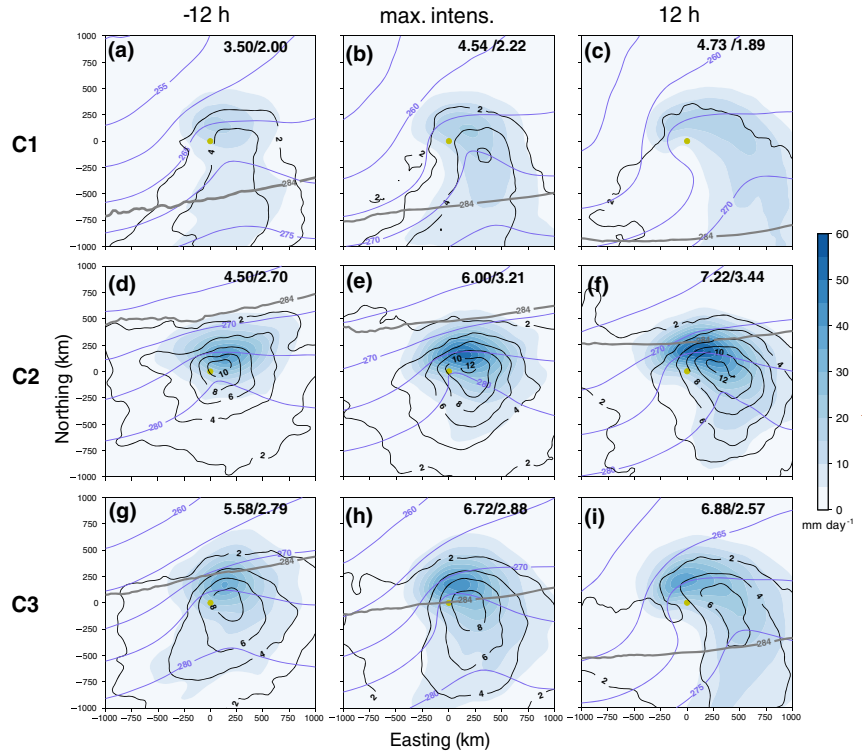

FIGURE 7 Composite evolution of cyclone-centred large-scale precipitation rate (blue shading, mm·day^{-1}), convective precipitation rate (black contours, mm·day^{-1}), and temperature at 850 hPa (purple contours, interval: 5 K). Panel setup and SST front position as in Figures 4–6. Numbers in the top right of each panel represent the average large-scale/convective precipitation in the composite domain

availability and cyclone intensity in C2 compared with C1.

The average large-scale precipitation in the Gulf Stream region was similar for C1 and C2, with the respective moisture availability being large for both categories, though slightly higher for C2 (TSS20). In the Kuroshio region, cyclones in C2 are stronger than those in C1 and associated with higher moisture content, resulting in the higher large-scale precipitation in C2 for the Kuroshio region.

Likewise, the convective precipitation is higher in C2 compared with C1 (Figure 7a–f). The maximum intensity of the convective precipitation for C2 occurs at a later stage of the development (0 hr and 12 hr), exceeding 12 mm day^{-1} approximately 200 km to the east of the cyclone core (Figure 7e,f). In C2, convective precipitation increases with cyclone intensity from 0 to 12 hr (Figure 7e,f), whereas for C1 it decreases for the same time period (Figure 7b,c). C1 thus shows that, in contrast to large-scale precipitation, convective precipitation does not necessarily increase with cyclone intensity. Conversely, convective precipitation evolves in tandem with the SSTs around the cyclone, indicating that local evaporation plays an important role for convective precipitation (consistent with Hand *et al.*, 2014; Pfahl and Sprenger, 2016; TSS20).

In addition to the quantitative difference, the structure of precipitation is different for C1 and C2. The maximum convective and large-scale precipitation is located closer to the cyclone centre in C2 than in C1 (Figure 7a–f). The same spatial distribution of precipitation was also observed for the Gulf Stream region (TSS20), with higher precipitation for C1, due to cyclones propagating over slightly higher SSTs and associated with higher low-level baroclinicity than in the Kuroshio region.

In contrast to C1, cyclones in C2 propagate in the subtropics, over an area with both high SSTs (Figure 1c) and moderate, but still substantial, baroclinicity (Figure 4). Such an environment is favourable for the development of hybrid cyclones (e.g., Guishard *et al.*, 2009; Yanase *et al.*, 2014; Yanase and Niino, 2019). In particular, Yanase and Niino (2019) pointed out the presence of a convective core in hybrid cyclones, which would explain why the

precipitation in C2 is more confined around the cyclone centre. This interpretation is also consistent with Pfahl *et al.* (2015), who found that the precipitation band was located closer to the cyclone centre when increasing global mean surface temperature. In synthesis, all these results show that the absolute SST around the cyclone shapes the spatial distribution of precipitation around the cyclone centre.

C3 is associated with the highest average large-scale precipitation among the three categories up to maximum intensification (Figure 7g,h). There is a steady increase of average large-scale precipitation until maximum intensification with only a slight increase afterwards, whereas convective precipitation remains roughly unchanged up until the cyclones cross the SST front (Figure 7g,h) and decays slightly from 0h to 12 hr (Figure 7i). A similar decrease of convective precipitation was discussed before also for C1, despite the higher cyclone intensity. Thus, whereas large-scale precipitation evolves in tandem with cyclone intensity, the convective precipitation co-evolves more closely with the underlying SST.

The increase of large-scale precipitation over time is more pronounced for the Gulf Stream region, where stronger low-level baroclinicity leads to enhanced ascent along the steeper slopes of isentropic surfaces (cf. TSS20). Low-level baroclinicity is generally weaker in the Kuroshio region, such that this factor explains less of the observed differences and evolution of cyclones in the Kuroshio region. Instead, the increase in large-scale precipitation observed during the evolution of cyclones in C3 can mainly be explained by the higher cyclone intensity (Figures 4h,i and 7h,i). Further, the more intense precipitation for categories C2 and C3 compared with C1 follows from a combination of stronger cyclones and higher moisture content (Figure 7).

3.6 | Cyclone-relative geopotential and wind at 300 hPa

So far, we have attempted to explain cyclone intensification in terms of low-level baroclinicity and moisture availability. Cyclones in C3 have more low-level baroclinicity than cyclones in C2, which can explain their slightly faster intensification despite the fact that C2 has more moisture available. However, C1 is characterised by similar low-level baroclinicity as C3, but cyclones in C1 intensify considerably less. Moreover, cyclones in C2 intensify much faster in the Kuroshio than in the Gulf Stream region, despite similar baroclinicity and more available moisture in the Gulf Stream region. Therefore, we need to also consider upper-level forcing and the jet as a potential third factor accounting for differences between our cyclone categories.

Cyclones in C1 propagate at a larger distance from the climatological position of the Pacific jet compared with C2 and C3 (Figures 1a, 2b,c). Consequently, the wind-speed maximum at 300 hPa is furthest away from the cyclone centre in C1 (Figure 8a–c). The wavy structure in both geopotential and wind suggests that cyclones are typically associated with an upper-level trough to the northwest of the cyclone. During the evolution in C1, the wind maximum shifts eastward (Figure 8b,c), following the development of the trough to the northwest (Figure 8a–c).

For C2, the isohypses are generally spaced more closely than in C1 (Figure 8a–f). Consistently, C2 is the category with the highest wind speed at 300 hPa, associated with a jet streak of 60–70 $m \cdot s^{-1}$, 750 km to the west–southwest of the cyclone centre 12 hr before maximum intensification (Figure 8d). Cyclones in C2 propagate close to the jet and stay in the left exit region of the jet throughout the evolution shown (Figure 8d–f). In contrast, in the Gulf Stream region, cyclones in C2 evolve at a greater distance from the climatological position of a weaker upper-level jet, compared with the Pacific, and are associated with the lowest wind-speed maximum at 300 hPa during maximum intensification among the three categories (TSS20).

As before, C3 can be interpreted as a combination in C1 and C2. Initially, the position relative to the jet is similar to C2 (Figure 8g), but during the evolution the cyclones propagate northward and away from the jet (Figure 8g,h). Twelve hours past maximum intensification (Figure 8i), the distribution of geopotential height and wind speed is approaching that in C1, with the presence of an upper-level trough in the northwest quadrant of the cyclone composite. Wind speeds remain higher in C3 than in C1, but at this point in time both wind maxima are located at a distance of more than 800 km to the south of the cyclone centre (Figure 8c,i).

Based on these results, it seems likely that upper-level forcing contributed to the more rapid deepening in C2 and C3 compared with C1 (Figure 1b). Up until the time of maximum intensification, cyclones in both C2 and C3 are located near the left exit of the jet (Figure 8d–i), whereas cyclones in C1 are further away from the jet (Figure 8a–c). The forced ascent at the left exit of the jet likely contributes to the more intense large-scale precipitation for C2 in the Kuroshio compared with the Gulf Stream region. The position relative to the upper-level jet thus appears to be an important contributor to cyclone intensification in the Kuroshio region and can explain the higher intensification of cyclones for C2 and C3 compared with cyclones in C1, as well as the higher intensification of C2 cyclones in the Pacific compared with the Atlantic. With C3 also

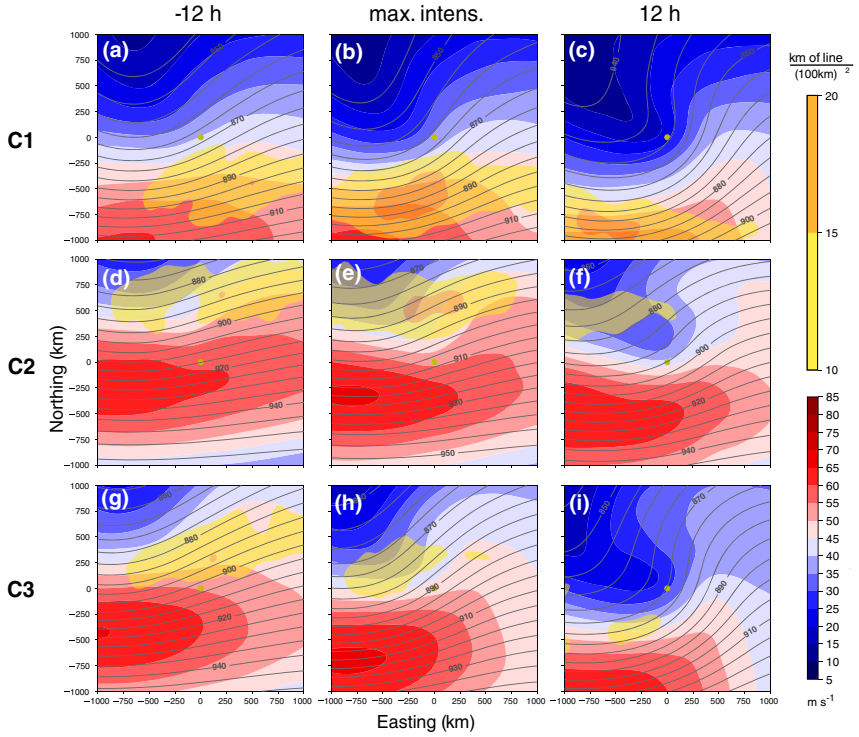

FIGURE 8 Composite evolution of cyclone-centred SST front density (yellow shading, in 10^{-5} km^{-1}), wind speed at 300 hPa (blue-red shading, m s^{-1}), and geopotential height at 300 hPa (grey contours, interval: 5 gpdm). Panel setup as in Figures 4–7

being associated with stronger low-level baroclinicity than C2 (see temperature gradient at 850 hPa in Figure 4d–i), the higher intensification of cyclones in C3 is related to a combination of both upper- and lower-level forcing.

4 | CONCLUDING REMARKS

We identified the main characteristics for categories of cyclones differing in their propagation relative to the SST front in the Kuroshio region. The SST front was detected automatically using an established algorithm and we considered cyclones remaining either on the cold (C1) or warm (C2) side of the SST front, as well as those crossing the SST front from the warm to the cold side (C3). We examined the potential role of the SST front in cyclone intensification and identified the mechanisms promoting cyclone intensification for these categories by compositing the evolution of these cyclones around their time of maximum intensification. As mechanisms, our analysis included low-level baroclinicity and upper-level forcing by the jet, as well as moisture transport and precipitation. The results aid our understanding of the role of the SST front along the Kuroshio Extension for cyclone intensification and enable us to generalise the results of TSS20 for the Gulf Stream region to western boundary currents in general.

Cyclones on the warm side of the SST front (C2) deepen more rapidly compared with cyclones on the cold side (C1) (Figure 1b). This supports previous studies that demonstrated that higher SSTs can lead to more intense cyclones (e.g., Reed *et al.*, 1993; Hirata *et al.*, 2018). A comparison with C2 in the Gulf Stream region, however, demonstrates that this relation must be more complex, as Atlantic C2 cyclones propagate over even higher SSTs than the corresponding ones in the Kuroshio region, yet they intensify the least of all Atlantic categories and also less than Pacific C2. Further, in both the Kuroshio and the Gulf Stream region, cyclones in C3 intensify the most, although they consistently propagate over lower SSTs than those in C2. Given these discrepancies, our results suggest that, even if higher SSTs can affect the intensification of cyclones, this effect is secondary to other effects on synoptic time-scales.

Nevertheless, SSTs strongly modulate the local surface heat fluxes and convective precipitation, as well as

the climatological moisture availability. Cyclones on the cold side of the SST front have, on average, less moisture available and are associated with weaker surface fluxes. Consistent with the overall lower SSTs in the Kuroshio region compared with the Gulf Stream region, cyclones in the Kuroshio region are also, in general, associated with less convective precipitation.

We identified clear differences in the mechanisms responsible for cyclone intensification between the Kuroshio and the Gulf Stream region. Low-level baroclinicity is generally weaker around the Kuroshio than around the Gulf Stream. In addition, cyclones have, on average, less moisture available. Consequently, both low-level baroclinicity and moisture availability play a less important role for cyclone intensification in the Kuroshio region and account for a smaller part of the differences between the categories. Even though the SST contrast across the Kuroshio is weaker than across the Gulf Stream, we mainly attribute the weaker baroclinicity to the greater distance of the Kuroshio region to the Asian continent. Even if Pacific cyclones in C3 propagate slightly closer to the Asian continent than those in C2 (Figure 2b,c), these cyclones are still much further away from the continent than all cyclone categories in the North Atlantic (cf. TSS20).

With their reduced importance, low-level baroclinicity and moisture availability alone cannot explain the observed differences in the intensification of cyclones. We therefore also considered the upper-level forcing. The higher intensification of both C2 and C3 cyclones in the Kuroshio region is consistent with their location close to the left exit of an intense upper-tropospheric jet stream (Figure 8d–i), a position favourable for cyclone intensification. The forced ascent at the left exit of the jet likely also contributes to the higher observed precipitation for C2.

Overall, our feature-based analysis identified several mechanisms leading to cyclone intensification that allowed us to estimate the relative contribution of the SST front to the evolution of these cyclones. We highlighted the importance of both the upper-level jet and low-level baroclinicity for cyclone intensification in the Kuroshio region. The propagation of C2 cyclones near the left exit region of the jet can explain both the higher cyclone intensification and increased large-scale precipitation compared with the Atlantic region, despite the more limited moisture availability in the Kuroshio region. Even though our results do not suggest a direct impact of the SST front on the intensification of cyclones, we suggest that the higher baroclinicity observed for cyclones in C3 is partially attributable to the SST front, providing a conducive environment for cyclone growth. We did not find a clear signal of land–sea contrast in the low-level baroclinicity in the Kuroshio region and thus conclude that the land–sea contrast is less effective in providing low-level baroclinicity in the Kuroshio region compared with the Gulf Stream region.

ACKNOWLEDGEMENTS

We thank ECMWF for providing the ERA-Interim data. We thank two anonymous referees for their feedback and insightful comments. This work was supported by the Research Council of Norway (RCN) project UNPACC (Unifying Perspectives on Atmosphere-Ocean Interactions during Cyclone Development).

ORCID

Leonidas Tsopouridis https://orcid.org/0000-0002-2043-0871
Clemens Spensberger https://orcid.org/0000-0002-9649-6957
Thomas Spengler https://orcid.org/0000-0002-1747-6385

REFERENCES

Berry, G., Reeder, M.J. and Jakob, C. (2011) A global climatology of atmospheric fronts. *Geophysical Research Letters*, 38, L04809.

Brayshaw, D.J., Hoskins, B. and Blackburn, M. (2009) The basic ingredients of the North Atlantic storm track. Part I: Land–sea contrast and orography. *Journal of the Atmospheric Sciences*, 66, 2539–2558.

Chagnon, J.M. and Gray, S.L. (2015) A diabatically generated potential vorticity structure near the extratropical tropopause in three simulated extratropical cyclones. *Monthly Weather Review*, 143, 2337–2347.

Cione, J.J., Raman, S. and Pietrafesa, L.J. (1993) The effect of Gulf Stream-induced baroclinicity on U.S. East Coast winter cyclones. *Monthly Weather Review*, 121, 421–430.

Dee, D.P., Uppala, S.M., Simmons, A.J., Berrisford, P., Poli, P., Kobayashi, S., Andrae, U., Balmaseda, M.A., Balsamo, G., Bauer, P., Bechtold, P., Beljaars, A.C.M., van de Bergd, L., Bidlot, J., Bormann, N., Delsol, C., Dragani, R., Fuentes, M., Geer, A.J., Haimberger, L., Healy, S.B., Hersbach, H., Holm, E.V., Isaksen, L., Kållberg, P., Köhler, M., M, M., McNally, A.P., Monge-Sanz, B.M., Morcrette, J.-J., Park, B.-K., Peubey, C., de Rosnay, P., Tavolato, C., Thepaut, J.-N. and Vitart, F. (2011) The ERA-Interim reanalysis: configuration and performance of the data assimilation system. *Quarterly Journal of the Royal Meteorological Society*, 137, 553–587.

Fink, A.H., Pohle, S., Pinto, J.G. and Knippertz, P. (2012) Diagnosing the influence of diabatic processes on the explosive deepening of extratropical cyclones. *Geophysical Research Letters*, 39(7), https://doi.org/10.1029/2012GL051025.

Guishard, M.P., Evans, J.L. and Hart, R.E. (2009) Atlantic subtropical storms. Part II: Climatology. *Journal of Climate*, 22, 3574–3594.

Hand, R., Keenlyside, N., Omrani, N.-E. and Latif, M. (2014) Simulated response to inter-annual SST variations in the Gulf Stream region. *Climate Dynamics*, 42, 715–731.

Hirata, H., Kawamura, R., Kato, M. and Shinoda, T. (2018) A positive feedback process related to the rapid development of an extratropical cyclone over the Kuroshio/Kuroshio Extension. *Monthly Weather Review*, 146, 417–433.

Hoskins, B.J. and Hodges, K.I. (2002) New perspectives on the Northern Hemisphere winter storm tracks. *Journal of the Atmospheric Sciences*, 59, 1041–1061.

Hotta, D. and Nakamura, H. (2011) On the significance of sensible heat supply from the ocean in the maintenance of mean baroclinicity along storm tracks. *Journal of Climate*, 24, 3377–3401.

Inatsu, M., Mukougawa, H. and Xie, S.-P. (2000) Formation of subtropical westerly jet core in an idealized GCM without mountains. *Geophysical Research Letters*, 27, 529–532.

Iwao, K., Inatsu, M. and Kimoto, M. (2012) Recent changes in explosively developing extratropical cyclones over the winter Northwestern Pacific. *Journal of Climate*, 25, 7282–7296.

Jacobs, N., Raman, S., Lackmann, G. and Childs, P., Jr. (2008) The influence of the Gulf Stream induced SST gradients on the US East Coast winter storm of 24–25 January 2000. *International Journal of Remote Sensing*, 29, 6145–6174.

Jaffe, S.C., Martin, J.E., Vimont, D.J. and Lorenz, D.J. (2011) A synoptic climatology of episodic, subseasonal retractions of the Pacific jet. *Journal of Climate*, 24, 2846–2860.

Jenkner, J., Sprenger, M., Schwenk, I., Schwierz, C., Dierer, S. and Leuenberger, D. (2010) Detection and climatology of fronts in a high-resolution model reanalysis over the Alps. *Meteorological Applications*, 17, 1–18.

Josey, S.A., Kent, E.C. and Taylor, P.K. (1998) *The Southampton Oceanography Centre (SOC) Ocean–Atmosphere Heat, Momentum and Freshwater Flux Atlas*. Southampton, UK: Southampton Oceanography Centre.

Kuo, Y.-H., Shapiro, M.A. and Donall, E.G. (1991) The interaction between baroclinic and diabatic processes in a numerical simulation of a rapidly intensifying extratropical marine cyclone. *Monthly Weather Review*, 119, 368–384.

Kuwano-Yoshida, A. and Asuma, Y. (2008) Numerical study of explosively developing extratropical cyclones in the northwestern Pacific region. *Monthly Weather Review*, 136, 712–740.

Masunaga, R., Nakamura, H., Miyasaka, T., Nishii, K. and Tanimoto, Y. (2015) Separation of climatological imprints of the Kuroshio Extension and Oyashio Fronts on the wintertime atmospheric boundary layer: their sensitivity to SST resolution prescribed for atmospheric reanalysis. *Journal of Climate*, 28, 1764–1787.

Michel, C., Terpstra, A. and Spengler, T. (2018) Polar mesoscale cyclone climatology for the Nordic Seas based on ERA-Interim. *Journal of Climate*, 31, 2511–2532.

Minobe, S., Kuwano-Yoshida, A., Komori, N., Xie, S.-P. and Small, R.J. (2008) Influence of the Gulf Stream on the troposphere. *Nature*, 452, 206–210.

Murray, R.J. and Simmonds, I. (1991a) A numerical scheme for tracking cyclone centres from digital data. Part I: development and operation of the scheme. *Australian Meteorological Magazine*, 39, 155–166.

Murray, R.J. and Simmonds, I. (1991b) A numerical scheme for tracking cyclone centres from digital data. Part II: application to January and July general circulation model simulations. *Australian Meteorological Magazine*, 39, 167–180.

Nakamura, H. (1992) Midwinter suppression of baroclinic wave activity in the Pacific. *Journal of the Atmospheric Sciences*, 49, 1629–1642.

Nakamura, H., Sampe, T., Goto, A., Ohfuchi, W. and Xie, S.-P. (2008) On the importance of midlatitude oceanic frontal zones for the mean state and dominant variability in the tropospheric circulation. *Geophysical Research Letters*, 35(15), https://doi.org/10.1029/2008GL034010.

Nakamura, H., Sampe, T., Tanimoto, Y. and Shimpo, A. (2004) Observed associations among storm tracks, jet streams and midlatitude oceanic fronts. *Geophysical Monograph Series*, 147, 329–345.

Nakamura, M. and Yamane, S. (2009) Dominant anomaly patterns in the near-surface baroclinicity and accompanying anomalies in the atmosphere and oceans. Part I: North Atlantic basin. *Journal of Climate*, 22, 880–904.

Nuss, W.A. and Anthes, R.A. (1987) A numerical investigation of low-level processes in rapid cyclogenesis. *Monthly Weather Review*, 115, 2728–2743.

Ogawa, F. and Spengler, T. (2019) Prevailing surface wind direction during air–sea heat exchange. *Journal of Climate*, 32, 5601–5617.

Oruba, L., Lapeyre, G. and Rivière, G. (2013) On the poleward motion of midlatitude cyclones in a baroclinic meandering jet. *Journal of the Atmospheric Sciences*, 70, 2629–2649.

Papritz, L. and Spengler, T. (2015) Analysis of the slope of isentropic surfaces and its tendencies over the North Atlantic. *Quarterly Journal of the Royal Meteorological Society*, 141, 3226–3238.

Parfitt, R., Czaja, A., Minobe, S. and Kuwano-Yoshida, A. (2016) The atmospheric frontal response to SST perturbations in the Gulf Stream region. *Geophysical Research Letters*, 43, 2299–2306.

Petterssen, S. and Smebye, S.J. (1971) On the development of extratropical cyclones. *Quarterly Journal of the Royal Meteorological Society*, 97, 457–482.

Pfahl, S., O'Gorman, P.A. and Singh, M.S. (2015) Extratropical cyclones in idealized simulations of changed climates. *Journal of Climate*, 28, 9373–9392.

Pfahl, S. and Sprenger, M. (2016) On the relationship between extratropical cyclone precipitation and intensity. *Geophysical Research Letters*, 43, 1752–1758.

Reed, R.J. and Albright, M.D. (1986) A case study of explosive cyclogenesis in the eastern Pacific. *Monthly Weather Review*, 114, 2297–2319.

Reed, R.J., Grell, G.A. and Kuo, Y.-H. (1993) The Erica IOP 5 storm. Part II: Sensitivity tests and further diagnosis based on model output. *Monthly Weather Review*, 121, 1595–1612.

Riehl, H., Alaka, M., Jordan, C. and Renard, R. (1954) The jet stream in relation to middle latitude cyclones. In: *The Jet Stream*, pp. 38–47. Boston, MA: Springer.

Ritchie, E.A. and Elsberry, R.L. (2003) Simulations of the extratropical transition of tropical cyclones: contributions by the midlatitude upper-level trough to reintensification. *Monthly Weather Review*, 131, 2112–2128.

Riviere, G. and Joly, A. (2006) Role of the low-frequency deformation field on the explosive growth of extratropical cyclones at the jet exit. Part II: Baroclinic critical region. *Journal of the Atmospheric Sciences*, 63, 1982–1995.

Roebber, P.J. (1989) On the statistical analysis of cyclone deepening rates. *Monthly Weather Review*, 117, 2293–2298.

Rudeva, I. and Gulev, S.K. (2011) Composite analysis of North Atlantic extratropical cyclones in NCEP–NCAR reanalysis data. *Monthly Weather Review*, 139, 1419–1446.

Sanders, F. (1986) Explosive cyclogenesis in the west-central North Atlantic Ocean, 1981–84. Part I: Composite structure and mean behavior. *Monthly Weather Review*, 114, 1781–1794.

Sanders, F. and Gyakum, J.R. (1980) Synoptic–dynamic climatology of the "bomb". *Monthly Weather Review*, 108, 1589–1606.

Schemm, S., Rudeva, I. and Simmonds, I. (2015) Extratropical fronts in the lower troposphere–global perspectives obtained from two automated methods. *Quarterly Journal of the Royal Meteorological Society*, 141, 1686–1698.

Schultz, D.M., Keyser, D. and Bosart, L.F. (1998) The effect of large-scale flow on low-level frontal structure and evolution in midlatitude cyclones. *Monthly Weather Review*, 126, 1767–1791.

Sinclair, M.R. and Revell, M.J. (2000) Classification and composite diagnosis of extratropical cyclogenesis events in the southwest Pacific. *Monthly Weather Review*, 128, 1089–1105.

Spensberger, C. and Spengler, T. (2020) Feature-based jet variability in the upper troposphere. *Journal of Climate*, 33(16), 6849–6871.

Spensberger, C., Spengler, T. and Li, C. (2017) Upper-tropospheric jet axis detection and application to the boreal winter 2013/14. *Monthly Weather Review*, 145, 2363–2374.

Tozuka, T., Ohishi, S. and Cronin, M.F. (2018) A metric for surface heat flux effect on horizontal sea-surface temperature gradients. *Climate Dynamics*, 51, 547–561.

Tsopouridis, L., Spensberger, C. and Spengler, T. (2020) Characteristics of cyclones following different pathways in the Gulf Stream region. *Quarterly Journal of the Royal Meteorological Society*. https://doi.org/10.1002/qj.3924.

Uccellini, L.W. (1990) Processes contributing to the rapid development of extratropical cyclones. In: *Extratropical Cyclones*, pp. 81–105: Boston, MA: Springer.

Uccellini, L.W., Kocin, P.J., Petersen, R.A., Wash, C.H. and Brill, K.F. (1984) The Presidents' Day cyclone of 18–19 February 1979: synoptic overview and analysis of the subtropical jet streak influencing the pre-cyclogenetic period. *Monthly Weather Review*, 112, 31–55.

Vannière, B., Czaja, A. and Dacre, H.F. (2017) Contribution of the cold sector of extratropical cyclones to mean state features over the Gulf Stream in winter. *Quarterly Journal of the Royal Meteorological Society*, 143, 1990–2000.

Wang, C.-C. and Rogers, J.C. (2001) A composite study of explosive cyclogenesis in different sectors of the North Atlantic. Part I: cyclone structure and evolution. *Monthly Weather Review*, 129, 1481–1499.

Wang, L., Hu, H. and Yang, X. (2019) The atmospheric responses to the intensity variability of subtropical front in the wintertime north Pacific. *Climate Dynamics*, 52, 5623–5639.

Yanase, W. and Niino, H. (2019) Parameter sweep experiments on a spectrum of cyclones with diabatic and baroclinic processes. *Journal of the Atmospheric Sciences*, 76, 1917–1935.

Yanase, W., Niino, H., Hodges, K. and Kitabatake, N. (2014) Parameter spaces of environmental fields responsible for cyclone development from tropics to extratropics. *Journal of Climate*, 27, 652–671.

Yao, Y., Zhong, Z. and Yang, X.-Q. (2016) Numerical experiments of the storm track sensitivity to oceanic frontal strength within the Kuroshio/Oyashio extensions. *Journal of Geophysical Research: Atmospheres*, 121, 2888–2900.

Yoshida, A. and Asuma, Y. (2004) Structures and environment of explosively developing extratropical cyclones in the northwestern Pacific region. *Monthly Weather Review*, 132, 1121–1142.

How to cite this article: Tsopouridis L, Spensberger C, Spengler T. Cyclone intensification in the Kuroshio region and its relation to the sea surface temperature front and upper-level forcing. *Q.J.R. Meteorol. Soc*. 2020;1–16. https://doi.org/10.1002/qj.3929

APPENDIX

Figure A1 shows the distribution of SST and SST fronts prior to and after the ERA-Interim resolution change.

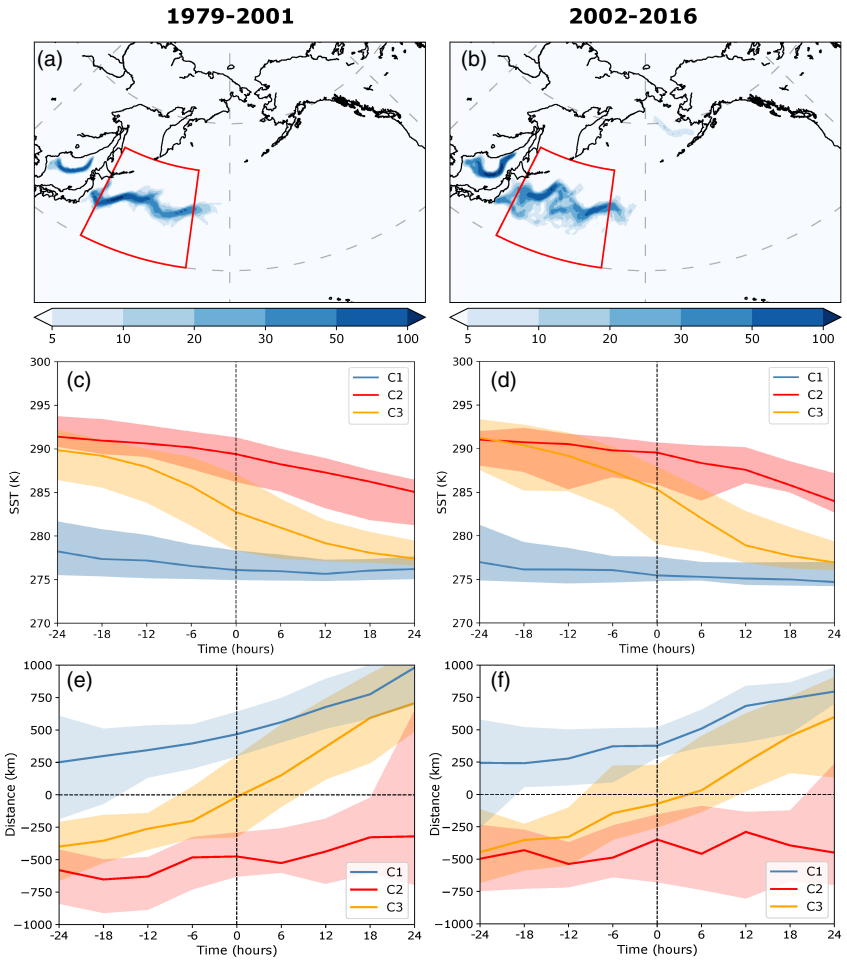

FIGURE A1 (a) Density of SST fronts (km of line (100 km)$^{-2}$) for the winter seasons in 1979–2001 for the North Pacific. The Kuroshio region is marked with a red box. (b) As (a), but for 2002–2016. (c) SST (K) for the three categories relative to the time of maximum intensification for the winter seasons in 1979–2001. Lines indicate the median and the shading the interquartile range. (d) As (c), but for 2002–2016. (e) Distance (km) between cyclone centres and the SST front relative to the time of maximum intensification for the winter seasons in 1979–2001. (f) As (e), but for 2002–2016

Paper III

SST fronts along the Gulf Stream and Kuroshio affect the winter climatology primarily in the absence of cyclones

Tsopouridis L, Spengler T, Spensberger C.
Weather and Climate Dynamics, (2020)
https://doi.org/10.5194/wcd-2020-50

https://doi.org/10.5194/wcd-2020-50
Preprint. Discussion started: 12 October 2020

Weather and Climate Dynamics Discussions
Open Access
EGU

SST fronts along the Gulf Stream and Kuroshio affect the winter climatology primarily in the absence of cyclones

Leonidas Tsopouridis[1], Thomas Spengler[1], and Clemens Spensberger[1]
[1]Geophysical Institute, University of Bergen, and Bjerknes Centre for Climate Research, Bergen, Norway
Correspondence: leonidas.tsopouridis@uib.no

Abstract. The Gulf Stream and Kuroshio regions feature strong sea surface temperature (SST) gradients that influence cyclone development and the storm track. Smoothing the SSTs in either the North Atlantic or North Pacific has been shown to yield a reduction in cyclone activity, surface heat fluxes, and precipitation, as well as a southward shift of the storm track and the upper-level jet. To what extent these changes are attributable to changes in individual cyclone behaviour, however, remains unclear. Comparing simulations with realistic and smoothed SSTs in the atmospheric general circulation model AFES, we find that the intensification of individual cyclones in the Gulf Stream or Kuroshio region is only marginally affected by reducing the SST gradient. In contrast, we observe considerable changes in the climatological mean state, with a reduced cyclone activity in the North Atlantic and North Pacific storm tracks that are also shifted equator-ward in both basins. The upper-level jet in the Atlantic also shifts equator-ward, while the jet in the Pacific strengthens in its climatological position and extends further east. Surface heat fluxes, specific humidity, and precipitation also respond strongly to the smoothing of the SST, with a considerable decrease of their mean values on the warm side of the SST front. This decrease is more pronounced in the Gulf Stream than in the Kuroshio region, due to the amplified decrease in SST along the Gulf Stream SST front. Subdividing the winter climatology into dates with/without cyclones present in the Gulf Stream and Kuroshio regions, we find that cyclones play only a secondary role in explaining the mean states differences between the smoothed and realistic SST experiments.

1 Introduction

The Gulf Stream and Kuroshio region with their strong sea surface temperature (SST) gradients are preferential locations for cyclogenesis (e.g., Hoskins and Hodges, 2002; Nakamura et al., 2004) and are found to determine the location and structure of storm tracks (e.g., Chen et al., 2010; Ogawa et al., 2012; Ma et al., 2015; Yao et al., 2018). Sensitivity tests with smoothed SSTs and a weaker SST gradient yield a reduced cyclone activity. In addition, these experiments feature an equator-ward shift of both the storm track as well as the upper level jet (e.g., Ma et al., 2015; Zhang et al., 2020) and a decrease of surface heat fluxes as well as precipitation on the warm side of the SST front (e.g., Kuwano-Yoshida et al., 2010b; Kuwano-Yoshida and

https://doi.org/10.5194/wcd-2020-50
Preprint. Discussion started: 12 October 2020

Weather and Climate Dynamics Discussions
Open Access
EGU

Minobe, 2017). However, as it remains unclear if the latter changes can be attributed to the changes in cyclone activity, we quantify the contribution of cyclones to the documented differences in the Gulf Stream and Kuroshio region.

SST gradients also influence individual cyclone intensification (e.g., Sanders, 1986; Wang and Rogers, 2001; Jacobs et al., 2008), where the intensification has been associated to low-level baroclinicity originating from sensible heat fluxes (e.g., Hotta and Nakamura, 2011) and latent heating (e.g., Papritz and Spengler, 2015) along the SST front. However, other studies related the intensification of individual cyclones in the western Atlantic to the low-level baroclinicity associated with the pronounced land-sea contrast (e.g., Brayshaw et al., 2009; Tsopouridis et al., 2020a). Thus, while several studies highlighted the sensitivity of cyclogenesis and the storm track to a smoothing of the SST (e.g., Nakamura et al., 2008; Kuwano-Yoshida and Minobe, 2017; Ma et al., 2017; Zhang et al., 2020), the impact of a weaker SST gradient on the intensification of individual cyclones remains unclear.

Randomly selecting 24 individual cyclones that occurred in the Gulf Stream region, de Vries et al. (2019) highlighted the reduction of surface latent heat fluxes and low-level baroclinicity when smoothing the SST. They, however, emphasised that these changes vary based on the position of each storm relative to the SST front. Similarly, Tsopouridis et al. (2020a) found cyclones following different pathways with respect to the SST front position to be associated with different characteristics. They, however, attributed the structural changes primarily to the absolute SST over which the cyclone is propagating rather than the SST front itself. Along the same lines, Booth et al. (2012) found storm strength to increase in the Gulf Stream region with increased SSTs, even if only a weak SST gradient is present. Given the twofold dependence on both the absolute SST and the strength of the SST front, the sensitivity of cyclone development with respect to either absolute SST or SST fronts needs to be further clarified.

In addition to low-level baroclinicity, upper-level forcing by the jet stream is known to contribute to cyclogenesis (e.g., Sanders and Gyakum, 1980; Uccellini et al., 1984; Sinclair and Revell, 2000; Yoshida and Asuma, 2004) and can influence cyclone intensification (e.g., Evans et al., 1994; Schultz et al., 1998; Riviere and Joly, 2006; Tsopouridis et al., 2020b). At the same time, the very existence of the extratropical jet depends on the cyclones maintaining the storm track (Hoskins and Valdes, 1990; Holton and Hakim, 2012; Papritz and Spengler, 2015). Accordingly, using experiments with realistic and smoothed SSTs, Kuwano-Yoshida and Minobe (2017) argued that the increased cyclone activity over the SST front influences the upper-level jet, causing its meandering over the North Pacific.

In the light of this tight coupling between the jet and the storm track, it is not surprising that a smoothing of the SST can affect the upper-level flow. Indeed both the storm track (e.g., Small et al., 2014; Ma et al., 2015; Piazza et al., 2016; Zhang et al., 2020) and the upper-level jet (e.g., Ma et al., 2017; O'Reilly et al., 2017) were shown to shift equatorward in the North Atlantic and Pacific ocean when the SSTs were smoothed. Kuwano-Yoshida and Minobe (2017) showed that smoother SST in the Kuroshio region resulted in a more zonally oriented storm track and argued that a weaker SST front is not able to anchor the upper-level flow. A southward shift of both the storm track density and the upper-level jet when smoothing the SST has also been documented in the North Atlantic region by Piazza et al. (2016), though their shift of the storm track was smaller compared to the one in the study of Small et al. (2014). They related this difference to the stronger SST smoothing in the study of Small et al. (2014). Based on the aforementioned arguments, a smoothing of an already climatologically weaker SST front

https://doi.org/10.5194/wcd-2020-50
Preprint. Discussion started: 12 October 2020

in the Kuroshio region (e.g., Nakamura et al., 2004; Tsopouridis et al., 2020b) should have a comparatively minor impact on the storm track and the upper-level wind speed compared to the Gulf Stream region.

Focusing on mesoscale aspects of the atmospheric response to a smoothing of the SSTs, Piazza et al. (2016) documented a considerable decrease in the surface heat fluxes (30-50%) and convective precipitation (up to 60%) over the warm side of the North-Atlantic SST front after they removed small-scale SST features. Consistently, Zhang et al. (2020) found a similar, yet significantly smaller, decrease of the surface heat fluxes (5%) and precipitation (7%) within the Kuroshio and Oyashio confluence region. Atmospheric general circulation model (AGCM) experiments with real and smoothed SSTs revealed that the SST front is important to maintain convective precipitation (in line with Minobe et al., 2008), with the atmospheric response of the SST smoothing being stronger in the Gulf Stream than in the Kuroshio region (Kuwano-Yoshida et al., 2010b). Indeed, comparing differences in precipitation between the original and smoothed SSTs as well as between the Atlantic (Minobe et al., 2008) and the Pacific (Kuwano-Yoshida and Minobe, 2017), the decrease of precipitation is more pronounced in the Gulf Stream region. Thus, surface heat fluxes and precipitation are considerably affected by the strength of the SST gradient, with the effect being stronger in the Gulf Stream than in the Kuroshio region. However, whether surface heat fluxes and precipitation are only altered by the SST gradients or to what extent changes in the occurrence of cyclones contribute to their distribution remains ambiguous.

While the ability of extratropical cyclones to strongly modulate the moisture transport (e.g., Ruprecht et al., 2002; Chang and Song, 2006) and precipitation (e.g., Bjerknes, 1922; Pfahl and Wernli, 2012; Hawcroft et al., 2012) is commonly accepted, a similar association between cyclones and heat fluxes is under debate. Some studies suggest a close relationship between the surface heat fluxes and cyclones in the midlatitudes on both synoptic (e.g., Alexander and Scott, 1997; Schemm et al., 2015; Dacre et al., 2020) and longer time scales (e.g., Parfitt et al., 2016; Ogawa and Spengler, 2019). Using a more statistical approach, Zolina and Gulev (2003) argued that the surface fluxes mainly occur on synoptic time scales. However, based on a composite analysis Rudeva and Gulev (2011) actually indicated that cyclones in the North Atlantic do not contribute significantly to the climatological surface heat fluxes in this region. Furthermore, Tanimoto et al. (2003) noted that in regions with active ocean dynamics, such as along the western boundary currents, the SST anomalies mainly regulate the surface heat fluxes and not the cyclones.

To shed light to the outlined uncertainties, we assess the effect of a weak or strong SST gradient using an atmospheric general circulation model (AFES 3) based on simulations with realistic and smoothed SSTs in the Gulf Stream and Kuroshio region. Our analysis of these simulations is twofold. Firstly, we follow the approach of Tsopouridis et al. (2020a, b, hereafter TSSa,TSSb) and investigate the effect of the smoothed SSTs on the structure of individual cyclones. Secondly, we examine the contributions of cyclones on the different winter climatologies between the realistic and smoothed simulations (similar to Ma et al., 2015). This two-pronged approach allows us to establish a link between changes in the structure of individual cyclones and changes in the winter climatology. As we will show, the impact on individual cyclones is markedly smaller compared to changes in the winter climatology, suggesting potential answers to the questions raised above.

https://doi.org/10.5194/wcd-2020-50
Preprint. Discussion started: 12 October 2020

Weather and Climate Dynamics Discussions
Open Access
EGU

2 Data and Methods

2.1 Data

We use data from version 3 of the Atmospheric General Circulation Model (AGCM) for the Earth Simulator (AFES) developed by the Earth Simulator Center of the Japan Agency for Marine Earth Science and Technology (Ohfuchi et al., 2004; Enomoto et al., 2008; Kuwano-Yoshida et al., 2010a). This version of AFES has been first used by Kuwano-Yoshida and Minobe (2017) and O'Reilly et al. (2017), and has a horizontal resolution of T239 (approximately 50 km) and 48 sigma levels in the vertical. The model was integrated from 1 September 1981 to 31 August 2001, where we only focus on the winter periods December to February, hereafter DJF. In the production of the AFES data, NOAA 0.25° daily SST data (Reynolds et al., 2007) were used as boundary conditions. More information about the model configuration can be found in Kuwano-Yoshida and Minobe (2017).

Kuwano-Yoshida and Minobe (2017), using AFES 3 produced two experiments for the North Pacific. Firstly, the control experiment (hereafter CNTL) that uses the original global SST data and secondly an experiment that uses smoothed SSTs over the Northwestern Pacific (hereafter SMTHK). They also composed an analogous experiment with spatially smoothed SSTs over the Northwestern Atlantic (hereafter SMTHG). In both cases, the NOAA 0.25° daily SST were smoothed by applying a 1-2-1 running mean filter 200 times in the zonal and meridional direction.

We use SST, latent and sensible heat fluxes, large-scale and convective precipitation, specific humidity at 850 hPa, and wind at 300 hPa for our analysis. We also compare the model simulations with the same variables from the ERA-Interim reanalysis that was created using a four-dimensional variational data assimilation scheme and a spectral truncation of T255 and 60 levels in the vertical (Dee et al., 2011).

2.2 SST front and jet stream detection

We identify the position of SST fronts using an objective frontal detection scheme based on the "thermal" method, as described in detail by Tsopouridis et al. (2020a). This method has also been used to detect atmospheric fronts (Jenkner et al., 2010; Berry et al., 2011; Schemm et al., 2015). To capture the most prominent SST fronts, we have chosen a SST gradient threshold of 2K/100km for the Atlantic and a smaller threshold of 1.25K/100km for the Pacific region. The smaller threshold in the Pacific is due to the weaker SST gradient, as documented by Nakamura et al. (2004), and in line with the previous studies of TSSa for the Atlantic and TSSb for the Pacific.

To assess the potential impact of the SST smoothing on the upper levels, we detect the jet stream position in both basins for the three experiments using the method and criteria of Spensberger et al. (2017), which identifies lines separating cyclonic from anticyclonic wind shear yielding automatically detected jet axes.

https://doi.org/10.5194/wcd-2020-50
Preprint. Discussion started: 12 October 2020

Weather and Climate Dynamics Discussions
Open Access
EGU

2.3 Cyclone detection and tracking

We employ the University of Melbourne cyclone detection and tracking algorithm (Murray and Simmonds, 1991a, b). The algorithm detects maxima in the Laplacian of the MSLP field and tracks them over time using a nearest-neighbour method together with the most likely direction of propagation (Murray and Simmonds, 1991a, b; Michel et al., 2018; TSSa; TSSb).

Analogous to TSSa; TSSb, we take into account only cyclones propagating for at least 12 hours (three consecutive time-steps) in the Gulf Stream region (30-50°N and 290-310°E) and the Kuroshio Extension region (30-50°N and 145-170°E). We also require the great circle distance between cyclogenesis and cyclolysis to be greater than 300 km in order to remove quasi-stationary systems.

2.4 Classification of cyclone tracks based on their position relative to the SST front

We categorise the identified cyclone tracks with a maximum intensification in either the Gulf Stream region or the Kuroshio region based on their propagation relative to the SST front. Firstly, we identify the shortest distance between each cyclone position and the SST front for every time-step along the cyclone track and define a vector pointing to the cyclone. Then, we follow TSSa and TSSb and focus on cyclones that always stay on the cold (C1) or warm (C2) side of the SST front, and those that cross the SST front from the warm to the cold side (C3).

We categorise the cyclones for the SMTHG and SMTHK experiments analogously to the CNTL experiment. However, as the SST gradient in the smoothed experiments is too weak to qualify as a front, we instead use the front positions from the CNTL experiment for the classification. We thus categorise cyclone tracks based on similarities in their geographical location and propagation direction to achieve a consistent classification of the cyclone tracks across all AFES experiments. For simplicity we still refer to C1-3 as the cold, warm, and crossing cases for the smooth experiments, even though, strictly speaking, no front is crossed.

2.5 Decomposition of climatological differences

In addition to the cyclone track classification, we decompose the winter climatology into dates with and without cyclones present the Gulf Stream or the Kuroshio region, respectively. This decomposition allows us to assess how much of the climatological differences in the smoothed experiment arise while cyclones are present in the respective region, and thus how much of the climatological differences are directly or indirectly associated with cyclones. For this analysis, we consider all cyclones that pass through either the Gulf Stream or the Kuroshio region during their evolution, irrespective of their direction of propagation and the location of their maximum intensification.

https://doi.org/10.5194/wcd-2020-50
Preprint. Discussion started: 12 October 2020

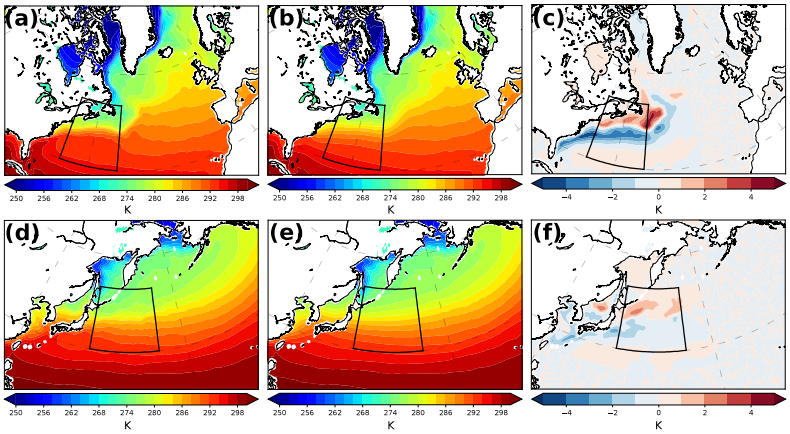

Figure 1. (a) Climatological SSTs in DJF for (a) CNTL, (b) SMTHG, and (c) the difference between SMTHG and CNTL (K). (d-f) as (a-c), but for the North Pacific.

3 Results and Discussion

3.1 SST front and SST/SST gradient distribution between the experiments

Analysing the SST (Fig. 1a) and SST gradient (Fig. 2a) distribution in the Gulf Stream region for CNTL, we note a remarkable SST contrast across the Gulf Stream, which results in a strong SST gradient (Fig. 2a) and in locally well-confined SST front detections (Fig. 3a), consistent with an oceanographic viewpoint (Meinen and Luther, 2016). The SST front distribution also resembles the correspondent feature presented in TSSa for the same region, but based on a different period and dataset.

Across the Kuroshio, we observe an overall similar, but less spatially confined, SST contrast compared to the Gulf Stream region (compare Fig. 1a with Fig. 1d), which results in a weaker SST gradient in the Kuroshio region (Fig. 2d). Consequently, the detected SST fronts are more wide-spreadly distributed in the Pacific (Fig. 3b), but remain collocated with the region of the climatologically largest SST gradient (in line with, e.g., Tozuka et al., 2018; Wang et al., 2019). The less pronounced SST gradient in the Pacific compared to the Atlantic is also evident in the ERA-Interim winter climatology (Fig. A1b,e), with the differences between the reanalysis and AFES simulations arising from the coarser SST resolution used in ERA-Interim prior to 2002 (e.g., Masunaga et al., 2015; Parfitt et al., 2017).

Compared to CNTL, the SSTs in SMTHG are smoother and their gradient is more widely distributed (compare Fig. 1a and Fig. 1b). In the western Atlantic, we also observe that the smoothing affects SSTs at a considerable distance from the Gulf

https://doi.org/10.5194/wcd-2020-50
Preprint. Discussion started: 12 October 2020

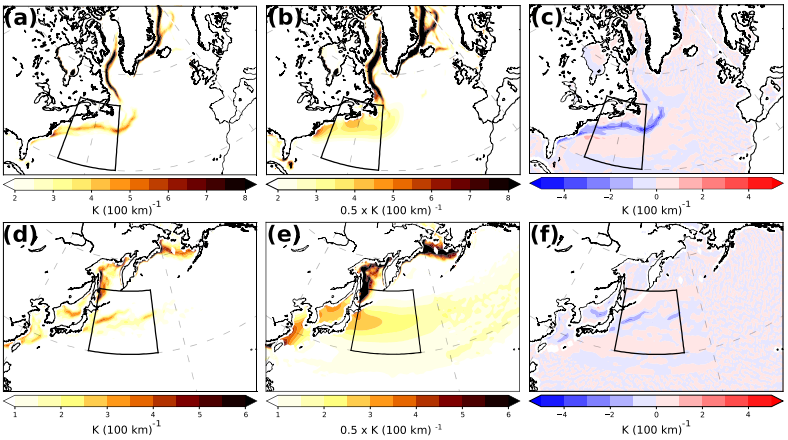

Figure 2. (a) Climatological SST gradient in DJF for (a) CNTL [K (100 km)$^{-1}$], (b) SMTHG [0.5 K (100 km)$^{-1}$], and (c) the difference between SMTHG and CNTL [K (100 km)$^{-1}$]. (d-f) as (a-c), but for the North Pacific.

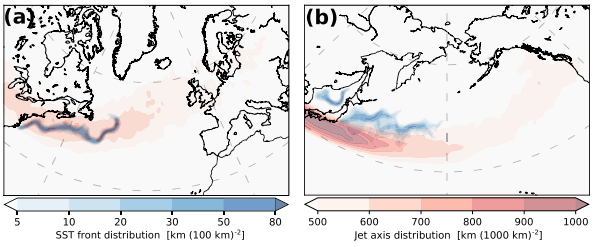

Figure 3. (a) SST front distributions (blue shading, km of line (100 km)$^{-2}$) and jet axis distributions (orange shading, km of jet axis line (1000 km)$^{-2}$) for the North Atlantic. (b) as (a), but for the North Pacific

Stream SST front (Fig. 3a), for example reducing the SST to the east of the Florida Peninsula (Fig. 1a,b). At approximately 40°N, the SST differences exhibit a clear dipole, with increased SST to the north and decreased SST to the south, following the position of the SST front (Fig. 1c, Fig. 3a). The largest differences occur offshore off the central US East coast ($\Delta\text{SST} < -4K$) as well as off the coast of Newfoundland ($\Delta\text{SST} > 4K$; Fig. 1c).

https://doi.org/10.5194/wcd-2020-50
Preprint. Discussion started: 12 October 2020

Weather and Climate Dynamics Discussions
Open Access
EGU

The SST distribution in SMTHK (Fig. 1e) is similar to CNTL, though smoother, and the region with the strongest gradients off the east coast of Japan is oriented slightly more zonally (Fig. 1d). Contrary to the Gulf Stream region, the SSTs outside the Kuroshio region remain largely unaffected. As in the Gulf Stream region, the SST differences between the two experiments follow a bipolar structure (Fig. 1f), but they are considerably weaker. The smoothing results in a maximum decrease (increase) of 2K (3K) south (north) of the SST front (Fig. 1f), with the SST differences being more pronounced in the western part of the domain close to Japan (Fig. 1f).

3.2 Cyclone Density and Upper-level Wind

To evaluate the potential impact of the upper-level forcing on cyclones, we present the climatological position of the jet stream over the two ocean basins. The position of the North Atlantic jet coincides with the location of the SST front (Fig. 3a), whereas the Pacific jet is located south of the Kuroshio SST front (Fig. 3b). The Pacific jet is stronger, meridionally more confined, and located over lower latitudes compared to the Atlantic jet, which is consistent with previous studies (e.g., Nakamura, 1992; Spensberger and Spengler, 2020). Both the strength and the position of the jet axes distribution in the North Atlantic are analogous to the study of TSSa, while for the Pacific we observe fewer jets in the region to the south of Japan compared to TSSb.

The changes in the SST field between CNTL and SMTHG/SMTHK introduce differences in both cyclone density and the climatological jet stream position. We observe an equatorward shift in the maximum cyclone density in both the North Atlantic and North Pacific, particularly in the central and eastern part of the basins (Fig. 4a,c). We also notice an analogous shift in the upper-level jet in the North Atlantic (Fig. 4b), with negative anomalies in the northern part of the basin and positive anomalies mainly to the east of the Gulf Stream region. However, a similar shift of the upper-level jet is not observed in the North Pacific, where the position of the jet remains rather unchanged, with a more confined and zonal distribution of the jet in SMTHK (Fig. 4d). We relate the lack of a shift in the upper-level jet in the North Pacific to the small SST difference after the SST smoothing ($\Delta\text{SST} = 1K$; Fig. 1f), whereas in the Atlantic the jet is located near the region with the most pronounced SST changes ($\Delta\text{SST} > 4K$; Fig. 1c).

Analogously, the sharper SST gradient in the Gulf Stream region (Fig. 2c,f) leads to larger changes in storm track activity in the Northwestern Atlantic, with a more pronounced decrease in cyclone density in the Gulf Stream region compared to the Kuroshio region (Fig. 4a,c). This is consistent with Kuwano-Yoshida et al. (2010b) and in line with Nakamura et al. (2008), who found the storm track activity in the Southern Ocean to be substantially weaker after the removal of the strong SST front.

Thus, while differences in cyclone density (Fig. 4a) and jet occurrence (Fig. 4b) are generally collocated in the Atlantic, they are displaced from each other in the Pacific region (Fig. 4c,d), where a considerable increase in cyclone density in the Northeast Pacific (Gulf of Alaska, Fig. 4c) is contrasted by a decrease in the upper-level wind speed (Fig. 4d). Zhang et al. (2020) found a similar decrease in the upper-level response in the northeastern Pacific, expressed by differences of meridional eddy wind variance and eddy kinetic energy at 300 hPa. However, they showed that the upper-level decrease was not accompanied by a reciprocal negative anomaly in the low-level storm track and thus documented a different response of the SST smoothing in the lower and upper levels in the Pacific.

https://doi.org/10.5194/wcd-2020-50
Preprint. Discussion started: 12 October 2020

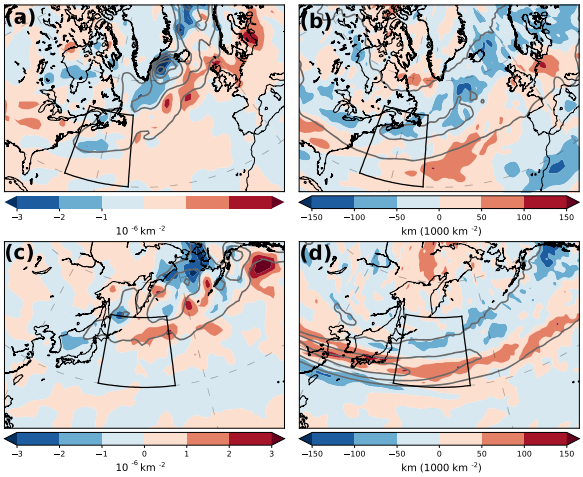

Figure 4. (a) Difference in the climatological cyclone density between SMTHG and CNTL (shading, 10^{-6} km^{-2}) and cyclone density (contours, first contour: 6*10^{-6} km^{-2}, interval 3*10^{-6} km^{-2}) for the CNTL experiment (b) difference in the climatological jet stream (shading, km of jet axis line (1000 km)$^{-2}$) and jet stream density (contours, first contour: 400 km of jet axis line (1000 km)$^{-2}$, interval: 200 km of jet axis line (1000 km)$^{-2}$. (c,d) As (a,b), but for the Kuroshio region. The Gulf Stream and Kuroshio regions are marked with a black box, respectively.

3.3 Categorisation and Intensification of Cyclones

To assess the effect of smoothing the SSTs on the evolution of individual cyclones, we now restrict our focus to cyclones with maximum intensification in the Gulf Stream or Kuroshio region (details in section 2.4). For the Atlantic CNTL, 57 cyclones consistently stay on the cold side of the Gulf Stream SST front (C1), 27 cyclones stay on the warm side (C2), and 40 cyclones cross the SST front from the warm to the cold side (C3). In SMTHG, 62, 30, and 25 cyclones belong to C1, C2, and C3, respectively. Comparing these numbers, we notice that the number of cyclones staying on either side of the SST front is nearly unaffected by the smoothing, whereas the number of crossing cyclones is substantially reduced. This implies an overall reduction in the number of cyclones, which is in line with the decreased cyclone density along the Gulf Stream SST front in SMTHG (Fig. 3a, Fig. 4a).

In the Kuroshio region, the number of cyclones in C1 (86/81) and C3 (59/60) is more or less unchanged between CNTL/SMTHK, whereas cyclones in C2 (24/14) decrease slightly in number. The restricted number of cyclones in C2, particularly in SMTHK,

https://doi.org/10.5194/wcd-2020-50
Preprint. Discussion started: 12 October 2020

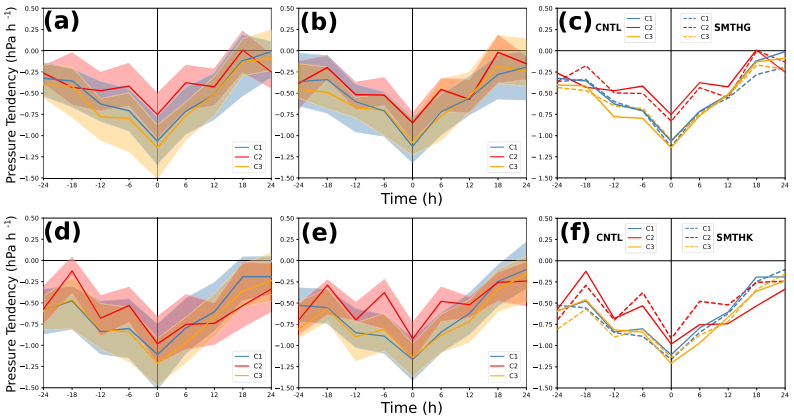

Figure 5. Pressure tendency (hPa h^{-1}) for the three categories relative to the time of maximum intensification for (a) CNTL and (b) SMTHG. Lines indicate the median and the shading the interquartile range. (c) Medians of the pressure tendency (hPa h^{-1}) for the three categories relative to the time of maximum intensification for CNTL (solid lines) and SMTHG (dashed lines). (d-f) As (a-c), but for the North Pacific.

implies some uncertainty for the corresponding results. Note that in contrast to the Atlantic, there is no reduction in cyclones crossing the SST front, potentially because the SST gradient in the Pacific is already comparatively weak in CNTL (compare Figs. 2a, d).

The more pronounced reduction of cyclones crossing the SST front in SMTHG compared to SMTHK highlights the significance of a strong SST gradient to anchor the position of the storm track, as discussed in previous studies (e.g., Nakamura et al., 2004, 2008; Sampe et al., 2010). Our results confirm these studies not only based on the number of cyclones, but also based on the location of cyclones during their maximum intensification. In CNTL, most cyclones undergo their most rapid intensification close to the SST front (Fig. A3b), whereas the location of most rapid intensification is distributed over a wider region in SMTHG (Fig. A3e).

Among the three categories, Atlantic cyclones of C3 and C1 are deepening the most in CNTL, with a maximum 6-hourly intensification corresponding to approximately 28 and 25 hPa/day, respectively. Conversely, cyclones of C2 are characterised by a weaker intensification throughout their evolution (Fig. 5a). In SMTHG, cyclones intensify similarly fast as in CNTL (Fig. 5a,b). In particular, cyclones of C3 experience only a slightly weaker intensification in SMTHG, although the SST front that they cross is barely existing in SMTHG. These results support the findings of TSSa, who related the intensification of cyclones in the Gulf Stream region to the low-level baroclinicity associated with the land-sea contrast, hypothesising that a strong SST

https://doi.org/10.5194/wcd-2020-50
Preprint. Discussion started: 12 October 2020

Weather and Climate Dynamics Discussions
Open Access
EGU

gradient only weakly modifies the deepening of the cyclones. Nevertheless, the distinction between the categories becomes less clear in SMTHG, where the interquartile ranges of the three categories overlap considerably.

In the Kuroshio region, cyclones of C3 are on average deepening the fastest (approx.30 hPa/day), followed by cyclones of C1 (approx. 25 hPa/day; Fig. 5d). In line with TSSb, C2 becomes the category with the larger deepening rate among the three categories after the time of maximum intensification. In contrast to TSSb, cyclones of C2, however, deepen the least before their maximum intensification in both CNTL and SMTHK (Fig. 5d,e). We relate this difference to cyclones in the AFES simulations being located further away from an upper-level jet stream than in the ERA-Interim data used in TSSb (not shown), where the upper levels proved to substantially influence the intensification of cyclones in the Kuroshio region. Moreover, the limited number of cyclones in the AFES simulations (24 cyclones in CNTL compared with 97 cyclones in TSSb) lowers the statistical robustness of these results.

In SMTHK, the cyclones in the three categories have similar pressure tendencies as in CNTL (Fig. 5e), which becomes even more apparent when comparing the median of their pressure tendencies (Fig. 5f). In particular, C3 on average intensifies virtually identically in the two experiments. In the light of the corresponding findings for the Gulf Stream region, this result is not surprising. Even for the more focused Gulf Stream SST front, the smoothing had only a minor impact on the evolution of C3 cyclones (Fig. 2c,f). A more pronounced effect is evident for C2 cyclones in the Kuroshio region, with cyclones intensifying slightly less after the smoothing. However, the number of cyclones is even smaller in SMTHK (14 cyclones) than in CNTL, making it difficult to draw conclusions from this difference.

Considering the evolution of the SST underneath the cyclone core, cyclones of C1 propagate over comparatively low SSTs, because they remain on the cold side of the SST front in both regions (Fig. 6a,d). In contrast, cyclones of C2 propagate over approximately 16 K higher SSTs than cyclones of C1 in the North Atlantic (Fig. 6a) and over 12K higher SSTs in the Pacific (Fig. 6d) during maximum intensification. However, during their evolution, cyclones gradually propagate towards lower SSTs. Cyclones of C3 propagate over higher SSTs at an early stage of their development and over lower SSTs after crossing the SST front. The latter is associated with the cross-frontal SST difference, which is more pronounced in the Atlantic (Fig. 6a) than in the Pacific (Fig. 6d) due to the sharper Gulf Stream SST front (consistent with Nakamura et al., 2004; Joyce et al., 2009; TSSb).

After the SST smoothing, cyclones of C1 propagate over approximately 1 K higher SSTs in both regions and cyclones of C2 over 1-2 K lower SSTs. Further, cyclones of C3 in the smoothed experiments experience a less sharp decrease in SST across the SST front compared to the CNTL experiment (Fig. 6b,c,e,f). The SST differences introduced by the smoothing are more pronounced before maximum intensification, because at this stage cyclones typically propagate in the western part of the regions of interest where the SST differences associated with the smoothing tend to be larger (Fig. 1c,f).

Overall, the considerable reduction in the number of cyclones of C3 after the smoothing of the SST in the Atlantic highlights the anchoring effect of a strong Gulf Stream SST front on the storm track. On the other hand, the already weak SST gradient in the Kuroshio prior to the smoothing leads to minor SST differences between CNTL and SMTHK and thus to a similar number of cyclones that cross the SST front. The rather similar cyclone intensification between the experiments indicate that the SST gradient is not particularly important for the intensification of individual cyclones (consistent with TSSa; TSSb).

https://doi.org/10.5194/wcd-2020-50
Preprint. Discussion started: 12 October 2020

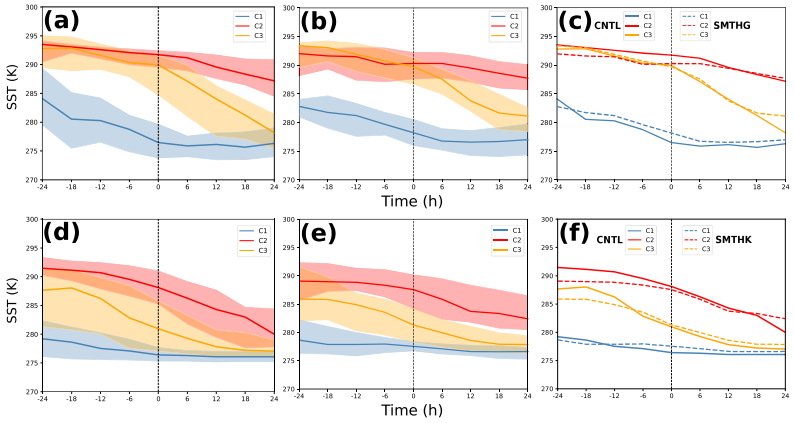

Figure 6. SSTs (K) for the three categories relative to the time of maximum intensification for (a) CNTL and (b) SMTHG. Lines indicate the median and the shading the interquartile range. (c) Medians of the SSTs (K) for the three categories relative to the time of maximum intensification for CNTL (solid lines) and SMTHG (dashed lines). (d-f) As (a-c), but for the North Pacific.

Our results thus suggest that the SST smoothing does not result in significant differences in the characteristics of individual cyclones. This result is supported by cyclone-relative composites of, for example, surface heat fluxes and precipitation, which exhibit only minor differences between the smooth and CNTL experiments for all cyclone categories (not shown). Nevertheless, we observe a latitudinal shift in the storm track and the jet stream climatologies associated with the SST smoothing (Fig. 4) and previous studies documented a significant reduction in the climatological surface heat fluxes and precipitation (e.g., Kuwano-Yoshida et al., 2010b; Kuwano-Yoshida and Minobe, 2017). This discrepancy raises the questions how the largely unaffected characteristics of individual cyclones relate to the evident changes in the climatological mean state of the storm track. In the following, we turn to this question by decomposing the winter climatology into dates with and without cyclones propagating through either the Gulf Stream or Kuroshio region.

3.4 Contribution of cyclones to the climatological differences introduced by smoothing the SST

3.4.1 Surface Heat Fluxes

In the CNTL climatology, we observe a maximum of latent and sensible surface heat fluxes on the warm side of both the Gulf Stream and the Kuroshio SST front (Fig. 7a,e). Peak latent heat fluxes are slightly offset to the south of the peak sensible heat fluxes. TSSb associated this offset with the increase of sea surface saturation mixing ratio with increasing SSTs, following

https://doi.org/10.5194/wcd-2020-50
Preprint. Discussion started: 12 October 2020

Weather and Climate Dynamics Discussions
Open Access
EGU

the Clausius-Clapeyron relation. In the North Atlantic, latent and sensible heat fluxes exceed 350 W m^{-2} and 80 W m^{-2}, respectively (Fig. 7a). Sensible heat fluxes are slightly larger in the North Pacific, whereas latent heat fluxes remain slightly weaker (Fig. 7e).

The surface heat fluxes are similarly distributed in the ERA-Interim dataset, though latent heat fluxes in CNTL are considerably larger compared to ERA-Interim (compare Fig. 7a with Fig. A1c, and Fig. 7e with Fig. A1f). This discrepancy most likely arises from the difference of the SST resolution between the AFES and ERA-Interim, with the latter having a lower resolution prior to 2002. Comparing the CNTL fluxes with the ERA-Interim winter climatology after 2002, the differences are significantly reduced (not shown).

The SST smoothing affects the amount of surface heat fluxes in both regions, though to a different extent. In the Gulf Stream region, we observe considerably weaker surface heat fluxes (Fig. 7b) along the weaker SST gradient (Fig. 2c). The maximum decrease of the latent heat fluxes is of the order of 120 W m^{-2}, while the reduction of sensible heat fluxes exceeds 30 W m^{-2} (in line with Small et al. (2014)). A slight increase of surface heat fluxes is observed mainly to the northeast and less in the southern parts of the Gulf Stream region (Fig. 7b), consistent with the increase of SSTs due to the smoothing (Fig. 1c). This dipole of positive and negative anomalies of the surface heat fluxes is less pronounced in the Kuroshio region (Fig. 7f), reaching only about half the amplitude compared to the Gulf Stream region. We attribute the reduced amplitude to the smaller impact of the SST smoothing on the SST distribution in the Kuroshio region (Fig. 1f).

To estimate the role of cyclones being present for the differences when smoothing the SST, we subdivide the differences between SMTHG/SMTHK and CNTL into time-steps with or without cyclones in the Gulf Stream or Kuroshio region, respectively (Fig. 7c,d,g,h). In the Gulf Stream region, cyclones are present about a third of the time-steps in both CNTL and SMTHG. In the Kuroshio region, cyclones are slightly more prevalent, and a cyclone is present in about 40% of the time-steps.

The division into cyclone/no-cyclone time-steps shows that the climatological differences between CNTL and SMTHG/SMTHK predominantly arise when no cyclones are present in the respective region (Fig. 7c,d,g,h). The contribution from no-cyclone time-steps is larger in amplitude and the distribution of the flux anomalies more closely resembles the climatological differences between the experiments (Fig. 7b,f). The largest differences in Fig. 7d arise close to the climatological SST front position and are clearly connected to the presence or absence of a sharp SST front. This can be explained by a cold air mass transitioning over a SST front experiencing less surface heating when the smoothing reduced the SSTs on the warm side of the SST front in SMTHG and SMTHK (see Fig. 1c,f; Zolina and Gulev, 2003 and Vanniere et al., 2017). The differences are more pronounced in the Gulf Stream region (Fig. 7c,d) compared to Kuroshio (Fig. 7g,h) due to the larger total mean differences of surface heat fluxes after the SST smoothing in the Atlantic (Fig. 7b,f).

Our results indicate that the smoothing of the SST front has only a minor effect when cyclones are present, which is confirmed by a cyclone-relative composite analysis, where surface heat fluxes are only moderately reduced by the smoothing of the SST front (not shown). Our findings are also in line with Rudeva and Gulev (2011), who indicated that cyclones in the North Atlantic sector do not contribute significantly to the climatological surface heat fluxes in the region.

https://doi.org/10.5194/wcd-2020-50
Preprint. Discussion started: 12 October 2020

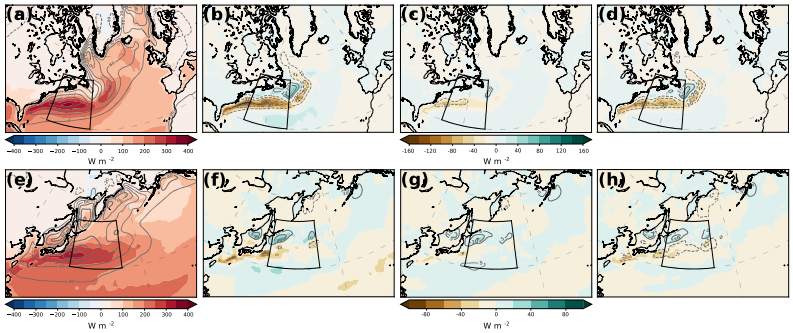

Figure 7. (a) Climatological latent (shading, W m^{-2}) and sensible heat fluxes (contours, W m^{-2}) for the North Atlantic for CNTL. (b) Difference of the heat fluxes climatologies between SMTHG and CNTL for latent (shading) and sensible heat fluxes (grey contours, interval: 10 W m^{-2}, zero contour omitted). (c,d) As (b), but only considering the dates with (c) or without (d) cyclones present in the Gulf Stream region. (e-h) As (a-d), but for the Kuroshio region. The Gulf Stream and Kuroshio regions are marked with a black box, respectively. Panels (c,d,g,h) are scaled such that their sum yields panels (b) and (f), respectively.

3.4.2 Precipitation

The precipitation distribution in the Atlantic in CNTL is characterised by a maximum of large-scale (> 6 mm day^{-1}) and convective precipitation (> 4 mm day^{-1}) along the Gulf Stream SST front extending eastward (Fig. 8a). The maximum values of precipitation are located along the SST front (Fig. 3a), with a well-defined convective rain-band displaced towards the warm side of the Gulf Stream SST front, consistent with the findings of Kuwano-Yoshida et al. (2010b).

In the Pacific, we observe an analogous spatial distribution of the precipitation pattern, but the amplitude is somewhat larger than in the Gulf Stream region (compare Fig. 8a with Fig. 8e). Further, the peaks of large-scale and convective precipitation are more collocated in the Kuroshio region, likely related to the weaker SST gradient (Fig. 2a,d). When compared to ERA-Interim (Fig. A2a,d), there is a good resemblance of the spatial distribution of precipitation, but we notice higher large-scale and convective precipitation in AFES, consistent with the larger latent heat flux.

Analogous to the surface heat fluxes, the smoothing of the SSTs affects precipitation in both regions. In the North Atlantic, the smoothing leads to a remarkable decrease of precipitation (Fig. 8b), in line with the study of Kuwano-Yoshida et al. (2010b). In the North Pacific, however, precipitation is reduced considerably less, with both large-scale and convective precipitation being reduced by less than 1 mm day^{-1} (consistent with Zhang et al. (2020)). We relate the more pronounced reduction of precipitation in the Gulf Stream to the originally sharper SST gradient (Fig. 2). We also observe a similar dipole pattern with reduced precipitation over the Gulf stream and Kuroshio core as well as increased precipitation in the southeast of both regions

https://doi.org/10.5194/wcd-2020-50
Preprint. Discussion started: 12 October 2020

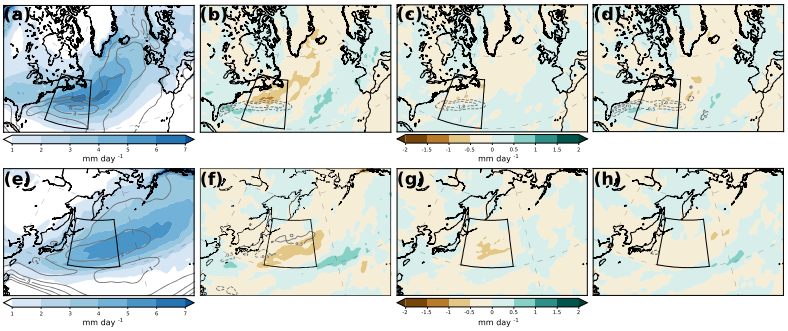

Figure 8. (a) Climatological large-scale precipitation (shading, mm day^{-1}) and convective precipitation (grey contours, interval: 1, mm day^{-1}, zero contour omitted) for the North Atlantic for CNTL. (b) Difference of the precipitation climatologies between SMTHG and CNTL for the large-scale (shading) and convective precipitation (grey contours, interval: 1, mm day^{-1}, zero contour omitted). (c,d) As (b), but only considering the dates with (c) or without (d) cyclones present in the Gulf Stream region. (e-h) As (a-d), but for the Kuroshio region. The Gulf Stream and Kuroshio regions are marked with a black box, respectively. Panels (c,d,g,h) are scaled such that their sum yields panels (b) and (f), respectively.

(Fig. 8b,f). This equatorward shift in precipitation is consistent with the equatorward shift of the storm track in the smoothed experiments (Fig. 4).

Among the two types of precipitation, convective precipitation is more sensitive to the SST smoothing. In SMTHG, the mean convective precipitation is reduced by half compared to CNTL and the narrow convective precipitation band observed in CNTL largely disappears in SMTHG (not shown). This finding is in line with Minobe et al. (2008) and Kuwano-Yoshida et al. (2010b), who showed that the Gulf Stream SST front is crucial for the distribution and amount of convective precipitation and found convective precipitation to be significantly reduced after heavily smoothing the SST distribution in their simulations with the same model.

Compared to the surface heat fluxes, the precipitation associated with cyclones is more influenced by the SST smoothing. There is a noticeable reduction in convective precipitation in the Gulf Stream region just south of the climatological position of the SST front (Fig. 8c), the region featuring the strongest decrease of SST due to the smoothing (Fig. 1c). This finding supports TSSa, who found convective precipitation to be closely related to the SSTs underneath the cyclone core. When no cyclone is present in the Gulf Stream region, the SST smoothing results in a reduction of both large-scale and convective precipitation almost everywhere in the Gulf Stream region.

Overall, cyclones account for a larger fraction of the precipitation differences than they did for the difference in surface heat fluxes when comparing CNTL and SMTHG. This result is in line with Hawcroft et al. (2012), who found the winter

https://doi.org/10.5194/wcd-2020-50
Preprint. Discussion started: 12 October 2020

Weather and Climate Dynamics Discussions
Open Access
EGU

precipitation in the Northern Hemisphere to be associated with extratropical cyclones. They also showed that the contribution of cyclones in the Gulf Stream region accounts for 55-80% of the total DJF precipitation. This considerable fraction suggests that precipitation should significantly shift equatorward along with the cyclone track density, which is consistent with our analysis (Figs. 4a, 8c).

In the Kuroshio region we note a rather equal influence of the SST smoothing on precipitation when cyclones are present or absent. These differences mainly concern the large-scale precipitation and are more evident to the east of the Kuroshio region in the no-cyclone case (Fig. 8h), forming a dipole of reduced precipitation to the north and increased precipitation to the south, similar to the Atlantic (Fig. 8d). Interestingly, we note a slightly higher decrease of large-scale precipitation (approx. 0.25 mm day^{-1}) when cyclones are present in the Kuroshio region, which is most likely related to a diminished cyclone density in SMTHK compared to CNTL (Fig. 4c).

3.4.3 Specific Humidity at 850 hPa

Higher values of specific humidity are observed to the south of the Gulf Stream and Kuroshio region (Fig. 9a,e) due to the Clausius-Clapeyron relation with higher SSTs (Fig. 1a,d). The specific humidity maximum exceeds 6 g kg^{-1} in the Gulf Stream region, while lower maximum values (5 g kg^{-1}) are found in the southeastern part of the Kuroshio region (Fig. 9a,e). The values are comparable to ERA-Interim (Fig. A2b,e).

Analogous to the surface heat fluxes (Fig. 7b,f), smoothing the SST causes a noticeable decrease in specific humidity to the south of the SST front (Fig. 9b,f), where the SSTs are lower than in CNTL (Fig. 1c,f). The decrease in specific humidity is more pronounced in the Gulf Stream region, following the larger SST decrease in the Atlantic when the SSTs are smoothed. Our findings are consistent with the results of Zhang et al. (2020), who analysed the meridional eddy specific humidity flux instead of specific humidity.

For specific humidity, cyclones account only for a small part of the climatological differences between CNTL and SMTHG (Fig. 9c,d). In addition to the larger amplitudes of the differences when no cyclones are present in the Gulf Stream, also the structure is slightly different, with the negative anomalies being more zonally oriented than when cyclones propagate in the region. In the presence of cyclones, specific humidity is generally reduced in SMTHG (Fig. 9c). In contrast, in the absence of cyclones, a slight increase in specific humidity is evident to the north of the SST front, where the smoothing leads to an SST increase (Fig. 9d). The largest differences in Fig. 9d arise towards the warm flank of the climatological SST front and are clearly related to the largest decrease in the SST between SMTHG and CNTL (Fig. 1c). The more pronounced decrease of specific humidity in the absence of cyclones in the Gulf Stream region resembles the decrease in surface heat fluxes (Fig. 7c,d), which was also larger in the absence of cyclones.

In the Kuroshio region, the difference in specific humidity (Fig. 9f) is distributed more equally between time-steps with and without cyclones present (Fig. 9g,h). Indeed, cyclones even contribute more to the reduction in specific humidity in the southern half of the Kuroshio region (Fig. 9g) than no-cyclone time-steps (Fig. 9h). The reduction in specific humidity likely explains the reduction of large-scale precipitation in the same location (Fig. 8g,h). Nonetheless, in absolute terms these differences remain small.

https://doi.org/10.5194/wcd-2020-50
Preprint. Discussion started: 12 October 2020

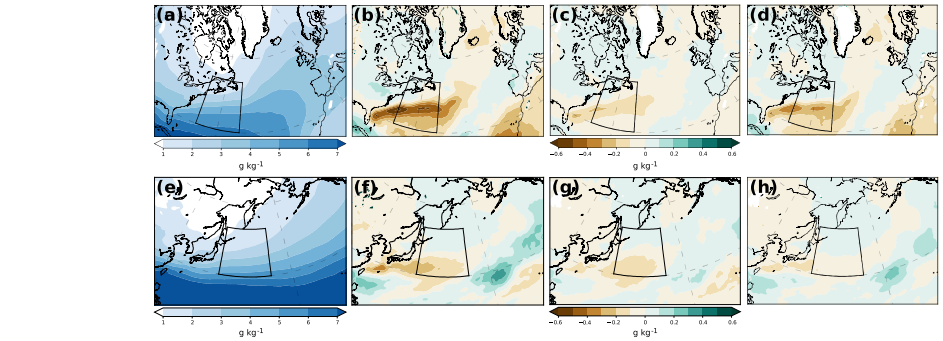

Figure 9. (a) Climatological specific humidity at 850 hPa (shading, g kg^{-1}) for the North Atlantic for CNTL. (b) Difference of climatological specific humidity between SMTHG and CNTL. (c,d) As (b), but only considering the dates with (c) or without (d) cyclones being present in the Gulf Stream region. (e-h) As (a-d), but for the Kuroshio region. The Gulf Stream and Kuroshio regions are marked with a black box, respectively. Panels (c,d,g,h) are scaled such that their sum yields panels (b) and (f), respectively.

We hypothesise that the different distribution of specific humidity between the dates with and without cyclones in the two regions arises from the different ratios of cyclones being present or absent in the Gulf Stream and the Kuroshio region, respectively. Cyclones are present in the Gulf Stream region in about 30% of the time-steps, whereas the respective percentage is higher in the Kuroshio region (about %40 of the time-steps). Therefore, the less pronounced decrease in humidity in the cyclone days in the Atlantic is most likely related to the smaller amount of time-steps, whereas the more equal split in decrease of specific humidity in the Pacific is attributable to the more equal split into cyclone/no-cyclone days.

Apart from the well-established Clausius-Clapeyron relationship between SSTs and moisture, several studies indicate the leading role of cyclones on the poleward transport of moisture (e.g., Peixoto and Oort, 1992; Nakamura et al., 2004; Chang and Song, 2006; Newman et al., 2012). However, based on the subdivision of the winter climatology into cyclone/no-cyclone dates, our results support instead that the SST is the dominating factor determining the distribution of specific humidity, with cyclones playing only a modulating role.

3.4.4 Upper-level Wind Speed at 300 hPa

In CNTL, the strongest climatological winds reach 40 m s^{-1} in the Gulf Stream region and occur in a southwest (SW) to northeast (NE) tilted band (Fig. 10a) that is located close to the position of the SST front (Fig. 3a). In the Kuroshio region, the climatological jet is more zonal than in the North Atlantic, exceeds 60 m s^{-1} (Fig. 10e), and is located somewhat to the south of the SST front (Fig. 3b). As for almost all the other fields, there is a good agreement between ERA-Interim and the AFES

https://doi.org/10.5194/wcd-2020-50
Preprint. Discussion started: 12 October 2020

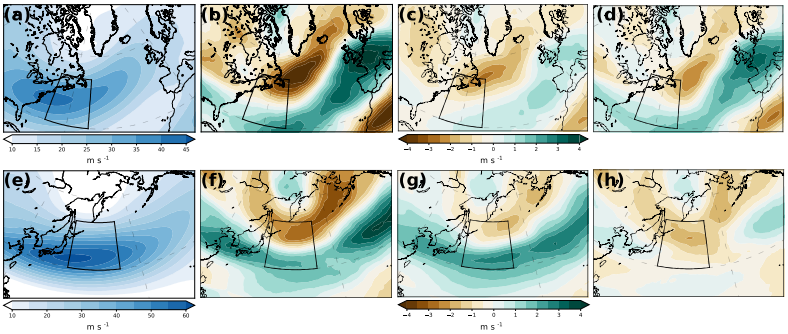

Figure 10. (a) Climatological wind speed at 300 hPa (shading, m s^{-1}) for the North Atlantic for CNTL. (b) Difference of the wind speed climatology between SMTHG and CNTL. (c,d) As (b), but only considering the dates with (c) and without (d) cyclones being present in the Gulf Stream region. (e-h) As (a-d), but for the Kuroshio region. The Gulf Stream and Kuroshio regions are marked with a black box, respectively. Panels (c,d,g,h) are scaled such that their sum yields panels (b) and (f), respectively.

simulations, with a slightly reduced maximum wind speed in the Gulf Stream region (approx. 5 m s^{-1}) and the maximum wind speed being geographically less extended over the North Pacific in the AFES climatology compared to ERA-Interim (compare Fig. 10a,e and Fig. A2c,f).

In both basins, we observe decreasing (increasing) wind speeds to the north (south) of the climatological jet position after the SST smoothing (Fig. 10b,f). This dipole is more pronounced downstream, in the central and eastern North Atlantic and Pacific, respectively. Kuwano-Yoshida and Minobe (2017) documented a similar difference pattern for the North Pacific jet.

The presence (Fig. 10c) or absence (Fig. 10d) of cyclones in the Gulf Stream region does not have a considerable imprint on the distribution of the observed upper-level wind speed differences, with dates with cyclones present accounting for less of the climatological wind differences. In the Pacific, however, the contribution from cyclones determines the overall dipolar structure of the wind speed differences (Fig. 10f-h). In contrast, in the absence of cyclones, wind speeds are reduced throughout the Kuroshio region as well as in most parts of the North Pacific (Fig. 10h).

This discrepancy between the contributions of cyclones in the North Atlantic versus North Pacific response to the smoothed SSTs might arise from the different relative shifts of cyclones and jets in these sectors (Fig. 4). Whereas cyclones and jets shift southward in tandem in the North Atlantic, it is mainly the cyclones that shift southward in the North Pacific, while the North Pacific jet intensifies in-place. Thus, the smoothed SSTs in the Kuroshio region allow cyclones to propagate closer to the

https://doi.org/10.5194/wcd-2020-50
Preprint. Discussion started: 12 October 2020

climatological position of the Pacific jet, thereby intensifying its eddy-driven component, while reducing the occurrence of a separate eddy-driven jet further north. This interpretation explains both the observed focusing and strengthening of the Pacific jet (Figs. 4d, 10f), and the larger contribution of cyclones to the upper-level response to the smoothed SSTs (Fig. 10g,h).

4 Conclusions

We quantified and attributed differences in the atmospheric response when using realistic (CNTL) and smooth SSTs for the North Atlantic (SMTHG) and North Pacific (SMTHK), respectively, based on simulations with the AFES 3 model. The CNTL simulation compares well to ERA-Interim, except for considerably larger latent heat fluxes in CNTL, but these are most likely associated with the lower SST resolution in ERA-Interim prior to 2002. Given the stronger SST gradient in the Atlantic, the effect of the smoothing on the SST front yields stronger SST differences between CNTL and the respective smooth experiments (see Fig. 1c,f) as well as a distinctly stronger reduction of the SST gradient in the Atlantic compared to the Pacific (see Fig. 2c,f).

We first examined the impact of the smoothing of the SST on the intensification of individual cyclones. Considering only cyclones with a maximum intensification in the Gulf Stream or the Kuroshio region, we classified them into 3 categories based on their propagation relative to the SST front, where cyclones either always stay on the cold (C1) or warm (C2) side of the SST front or they cross the SST front from the warmer to the colder side (C3). Similar deepening rates for all these cyclone-categories across all experiments reveal the rather minor role of the SST gradient on the intensification of individual cyclones. This result is valid for both ocean basins, though it is particularly relevant for the Gulf Stream region where the SST smoothing dramatically weakens the strong SST gradient.

Considering all cyclones propagating in either the North Atlantic or the North Pacific, we found the cyclone density in the storm track to decrease when the SSTs are smoothed in the Kuroshio and even more so in the Gulf Stream region. We relate the different response of the cyclone densities for the two regions to the more pronounced reduction of the SST gradient in SMTHG for the Atlantic compared to SMTHK for the Pacific. Overall, we observe an equator-ward shift in cyclone density in both regions, which is more pronounced over the central and eastern ocean basins. Both cyclone density differences have a distinct SW-NE tilt, basically following the storm track. An analogous southward shift is observed in the upper-level jet for the North Atlantic, whereas for the North Pacific such a shift is absent and the difference between the experiments instead reveals a more meridionally focused and zonally extended jet for smoother SST.

We found a considerable decrease of both latent and sensible heat fluxes along the SST front when smoothing the SSTs, which was more pronounced across the SST front in the Gulf Stream region compared to the Kuroshio. Analogous to the surface heat fluxes, precipitation in the Gulf Stream region is strongly reduced when smoothing the SST front, which is particularly evident for convective precipitation on the warm side of the Gulf Stream SST front. However, both types of precipitation are only slightly affected by the SST smoothing in the Kuroshio region. Differences in specific humidity at 850 hPa feature a similar reduction after smoothing the SST. The weaker reduction of moisture and precipitation in the Kuroshio region is

https://doi.org/10.5194/wcd-2020-50
Preprint. Discussion started: 12 October 2020

related to the smaller differences in the SST and SST front between CNTL and the smoothed fields in the Pacific compared the Atlantic.

To clarify whether the differences between the realistic and smooth experiments stem directly from differences in the SST or from the occurrence of cyclones, we subdivided the winter climatology into days with and without cyclones present in the Gulf Stream or Kuroshio region. We found the contribution from time-steps without cyclones in the Gulf Stream or Kuroshio region to more closely resemble the climatological differences in surface heat fluxes. Differences in precipitation, however, were more closely associated with cyclones being present in the Gulf Stream or Kuroshio region.

Differences in specific humidity in the Gulf Stream region between CNTL and SMTHG are mainly attributable to days when cyclones are not present in the region. For the Kuroshio, however, the differences are almost equally attributed between time-steps with and without cyclones present in the region. Likewise, while cyclones in the Gulf Stream region do not seem to have a considerable imprint on the differences in the upper-level wind, differences in the Kuroshio region are mainly attributable to time-steps when cyclones are present. We associate this discrepancy between the two basins to cyclones in the Pacific propagating more closely to the climatological jet position in SMTHK, thereby intensifying its eddy-driven component.

Overall, our analysis highlights that SST fronts only have a minor impact on the characteristics and intensification of individual cyclones propagating in the Gulf Stream or Kuroshio region. Nevertheless, we found a large-scale response with decreased cyclone density as well as an equator-ward shift of cyclone densities associated with the SST smoothing. Analogously, the upper-level jet shifts equator-ward in the North Atlantic, while the Pacific jet strengthens and extends more zonally eastward along its climatological location, which can be associated with the more collocated storm track. The effect of the SST smoothing was stronger in the Gulf Stream region, where the smoothing has a larger impact on the climatologically sharper SST front. Subdividing time-steps into those with and without cyclones in the two regions underlined the leading role of the SST to explain the differences in the heat fluxes, specific humidity, and convective precipitation, with cyclones generally playing a secondary modulating role.

Code availability. The codes to construct the figures in this study is available upon request.

Data availability. ERA-Interim data are provided by European Centre for Medium-Range Weather Forecasts (ECMWF) available online at https://www.ecmwf.int/en/forecasts/datasets/ reanalysis-datasets/era-interim (Dee et al., 2011)

Author contributions. LT carried out the bulk of the data analysis and writing. TS contributed to detailed discussion about the methods and interpretation of the findings as well as to the writing process. CS contributed to both data analysis and writing.

https://doi.org/10.5194/wcd-2020-50
Preprint. Discussion started: 12 October 2020

Weather and Climate Dynamics Discussions
Open Access
EGU

Competing interests. The authors declare that they have no conflict of interest.

Appendix A: ERA-INTERIM CLIMATOLOGIES AND CYCLONES LOCATION

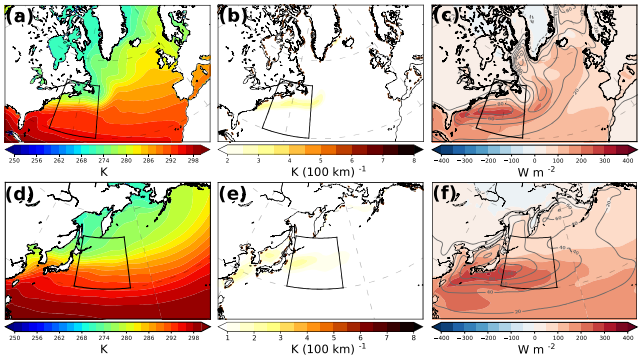

Figure A1. (a) DJF climatology over ERA-Interim period 1982-2000 for (a) the SSTs (K), (b) the SST gradient (K (100 km)$^{-1}$), (c) the latent (shading, W m^{-2}) and sensible heat fluxes (contours, W m^{-2}) for the North Atlantic. (d-f) As (a-c), but for the North Pacific. The Gulf Stream and Kuroshio regions are marked with a black box, respectively.

Acknowledgements. We thank ECMWF for providing the ERA-Interim data and Akira Kuwano-Yoshida and Akira Yamazaki, who provided the AFES 3 data. The AFES 3 data was supported by the Grant-in-Aid for Scientific Research on Innovative Areas 22106008 ("A 'hot spot' in the climate system: Extra-tropical air–sea interaction under the East Asian monsoon system") from the Ministry of Education, Culture, Sports, Science, and Technology of Japan, and calculated using the Earth Simulator under JAMSTEC support.

https://doi.org/10.5194/wcd-2020-50
Preprint. Discussion started: 12 October 2020

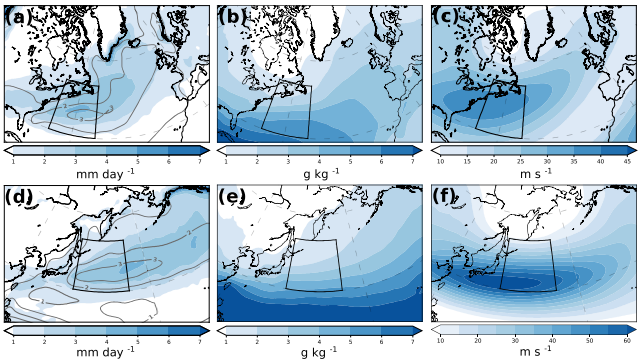

Figure A2. (a) DJF climatology over ERA-Interim period 1982-2000 for (a) the large-scale precipitation (shading, mm day^{-1}) and the convective precipitation (contours, mm day^{-1}) , (b), the specific humidity at 850 hPa (g kg^{-1}) and (c) the wind speed at 300 hPa (m s^{-1}) for the North Atlantic. (d-f) As (a-c), but for the North Pacific. The Gulf Stream and Kuroshio regions are marked with a black box, respectively.

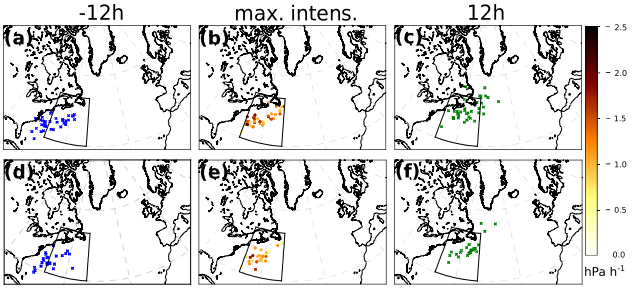

Figure A3. Locations of cyclones for C3 in the North Atlantic, (a) 12 hours prior to maximum intensification (blue crosses), (b) at the time of maximum intensification (dots colored depending on their pressure tendency, (hPa h^{-1})) and (c) 12 hours past maximum intensification (green crosses) in the CNTL experiment. (d-f) As (a-c), but for the SMTHG experiment. The Gulf Stream region is marked with a black box.

https://doi.org/10.5194/wcd-2020-50
Preprint. Discussion started: 12 October 2020

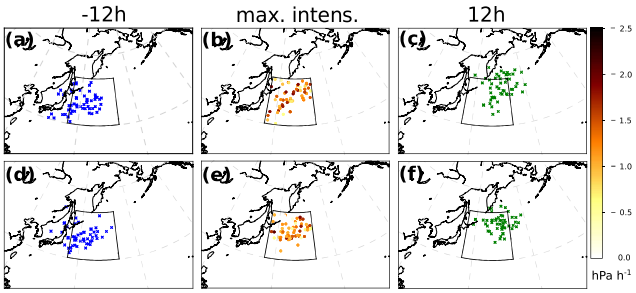

Figure A4. Locations of cyclones for C3 in the North Pacific, (a) 12 hours prior to maximum intensification (blue crosses), (b) at the time of maximum intensification (dots colored depending on their pressure tendency, (hPa h^{-1})) and (c) 12 hours past maximum intensification (green crosses) in the CNTL experiment. (d-f) As (a-c), but for the SMTHK experiment. The Kuroshio region is marked with a black box.

https://doi.org/10.5194/wcd-2020-50
Preprint. Discussion started: 12 October 2020

Weather and Climate Dynamics Discussions
Open Access
EGU

References

Alexander, M. A. and Scott, J. D.: Surface flux variability over the North Pacific and North Atlantic oceans, Journal of climate, 10, 2963–2978, 1997.

Berry, G., Reeder, M. J., and Jakob, C.: A global climatology of atmospheric fronts, Geophys. Res. Lett., 38, L04 809, https://doi.org/10.1029/2010GL046451, 2011.

Bjerknes, J.: Life cycle of cyclones and the polar front theory of atmospheric circulation, Geophys. Publik., 3, 1–18, 1922.

Booth, J. F., Thompson, L., Patoux, J., and Kelly, K. A.: Sensitivity of Midlatitude Storm Intensification to Perturbations in the Sea Surface Temperature near the Gulf Stream, Mon. Wea. Rev., 140, 1241–1256, https://doi.org/10.1175/MWR-D-11-00195.1, 2012.

Brayshaw, D. J., Hoskins, B., and Blackburn, M.: The basic ingredients of the North Atlantic storm track. Part I: Land–sea contrast and orography., J. Atmos. Sci., 66, 2539–2558, https://doi.org/10.1175/2009JAS3078.1, 2009.

Chang, E. K. and Song, S.: The seasonal cycles in the distribution of precipitation around cyclones in the western North Pacific and Atlantic, Journal of the atmospheric sciences, 63, 815–839, 2006.

Chen, G., Plumb, R. A., and Lu, J.: Sensitivities of zonal mean atmospheric circulation to SST warming in an aqua-planet model, Geophysical Research Letters, 37, 2010.

Dacre, H. F., Josey, S. A., and Grant, A. L.: Extratropical cyclone induced sea surface temperature anomalies in the 2013/14 winter, Weather Clim. Dyn., 1, 27–44, https://doi.org/10.5194/wcd-1-27-2020, 2020.

de Vries, H., Scher, S., Haarsma, R., Drijfhout, S., and Van Delden, A.: How Gulf-Stream SST-fronts influence Atlantic winter storms, Climate Dyn., 52, 5899–5909, https://doi.org/10.1007/s00382-018-4486-7, 2019.

Dee, D. P., Uppala, S. M., Simmons, A. J., Berrisford, P., Poli, P., Kobayashi, S., Andrae, U., Balmaseda, M. A., Balsamo, G., Bauer, P., Bechtold, P., Beljaars, A. C. M., van de Bergd, L., Bidlot, J., Bormann, N., Delsol, C., Dragani, R., Fuentes, M., Geer, A. J., Haimberger, L., Healy, S. B., Hersbach, H., Holm, E. V., Isaksen, L., Kållberg, P., M. Köhler, M. M., McNally, A. P., Monge-Sanz, B. M., Morcrette, J.-J., Park, B.-K., Peubey, C., de Rosnay, P., Tavolato, C., Thepaut, J.-N., and Vitart, F.: The ERA-Interim reanalysis: configuration and performance of the data assimilation system, Quart. J. Roy. Meteor. Soc., 137, 553–587, https://doi.org/10.1002/qj.828, 2011.

Enomoto, T., Kuwano-Yoshida, A., Komori, N., and Ohfuchi, W.: Description of AFES 2: Improvements for high-resolution and coupled simulations, in: High Resolution Numerical Modelling of the Atmosphere and Ocean, pp. 77–97, Springer, 2008.

Evans, M. S., Keyser, D., Bosart, L. F., and Lackmann, G. M.: A satellite-derived classification scheme for rapid maritime cyclogenesis, Monthly weather review, 122, 1381–1416, 1994.

Hawcroft, M., Shaffrey, L., Hodges, K., and Dacre, H.: How much Northern Hemisphere precipitation is associated with extratropical cyclones?, Geophysical Research Letters, 39, https://doi.org/10.1029/2012GL053866, 2012.

Holton, J. R. and Hakim, G. J.: An Introduction to Dynamic Meteorology, Academic Press, 2012.

Hoskins, B. J. and Hodges, K. I.: New perspectives on the Northern Hemisphere winter storm tracks, J. Atmos. Sci., 59, 1041–1061, https://doi.org/10.1175/1520-0469(2002)059<1041:NPOTNH>2.0.CO;2, 2002.

Hoskins, B. J. and Valdes, P. J.: On the existence of storm-tracks, Journal of the atmospheric sciences, 47, 1854–1864, 1990.

Hotta, D. and Nakamura, H.: On the significance of sensible heat supply from the ocean in the maintenance of mean baroclinicity along storm tracks, J. Climate, 24, 3377–3401, https://doi.org/10.1175/2010JCLI3910.1, 2011.

Jacobs, N., Raman, S., Lackmann, G., and Childs Jr, P.: The influence of the Gulf Stream induced SST gradients on the US East Coast winter storm of 24–25 January 2000, Int. J. Remote Sens., 29, 6145–6174, https://doi.org/10.1080/01431160802175561, 2008.

https://doi.org/10.5194/wcd-2020-50
Preprint. Discussion started: 12 October 2020

Jenkner, J., Sprenger, M., Schwenk, I., Schwierz, C., Dierer, S., and Leuenberger, D.: Detection and climatology of fronts in a high-resolution model reanalysis over the Alps, Meteorol. Appl., 17, 1–18, https://doi.org/10.1002/met.142, 2010.

Joyce, T. M., Kwon, Y.-O., and Yu, L.: On the relationship between synoptic wintertime atmospheric variability and path shifts in the Gulf Stream and the Kuroshio Extension, Journal of Climate, 22, 3177–3192, 2009.

Kuwano-Yoshida, A. and Minobe, S.: Storm-track response to SST fronts in the northwestern Pacific region in an AGCM, Journal of Climate, 30, 1081–1102, 2017.

Kuwano-Yoshida, A., Enomoto, T., and Ohfuchi, W.: An improved PDF cloud scheme for climate simulations, Quarterly Journal of the Royal Meteorological Society, 136, 1583–1597, 2010a.

Kuwano-Yoshida, A., Minobe, S., and Xie, S.-P.: Precipitation response to the Gulf Stream in an atmospheric GCM, Journal of Climate, 23, 3676–3698, 2010b.

Ma, X., Chang, P., Saravanan, R., Montuoro, R., Hsieh, J.-S., Wu, D., Lin, X., Wu, L., and Jing, Z.: Distant influence of Kuroshio eddies on North Pacific weather patterns?, Scientific reports, 5, 17 785, 2015.

Ma, X., Chang, P., Saravanan, R., Montuoro, R., Nakamura, H., Wu, D., Lin, X., and Wu, L.: Importance of resolving Kuroshio front and eddy influence in simulating the North Pacific storm track, Journal of Climate, 30, 1861–1880, 2017.

Masunaga, R., Nakamura, H., Miyasaka, T., Nishii, K., and Tanimoto, Y.: Separation of climatological imprints of the Kuroshio Extension and Oyashio fronts on the wintertime atmospheric boundary layer: Their sensitivity to SST resolution prescribed for atmospheric reanalysis, Journal of Climate, 28, 1764–1787, 2015.

Meinen, C. S. and Luther, D. S.: Structure, transport, and vertical coherence of the Gulf Stream from the Straits of Florida to the Southeast Newfoundland Ridge, Deep-Sea Res. Pt. I, 112, 137–154, https://doi.org/10.1016/j.dsr.2016.03.002, 2016.

Michel, C., Terpstra, A., and Spengler, T.: Polar mesoscale cyclone climatology for the Nordic Seas based on ERA-Interim, J. Climate, 31, 2511–2532, https://doi.org/10.1175/JCLI-D-16-0890.1, 2018.

Minobe, S., Kuwano-Yoshida, A., Komori, N., Xie, S.-P., and Small, R. J.: Influence of the Gulf Stream on the troposphere, Nature, 452, 206–210, https://doi.org/10.1038/nature06690, 2008.

Murray, R. J. and Simmonds, I.: A numerical scheme for tracking cyclone centres from digital data. Part I: Development and operation of the scheme, Aust. Met. Mag., 39, 155–166, 1991a.

Murray, R. J. and Simmonds, I.: A numerical scheme for tracking cyclone centres from digital data. Part II: application to January and July general circulation model simulations, Aust. Met. Mag., 39, 167–180, 1991b.

Nakamura, H.: Midwinter suppression of baroclinic wave activity in the Pacific, Journal of the atmospheric sciences, 49, 1629–1642, 1992.

Nakamura, H., Sampe, T., Tanimoto, Y., and Shimpo, A.: Observed associations among storm tracks, jet streams and midlatitude oceanic fronts, Geoph. Monog. Series, 147, 329–345, https://doi.org/10.1029/147GM18, 2004.

Nakamura, H., Sampe, T., Goto, A., Ohfuchi, W., and Xie, S.-P.: On the importance of midlatitude oceanic frontal zones for the mean state and dominant variability in the tropospheric circulation, Geophysical Research Letters, 35, 2008.

Newman, M., Kiladis, G. N., Weickmann, K. M., Ralph, F. M., and Sardeshmukh, P. D.: Relative contributions of synoptic and low-frequency eddies to time-mean atmospheric moisture transport, including the role of atmospheric rivers, Journal of climate, 25, 7341–7361, 2012.

Ogawa, F. and Spengler, T.: Prevailing Surface Wind Direction during Air–Sea Heat Exchange, J. Climate, 32, 5601–5617, https://doi.org/10.1175/JCLI-D-18-0752.1, 2019.

Ogawa, F., Nakamura, H., Nishii, K., Miyasaka, T., and Kuwano-Yoshida, A.: Dependence of the climatological axial latitudes of the tropospheric westerlies and storm tracks on the latitude of an extratropical oceanic front, Geophysical research letters, 39, 2012.

https://doi.org/10.5194/wcd-2020-50
Preprint. Discussion started: 12 October 2020

Ohfuchi, W., Nakamura, H., Yoshioka, M. K., Enomoto, T., Takaya, K., Peng, X., Yamane, S., Nishimura, T., Kurihara, Y., Ninomiya, K., et al.: 10-km mesh meso-scale resolving simulations of the global atmosphere on the Earth Simulator: Preliminary outcomes of AFES (AGCM for the Earth Simulator), J. Earth Simulator, 1, 8–34, 2004.

O'Reilly, C. H., Minobe, S., Kuwano-Yoshida, A., and Woollings, T.: The Gulf Stream influence on wintertime North Atlantic jet variability, Quarterly Journal of the Royal Meteorological Society, 143, 173–183, 2017.

Papritz, L. and Spengler, T.: Analysis of the slope of isentropic surfaces and its tendencies over the North Atlantic, Quart. J. Roy. Meteor. Soc., 141, 3226–3238, https://doi.org/10.1002/qj.260, 2015.

Parfitt, R., Czaja, A., Minobe, S., and Kuwano-Yoshida, A.: The atmospheric frontal response to SST perturbations in the Gulf Stream region, Geophys. Res. Lett., 43, 2299–2306, https://doi.org/10.1002/2016GL067723, 2016.

Parfitt, R., Czaja, A., and Kwon, Y.-O.: The impact of SST resolution change in the ERA-Interim reanalysis on wintertime Gulf Stream frontal air-sea interaction, Geophysical Research Letters, 44, 3246–3254, 2017.

Peixoto, J. P. and Oort, A. H.: Physics of climate, 1992.

Pfahl, S. and Wernli, H.: Quantifying the relevance of cyclones for precipitation extremes, Journal of Climate, 25, 6770–6780, 2012.

Piazza, M., Terray, L., Boé, J., Maisonnave, E., and Sanchez-Gomez, E.: Influence of small-scale North Atlantic sea surface temperature patterns on the marine boundary layer and free troposphere: A study using the atmospheric ARPEGE model, Climate dynamics, 46, 1699–1717, 2016.

Reynolds, R. W., Smith, T. M., Liu, C., Chelton, D. B., Casey, K. S., and Schlax, M. G.: Daily high-resolution-blended analyses for sea surface temperature, Journal of Climate, 20, 5473–5496, 2007.

Riviere, G. and Joly, A.: Role of the low-frequency deformation field on the explosive growth of extratropical cyclones at the jet exit. Part II: Baroclinic critical region, Journal of the atmospheric sciences, 63, 1982–1995, 2006.

Rudeva, I. and Gulev, S. K.: Composite analysis of North Atlantic extratropical cyclones in NCEP–NCAR reanalysis data, Mon. Wea. Rev., 139, 1419–1446, https://doi.org/10.1175/2010MWR3294.1, 2011.

Ruprecht, E., Schröder, S. S., and Ubl, S.: On the relation between NAO and water vapour transport towards Europe, Meteorologische Zeitschrift, 11, 395–401, 2002.

Sampe, T., Nakamura, H., Goto, A., and Ohfuchi, W.: Significance of a midlatitude SST frontal zone in the formation of a storm track and an eddy-driven westerly jet, Journal of Climate, 23, 1793–1814, 2010.

Sanders, F.: Explosive cyclogenesis in the west-central North Atlantic Ocean, 1981–84. Part I: Composite structure and mean behavior, Mon. Wea. Rev., 114, 1781–1794, https://doi.org/10.1175/1520-0493(1986)114<1781:ECITWC>2.0.CO;2, 1986.

Sanders, F. and Gyakum, J. R.: Synoptic-dynamic climatology of the "bomb", Mon. Wea. Rev., 108, 1589–1606, https://doi.org/10.1175/1520-0493(1980)108<1589:SDCOT>2.0.CO;2, 1980.

Schemm, S., Rudeva, I., and Simmonds, I.: Extratropical fronts in the lower troposphere–global perspectives obtained from two automated methods, Quart. J. Roy. Meteor. Soc., 141, 1686–1698, https://doi.org/10.1002/qj.2471, 2015.

Schultz, D. M., Keyser, D., and Bosart, L. F.: The effect of large-scale flow on low-level frontal structure and evolution in midlatitude cyclones, Monthly weather review, 126, 1767–1791, 1998.

Sinclair, M. R. and Revell, M. J.: Classification and composite diagnosis of extratropical cyclogenesis events in the southwest Pacific, Mon. Wea. Rev., 128, 1089–1105, https://doi.org/10.1175/1520-0493(2000)128<1089:CACDOE>2.0.CO;2, 2000.

Small, R. J., Tomas, R. A., and Bryan, F. O.: Storm track response to ocean fronts in a global high-resolution climate model, Climate dynamics, 43, 805–828, 2014.

https://doi.org/10.5194/wcd-2020-50
Preprint. Discussion started: 12 October 2020

Spensberger, C. and Spengler, T.: Feature-based Jet Variability in the Upper Troposphere, Journal of Climate, p. submitted, 2020.

Spensberger, C., Spengler, T., and Li, C.: Upper-tropospheric jet axis detection and application to the boreal winter 2013/14, Monthly Weather Review, 145, 2363–2374, 2017.

Tanimoto, Y., Nakamura, H., Kagimoto, T., and Yamane, S.: An active role of extratropical sea surface temperature anomalies in determining anomalous turbulent heat flux, Journal of Geophysical Research: Oceans, 108, 2003.

Tozuka, T., Ohishi, S., and Cronin, M. F.: A metric for surface heat flux effect on horizontal sea surface temperature gradients, Climate Dynamics, 51, 547–561, 2018.

Tsopouridis, L., Spensberger, C., and Spengler, T.: Characteristics of Cyclones Following Different Pathways in the Gulf Stream Region, Quarterly Journal of the Royal Meteorological Society;1-16, https://doi.org/10.1002/qj.3924, 2020a.

Tsopouridis, L., Spensberger, C., and Spengler, T.: Cyclone Intensification in the Kuroshio Region and its relation to the Sea Surface Temperature Front and Upper-Level Forcing, Quarterly Journal of the Royal Meteorological Society, https://doi.org/10.1002/qj.3929, 2020b.

Uccellini, L. W., Kocin, P. J., Petersen, R. A., Wash, C. H., and Brill, K. F.: The Presidents' Day cyclone of 18–19 February 1979: Synoptic overview and analysis of the subtropical jet streak influencing the pre-cyclogenetic period, Monthly weather review, 112, 31–55, 1984.

Vanniere, B., Czaja, A., Dacre, H. F., and Woollings, T.: A "Cold Path" for the Gulf Stream–Troposphere Connection, J. Climate, 30, 1363–1379, https://doi.org/10.1175/JCLI-D-15-0749.1, 2017.

Wang, C.-C. and Rogers, J. C.: A composite study of explosive cyclogenesis in different sectors of the North Atlantic. Part I: Cyclone structure and evolution, Mon. Wea. Rev., 129, 1481–1499, https://doi.org/10.1175/1520-0493(2001)129<1481:ACSOEC>2.0.CO;2, 2001.

Wang, L., Hu, H., and Yang, X.: The atmospheric responses to the intensity variability of subtropical front in the wintertime North Pacific, Climate Dynamics, 52, 5623–5639, 2019.

Yao, Y., Zhong, Z., and Yang, X.-Q.: Impacts of the subarctic frontal zone on the North Pacific storm track in the cold season: an observational study, International Journal of Climatology, 38, 2554–2564, 2018.

Yoshida, A. and Asuma, Y.: Structures and environment of explosively developing extratropical cyclones in the northwestern Pacific region, Monthly Weather Review, 132, 1121–1142, 2004.

Zhang, C., Liu, H., Xie, J., Lin, P., Li, C., Yang, Q., and Song, J.: North Pacific storm track response to the mesoscale SST in a global high-resolution atmospheric model, Climate Dynamics, 55, 1597–1611, 2020.

Zolina, O. and Gulev, S. K.: Synoptic variability of ocean–atmosphere turbulent fluxes associated with atmospheric cyclones, Journal of climate, 16, 2717–2734, 2003.

Bibliography

Allen, M. R., and W. J. Ingram (2002), Constraints on future changes in climate and the hydrologic cycle, *Nature*, *419*(6903), 228–232. 3.3

Baehr, C., B. Pouponneau, F. Ayrault, and A. Joly (1999), Dynamical characterization of the fastex cyclogenesis cases, *Quarterly Journal of the Royal Meteorological Society*, *125*(561), 3469–3494. 1.3.1

Bengtsson, L., K. I. Hodges, and E. Roeckner (2006), Storm tracks and climate change, *Journal of Climate*, *19*(15), 3518–3543. 1.2

Bjerknes, J. (1919), On the structure of moving cyclones, *Monthly Weather Review*, *47*(2), 95–99. 1.3

Bjerknes, J., and H. Solberg (1922), Life cycle of cyclones and the polar front theory of atmospheric circulation, *Geophys. Publik.*, *3*, 1–18. 1.3

Blackmon, M. L. (1976), A climatological spectral study of the 500 mb geopotential height of the northern hemisphere, *Journal of the Atmospheric Sciences*, *33*(8), 1607–1623. 1.2

Blackmon, M. L., J. M. Wallace, N.-C. Lau, and S. L. Mullen (1977), An observational study of the northern hemisphere wintertime circulation, *Journal of the Atmospheric Sciences*, *34*(7), 1040–1053. 1.2

Blackmon, M. L., Y. Lee, and J. M. Wallace (1984), Horizontal structure of 500 mb height fluctuations with long, intermediate and short time scales, *Journal of the atmospheric sciences*, *41*(6), 961–980. 1.2

Booth, J. F., L. A. Thompson, J. Patoux, K. A. Kelly, and S. Dickinson (2010), The signature of the midlatitude tropospheric storm tracks in the surface winds, *Journal of Climate*, *23*(5), 1160–1174. 1.1

Booth, J. F., L. Thompson, J. Patoux, and K. A. Kelly (2012), Sensitivity of midlatitude storm intensification to perturbations in the sea surface temperature near the Gulf Stream, *Mon. Wea. Rev.*, *140*, 1241–1256, doi:10.1175/MWR-D-11-00195.1. 1.3.1

Brayshaw, D. J. (2006), Large scale forcing of the north atlantic storm track, Ph.D. thesis, University of Reading. 1.1, 1.2

Brayshaw, D. J., B. Hoskins, and M. Blackburn (2008), The storm-track response to idealized sst perturbations in an aquaplanet gcm, *Journal of the Atmospheric Sciences*, *65*(9), 2842–2860. 1.2

Brayshaw, D. J., B. Hoskins, and M. Blackburn (2009), The basic ingredients of the North Atlantic storm track. Part I: Land–sea contrast and orography., *J. Atmos. Sci.*, *66*, 2539–2558, doi:10.1175/2009JAS3078.1. 1.2, 1.3.1

Brayshaw, D. J., B. Hoskins, and M. Blackburn (2011), The basic ingredients of the north atlantic storm track. part ii: Sea surface temperatures, *Journal of the Atmospheric Sciences*, *68*(8), 1784–1805. 1.2

Broccoli, A. J., and S. Manabe (1992), The effects of orography on midlatitude northern hemisphere dry climates, *Journal of Climate*, *5*(11), 1181–1201. 1.2

Catto, J., C. Jakob, G. Berry, and N. Nicholls (2012), Relating global precipitation to atmospheric fronts, *Geophysical Research Letters*, *39*(10). 1.3

Catto, J. L., L. C. Shaffrey, and K. I. Hodges (2010), Can climate models capture the structure of extratropical cyclones?, *Journal of Climate*, *23*(7), 1621–1635. 1.2

Centurioni, L. R., P. P. Niiler, and D.-K. Lee (2004), Observations of inflow of philippine sea surface water into the south china sea through the luzon strait, *Journal of Physical Oceanography*, *34*(1), 113–121. 1.1

Chagnon, J. M., and S. L. Gray (2015), A diabatically generated potential vorticity structure near the extratropical tropopause in three simulated extratropical cyclones, *Monthly Weather Review*, *143*(6), 2337–2347. 1.3.1

Chang, E. K. (2003), Midwinter suppression of the pacific storm track activity as seen in aircraft observations, *Journal of the atmospheric sciences*, *60*(11), 1345–1358. 1.2

Chang, E. K., S. Lee, and K. L. Swanson (2002), Storm track dynamics, *Journal of climate*, *15*(16), 2163–2183. 1.2, 1.3

Charney, J. (1947), The dynamics of long waves in a westerly baroclinic current, *J. Meteor*, *4*, 135–163. 1.3

Chelton, D. B., M. G. Schlax, M. H. Freilich, and R. F. Milliff (2004), Satellite measurements reveal persistent small-scale features in ocean winds, *science*, *303*(5660), 978–983. 1.1

Chen, S.-C., and K. E. Trenberth (1988), Forced planetary waves in the northern hemisphere winter: Wave-coupled orographic and thermal forcings, *Journal of the atmospheric sciences*, *45*(4), 682–704. 1.2

Christoph, M., U. Ulbrich, and P. Speth (1997), Midwinter suppression of northern hemisphere storm track activity in the real atmosphere and in gcm experiments, *Journal of the atmospheric sciences*, *54*(12), 1589–1599. 1.2

Dacre, H., M. Hawcroft, M. Stringer, and K. Hodges (2012), An extratropical cyclone atlas: A tool for illustrating cyclone structure and evolution characteristics, *Bulletin of the American Meteorological Society*, *93*(10), 1497–1502. 1.3

Dacre, H. F., and S. L. Gray (2009), The spatial distribution and evolution characteristics of north atlantic cyclones, *Monthly Weather Review*, *137*(1), 99–115. 1.3

Davis, C. A., and K. A. Emanuel (1991), Potential vorticity diagnostics of cyclogenesis, *Monthly weather review*, *119*(8), 1929–1953. 1.3

Davis, C. A., M. T. Stoelinga, and Y.-H. Kuo (1993), The integrated effect of condensation in numerical simulations of extratropical cyclogenesis, *Monthly weather review*, *121*(8), 2309–2330. 1.3.1

Deveson, A., K. Browning, and T. Hewson (2002), A classification of fastex cyclones using a height-attributable quasi-geostrophic vertical-motion diagnostic, *Quarterly Journal of the Royal Meteorological Society: A journal of the atmospheric sciences, applied meteorology and physical oceanography*, *128*(579), 93–117. 1.3

Eady, E. T. (1949), Long waves and cyclone waves, *Tellus*, *1*(3), 33–52. 1.3

Evans, M. S., D. Keyser, L. F. Bosart, and G. M. Lackmann (1994), A satellite-derived classification scheme for rapid maritime cyclogenesis, *Monthly weather review*, *122*(7), 1381–1416. 1.3.1

Feliks, Y., M. Ghil, and E. Simonnet (2004), Low-frequency variability in the midlatitude atmosphere induced by an oceanic thermal front, *Journal of the atmospheric sciences*, *61*(9), 961–981. 3.3

Fink, A. H., S. Pohle, J. G. Pinto, and P. Knippertz (2012), Diagnosing the influence of diabatic processes on the explosive deepening of extratropical cyclones, *Geophysical Research Letters*, *39*(7). 1.3.1

Gray, S. L., and H. F. Dacre (2006), Classifying dynamical forcing mechanisms using a climatology of extratropical cyclones, *Quarterly Journal of the Royal Meteorological Society: A journal of the atmospheric sciences, applied meteorology and physical oceanography*, *132*(617), 1119–1137. 1.3

Greeves, C., V. Pope, R. Stratton, and G. Martin (2007), Representation of northern hemisphere winter storm tracks in climate models, *Climate dynamics*, *28*(7-8), 683–702. 1.2

Guo, Y., T. Shinoda, J. Lin, and E. K. Chang (2017), Variations of northern hemisphere storm track and extratropical cyclone activity associated with the madden–julian oscillation, *Journal of Climate*, *30*(13), 4799–4818. 1.2

Hartmann, D. L. (1994), *Global Physical Climatology (International geophysics; v. 56)*, Academic Press. 1.3

Hartmann, D. L., A. M. K. Tank, M. Rusticucci, L. V. Alexander, S. Brönnimann, Y. A. R. Charabi, F. J. Dentener, E. J. Dlugokencky, D. R. Easterling, A. Kaplan, et al. (2013), Observations: atmosphere and surface, in *Climate change 2013 the physical science basis: Working group I contribution to the fifth assessment report of the intergovernmental panel on climate change*, pp. 159–254, Cambridge University Press. 3.3

Hawcroft, M., L. Shaffrey, K. Hodges, and H. Dacre (2012), How much Northern Hemisphere precipitation is associated with extratropical cyclones?, *Geophysical Research Letters*, *39*, doi:10.1029/2012GL053866. 1.3

Held, I. M., and B. J. Soden (2006), Robust responses of the hydrological cycle to global warming, *Journal of climate*, *19*(21), 5686–5699. 3.3

Hendry, R. (1988), A simple model of gulf stream thermal structure with application to the analysis of moored measurements in the presence of mooring motion, *Journal of Atmospheric and Oceanic Technology*, *5*(2), 328–339. 1.1

Hogg, N. G., and W. E. Johns (1995), Western boundary currents, *Reviews of Geophysics*, *33*(S2), 1311–1334. 1.1

Hoskins, B. J., and K. I. Hodges (2002), New perspectives on the Northern Hemisphere winter storm tracks, *J. Atmos. Sci.*, *59*, 1041–1061, doi:10.1175/1520-0469(2002)059<1041:NPOTNH>2.0.CO;2. 1.2

Hoskins, B. J., and D. J. Karoly (1981), The steady linear response of a spherical atmosphere to thermal and orographic forcing, *Journal of the Atmospheric Sciences*, *38*(6), 1179–1196. 1.2

Hoskins, B. J., and P. J. Valdes (1990), On the existence of storm-tracks, *Journal of the atmospheric sciences*, *47*(15), 1854–1864. 1.2, 1.3

Hoskins, B. J., M. E. McIntyre, and A. W. Robertson (1985), On the use and significance of isentropic potential vorticity maps, *Quarterly Journal of the Royal Meteorological Society*, *111*(470), 877–946. 1.3

Hotta, D., and H. Nakamura (2011), On the significance of sensible heat supply from the ocean in the maintenance of mean baroclinicity along storm tracks, *J. Climate*, *24*, 3377–3401, doi:10.1175/2010JCLI3910.1. 1.3, 1.3.1

Hu, D., L. Wu, W. Cai, A. S. Gupta, A. Ganachaud, B. Qiu, A. L. Gordon, X. Lin, Z. Chen, S. Hu, et al. (2015), Pacific western boundary currents and their roles in climate, *Nature*, *522*(7556), 299–308. 1.1

Inatsu, M., H. Mukougawa, and S.-P. Xie (2000), Formation of subtropical westerly jet core in an idealized GCM without mountains, *Geophys. Res. Lett.*, *27*, 529–532, doi:10.1029/1999GL010933. 1.2, 1.3.1

Kawai, H. (1972), Hydrography of the kuroshio extension, *Kuroshio, It's physical aspects*, pp. 235–352. 1.1

Kelly, K. A. (1991), The meandering gulf stream as seen by the geosat altimeter: Surface transport, position, and velocity variance from 73 to 46 w, *Journal of Geophysical Research: Oceans*, *96*(C9), 16,721–16,738. 1.1

Kelly, K. A., and S. Dong (2004), The relationship of western boundary current heat transport and storage to midlatitude ocean-atmosphere interaction, *Earths Climate: The Ocean–Atmosphere Interaction, Geophys. Monogr*, *147*, 347–363. 1.1

Kelly, K. A., R. J. Small, R. Samelson, B. Qiu, T. M. Joyce, Y.-O. Kwon, and M. F. Cronin (2010), Western boundary currents and frontal air–sea interaction: Gulf stream and kuroshio extension, *Journal of Climate*, *23*(21), 5644–5667. 1.1

Knauss, J. A. (1969), A note on the transport of the gulf stream, *Deep-Sea Res.*, *16*, 117–123. 1.1

Knutson, T. R., F. Zeng, and A. T. Wittenberg (2013), Multimodel assessment of regional surface temperature trends: Cmip3 and cmip5 twentieth-century simulations, *Journal of Climate*, *26*(22), 8709–8743. 3.3

Kuo, Y.-H., M. A. Shapiro, and E. G. Donall (1991), The interaction between baroclinic and diabatic processes in a numerical simulation of a rapidly intensifying extratropical marine cyclone, *Mon. Wea. Rev.*, *119*, 368–384, doi:10.1175/1520-0493(1991)119<0368:tibbad>2.0.co;2. 1.3.1

Kuwano-Yoshida, A., and S. Minobe (2017), Storm-track response to sst fronts in the northwestern pacific region in an agcm, *Journal of Climate*, *30*(3), 1081–1102. 1.2

Kuwano-Yoshida, A., S. Minobe, and S.-P. Xie (2010), Precipitation response to the gulf stream in an atmospheric gcm, *Journal of Climate*, *23*(13), 3676–3698. 1.2

Kwon, Y.-O., M. A. Alexander, N. A. Bond, C. Frankignoul, H. Nakamura, B. Qiu, and L. A. Thompson (2010), Role of the gulf stream and kuroshio–oyashio systems in large-scale atmosphere–ocean interaction: A review, *Journal of Climate*, *23*(12), 3249–3281. 1.1

Lau, N.-C., and E. O. Holopainen (1984), Transient eddy forcing of the time-mean flow as identified by geopotential tendencies, *Journal of the Atmospheric Sciences*, *41*(3), 313–328. 1.2

Leaman, K., E. Johns, and T. Rossby (1989), The average distribution of volume transport and potential vorticity with temperature at three sections across the gulf stream, *Journal of Physical Oceanography*, *19*(1), 36–51. 1.1

Liu, K.-K., L. Atkinson, R. Quiñones, and L. Talaue-McManus (2010), *Carbon and nutrient fluxes in continental margins: a global synthesis*, Springer Science & Business Media. 1.1

Ma, X., P. Chang, R. Saravanan, R. Montuoro, J.-S. Hsieh, D. Wu, X. Lin, L. Wu, and Z. Jing (2015), Distant influence of kuroshio eddies on north pacific weather patterns?, *Scientific reports*, *5*, 17,785. 1.2

McCabe, G. J., M. P. Clark, and M. C. Serreze (2001), Trends in northern hemisphere surface cyclone frequency and intensity, *Journal of Climate*, *14*(12), 2763–2768. 1.2

McClain, C. R., S. R. Signorini, and J. R. Christian (2004), Subtropical gyre variability observed by ocean-color satellites, *Deep Sea Research Part II: Topical Studies in Oceanography*, *51*(1-3), 281–301. 1.1

Meinen, C. S., and D. S. Luther (2016), Structure, transport, and vertical coherence of the Gulf Stream from the Straits of Florida to the Southeast Newfoundland Ridge, *Deep-Sea Res. Pt. I*, *112*, 137–154, doi:10.1016/j.dsr.2016.03.002. 1.1

Minobe, S., A. Kuwano-Yoshida, N. Komori, S.-P. Xie, and R. J. Small (2008), Influence of the Gulf Stream on the troposphere, *Nature*, *452*, 206–210, doi: 10.1038/nature06690. 3.3

Munk, W. H. (1950), On the wind-driven ocean circulation, *Journal of meteorology*, *7*(2), 80–93. 1.1

Murray, R. J., and I. Simmonds (1991a), A numerical scheme for tracking cyclone centres from digital data. Part I: Development and operation of the scheme, *Aust. Met. Mag.*, *39*, 155–166. 1.2

Murray, R. J., and I. Simmonds (1991b), A numerical scheme for tracking cyclone centres from digital data. Part II: application to January and July general circulation model simulations, *Aust. Met. Mag.*, *39*, 167–180. 1.2

Nakamura, H. (1992), Midwinter suppression of baroclinic wave activity in the pacific, *Journal of the atmospheric sciences*, *49*(17), 1629–1642. 1.2

Nakamura, H., T. Sampe, Y. Tanimoto, and A. Shimpo (2004), Observed associations among storm tracks, jet streams and midlatitude oceanic fronts, *Geoph. Monog. Series*, *147*, 329–345, doi:10.1029/147GM18. 1.1, 1.2, 1.3

Nakamura, H., A. Nishina, and S. Minobe (2012), Response of storm tracks to bimodal kuroshio path states south of japan, *Journal of climate*, *25*(21), 7772–7779. 1.1

Oruba, L., G. Lapeyre, and G. Rivière (2013), On the poleward motion of midlatitude cyclones in a baroclinic meandering jet, *Journal of the atmospheric sciences*, *70*(8), 2629–2649. 1.3.1

Papritz, L., and T. Spengler (2015), Analysis of the slope of isentropic surfaces and its tendencies over the North Atlantic, *Quart. J. Roy. Meteor. Soc.*, *141*, 3226–3238, doi:10.1002/qj.260. 1.3.1

Park, H.-S., J. C. Chiang, and S.-W. Son (2010), The role of the central asian mountains on the midwinter suppression of north pacific storminess, *Journal of the atmospheric sciences*, *67*(11), 3706–3720. 1.2

Peixoto, J. P., and A. H. Oort (1992), Physics of climate. 1.3

Petterssen, S., and S. J. Smebye (1971), On the development of extratropical cyclones, *Quarterly Journal of the Royal Meteorological Society*, *97*(414), 457–482. 1.3

Pfahl, S., and H. Wernli (2012), Quantifying the relevance of cyclones for precipitation extremes, *Journal of Climate*, *25*(19), 6770–6780. 1.3

Piazza, M., L. Terray, J. Boé, E. Maisonnave, and E. Sanchez-Gomez (2016), Influence of small-scale north atlantic sea surface temperature patterns on the marine boundary layer and free troposphere: A study using the atmospheric arpege model, *Climate dynamics*, *46*(5-6), 1699–1717. 1.2

Pinto, J. G., U. Ulbrich, G. Leckebusch, T. Spangehl, M. Reyers, and S. Zacharias (2007), Changes in storm track and cyclone activity in three sres ensemble experiments with the echam5/mpi-om1 gcm, *Climate Dynamics*, *29*(2-3), 195–210. 1.2

Qiu, B. (2001), Kuroshio and oyashio currents, *Ocean currents: a derivative of the encyclopedia of ocean sciences*, pp. 61–72. 1.1

Qiu, B. (2002), The kuroshio extension system: Its large-scale variability and role in the midlatitude ocean-atmosphere interaction, *Journal of Oceanography*, *58*(1), 57–75. 1.1

Rhines, P. B. (2002), Rossby waves, *Encyclopaedia of Atmospheric Sciences*, pp. 1–37. 1.3

Ritchie, E. A., and R. L. Elsberry (2003), Simulations of the extratropical transition of tropical cyclones: Contributions by the midlatitude upper-level trough to reintensification, *Monthly weather review*, *131*(9), 2112–2128. 1.3.1

Riviere, G., and A. Joly (2006), Role of the low-frequency deformation field on the explosive growth of extratropical cyclones at the jet exit. part ii: Baroclinic critical region, *Journal of the atmospheric sciences*, *63*(8), 1982–1995. 1.3.1

Robinson, W. A. (1996), Does eddy feedback sustain variability in the zonal index?, *Journal of the atmospheric sciences*, *53*(23), 3556–3569. 1.2

Roebber, P. J. (1989), The role of surface heat and moisture fluxes associated with large- scale ocean current meanders in maritime cyclogenesis, *Mon. Wea. Rev.*, *117*, 1676–1694, doi:10.1175/1520-0493(1989)117<1676:TROSHA>2.0.CO;2. 1.3.1

Rossby, C. (1939), Planetary flow patterns in the atmosphere, *Quart. J. Roy. Met. Soc*, *66*, 68. 1.3

Sampe, T., H. Nakamura, A. Goto, and W. Ohfuchi (2010), Significance of a midlatitude sst frontal zone in the formation of a storm track and an eddy-driven westerly jet, *Journal of Climate*, *23*(7), 1793–1814. 1.2

Sawyer, J. (1970), Observational characteristics of atmospheric fluctuations with a time scale of a month, *Quarterly Journal of the Royal Meteorological Society*, *96*(410), 610–625. 1.2

Schneider, T. (2006), The general circulation of the atmosphere, *Annual Review of Earth and Planetary Sciences*, *34*. 1.2

Schultz, D. M., and G. Vaughan (2011), Occluded fronts and the occlusion process: A fresh look at conventional wisdom, *Bulletin of the American Meteorological Society*, *92*(4), 443–466. 1.3

Schultz, D. M., D. Keyser, and L. F. Bosart (1998), The effect of large-scale flow on low-level frontal structure and evolution in midlatitude cyclones, *Monthly weather review*, *126*(7), 1767–1791. 1.1, 1.3.1

Schultz, D. M., L. F. Bosart, B. A. Colle, H. C. Davies, C. Dearden, D. Keyser, O. Martius, P. J. Roebber, W. J. Steenburgh, H. Volkert, et al. (2018), Extratropical cyclones: A century of research on meteorologys centerpiece, *Meteorological monographs*, *59*, 16–1. 1.3

Shapiro, M. A., and D. Keyser (1990), Fronts, jet streams and the tropopause, in *Extratropical cyclones*, pp. 167–191, Springer. 1.3

Shaw, T., M. Baldwin, E. A. Barnes, R. Caballero, C. Garfinkel, Y.-T. Hwang, C. Li, P. O'Gorman, G. Rivière, I. Simpson, et al. (2016), Storm track processes and the opposing influences of climate change, *Nature Geoscience*, *9*(9), 656–664. 1.2, 1.3

Siedler, G., S. M. Griffies, J. Gould, and J. A. Church (2013), *Ocean circulation and climate: a 21st century perspective*, Academic Press. 1.1

Sinclair, M., and S. Shami (1997), Evolving simple software agents: comparing genetic algorithm and genetic programming performance, in *Second International Conference On Genetic Algorithms In Engineering Systems: Innovations And Applications*, pp. 421–426, IET. 1.2

Sinclair, M. R. (1995), A climatology of cyclogenesis for the southern hemisphere, *Monthly Weather Review*, *123*(6), 1601–1619. 1.2

Small, R. d., S. P. deSzoeke, S. Xie, L. Oneill, H. Seo, Q. Song, P. Cornillon, M. Spall, and S. Minobe (2008), Air–sea interaction over ocean fronts and eddies, *Dynamics of Atmospheres and Oceans*, *45*(3-4), 274–319. 1.1

Small, R. J., R. A. Tomas, and F. O. Bryan (2014), Storm track response to ocean fronts in a global high-resolution climate model, *Climate dynamics*, *43*(3-4), 805–828. 1.2

Stocker, T., G. Clarke, H. Le Treut, R. Lindzen, V. Meleshko, R. Mugara, T. Palmer, R. Pierrehumbert, P. Sellers, K. Trenberth, et al. (2001), Physical climate processes and feedbacks, in *IPCC, 2001: Climate change 2001: The scientific basis. Contribution of working group I to the third assessment report of the intergovernmental panel on climate change*, pp. 417–470, Cambridge University Press. 3.3

Stommel, H. (1948), The westward intensification of wind-driven ocean currents, *Eos, Transactions American Geophysical Union*, *29*(2), 202–206. 1.1

Stommel, H. M. (1965), *The Gulf Stream: a physical and dynamical description*, Univ of California Press. 1.1

Sutcliffe, R. (1951), Mean upper contour patterns of the northern hemispherethe thermal-synoptic view-point, *Quarterly Journal of the Royal Meteorological Society*, *77*(333), 435–440. 1.2

Sverdrup, H. U. (1947), Wind-driven currents in a baroclinic ocean; with application to the equatorial currents of the eastern pacific, *Proceedings of the National Academy of Sciences of the United States of America*, *33*(11), 318. 1.1

Talley, L. D. (2011), *Descriptive physical oceanography: an introduction*, Academic press. 1.1

Tamarin, T., and Y. Kaspi (2017), Mechanisms controlling the downstream poleward deflection of midlatitude storm tracks, *Journal of the Atmospheric Sciences*, *74*(2), 553–572. 1.2

Tierney, G., D. J. Posselt, and J. F. Booth (2018), An examination of extratropical cyclone response to changes in baroclinicity and temperature in an idealized environment, *Climate Dynamics*, *51*(9-10), 3829–3846. 1.3

Tsopouridis, L., C. Spensberger, and T. Spengler (2020a), Characteristics of cyclones following different pathways in the gulf stream region, *Quarterly Journal of the Royal Meteorological Society;1-16, https://doi.org/10.1002/qj.3924*. 1.3.1, 3.1

Tsopouridis, L., C. Spensberger, and T. Spengler (2020b), Cyclone intensification in the kuroshio region and its relation to the sea surface temperature front and upper-level forcing, *Quarterly Journal of the Royal Meteorological Society;1-16, https://-doi.org/10.1002/qj.3929*. 3.1

Uccellini, L. W. (1990), Processes contributing to the rapid development of extratropical cyclones, in *Extratropical cyclones*, pp. 81–105, Springer. 1.3.1

Wallace, J. M., and P. V. Hobbs (2006), *Atmospheric science: an introductory survey*, vol. 92, Elsevier. 1.1

Wang, C.-C., and J. C. Rogers (2001), A composite study of explosive cyclogenesis in different sectors of the North Atlantic. Part I: Cyclone structure and evolution, *Mon. Wea. Rev.*, *129*, 1481–1499, doi:10.1175/1520-0493(2001)129<1481:ACSOEC>2.0.CO;2. 1.3.1

Whitaker, J. S., and C. A. Davis (1994), Cyclogenesis in a saturated environment, *Journal of the atmospheric sciences*, *51*(6), 889–908. 1.3

Willison, J., W. A. Robinson, and G. M. Lackmann (2013), The importance of resolving mesoscale latent heating in the north atlantic storm track, *Journal of the Atmospheric Sciences*, *70*(7), 2234–2250. 3.3

Xie, S.-P. (2004), Satellite observations of cool ocean–atmosphere interaction, *Bulletin of the American Meteorological Society*, *85*(2), 195–208. 1.1

Yin, J. H. (2005), A consistent poleward shift of the storm tracks in simulations of 21st century climate, *Geophysical Research Letters*, *32*(18). 1.2

Yu, L., and R. A. Weller (2007), Objectively analyzed air–sea heat fluxes for the global ice-free oceans (1981–2005), *Bulletin of the American Meteorological Society*, *88*(4), 527–540. 1.1

Zhang, C., H. Liu, J. Xie, P. Lin, C. Li, Q. Yang, and J. Song (2020), North pacific storm track response to the mesoscale sst in a global high-resolution atmospheric model, *Climate Dynamics*, *55*(5), 1597–1611. 1.2

Zhang, Y., and I. M. Held (1999), A linear stochastic model of a gcms midlatitude storm tracks, *Journal of the atmospheric sciences*, *56*(19), 3416–3435. 1.2

Zhao, Y., and X. San Liang (2019), Causes and underlying dynamic processes of the mid-winter suppression in the north pacific storm track, *Science China Earth Sciences*, *62*(5), 872–890. 1.2

Graphic design: Communication Division, UiB / Print: Skipnes Kommunikasjon AS

uib.no

ISBN: 9788230858578 (print)
9788230846698 (PDF)